Development of a disturbance compensation controller for an active damping system

L.Tulleken

Master of Science Thesis

Delft University of Technology

Delft Center for Systems and Control

Development of a disturbance compensation controller for an active damping system

Master of Science Thesis

For the degree of Master of Science in Systems and Control at Delft University of Technology

L.Tulleken

June 3, 2019

Faculty of Mechanical, Maritime and Materials Engineering (3mE) · Delft University of Technology

The work in this thesis was supported by ZF Friedrichshafen AG. Their cooperation is hereby gratefully acknowledged.

Delft
University of
Technology

Abstract

ZF Friedrichshafen AG is developing its own active suspension system designed as a single unit per corner to optimize the dynamic behavior of a vehicle. The innovative active damper design integrates all the essential components into one damper unit, with the aim to facilitate implementation. This master thesis in cooperation with ZF Friedrichshafen AG presents the development of a disturbance compensation controller for the active suspension unit. The goal is to suppress forces induced by road irregularities on the passenger cabin.
This work is divided into two parts.
The first part provides a theoretical background on active suspension systems in the form of a literature survey. It focuses on the purpose of a suspension, different suspension types and control techniques which can be found in previous studies on active suspensions. −This literature survey was separately graded and is not considered in the final assessment of this master thesis. It is provided here for convenience as it is referred to every now and then in the second part of this work and as conventions are introduced.−
The second part of this work is the actual master thesis report. It introduces the project's outline at ZF Friedrichshafen AG and explains the already existing modular vehicle controller structure and the working principle of the active damper unit. It presents a new signal based disturbance compensation algorithm and defines the corresponding required signal conditioning. This algorithm is validated by simulations on an augmented quarter car model, which includes a linear approximation of the active damper unit, before it is implemented in the project's test vehicle. Extensive real world tests are conducted and the results are evaluated by means of performance criteria, which use the insights gained in the simulations. Finally an adaptation logic is developed to enhance the controller's performance. It considers the physical limits of the active damper units and combines the disturbance compensation algorithm with Skyhook control. The control algorithms in combination with the adaptation logic are tested and the results are discussed.
The emphasis throughout this work lies on the implementation and applicability of the control algorithm.

Acknowledgements

I would like to thank my supervisor, Dr. Eckehard Münch, for his guidance during the past year at ZF and his assistance during the writing of this thesis.

I would also like to thank my colleague, Dr. Claudia Voicu, for the helpful feedback during the writing of this report and all my other colleagues, for the pleasant time at ZF.

Writing my thesis at an international company abroad was a great opportunity to broaden my knowledge and I would like to thank my supervisor at the TU Delft, Prof.dr.ir. J. Hellendoorn, for his support during this time and for his helpful feedback on this final report.

Delft, University of Technology L.Tulleken
June 3, 2019

Table of Contents

List of Figures

List of Tables

Chapter 1

Introduction

This work is made in cooperation with ZF Friedrichshafen AG and presents the development of a disturbance compensation controller for a passenger vehicle with an innovative active suspension system. The goal of the disturbance compensation controller is to suppress forces induced by road irregularities on the passenger cabin.
The proposed disturbance compensation algorithm is verified by means of simulations, before the controller is implemented and extensively tested under real world conditions in a test vehicle. The test results are evaluated by means of two performance criteria and an additional adaptation logic is developed to further enhance the controller's performance.
The emphasis throughout this work lies on the implementation and applicability of the control algorithm.

1-1 Motivation

In the early days of the automobile, automotive engineers focused primarily on the development of lightweight and efficient power trains to make the vehicles they developed faster. General chassis development lagged behind until in the 1930s the demand for reliability, comfort and safety increased. By that time, the focus of vehicle development shifted to suspension. [9]

Despite the fact that vehicle suspensions have been subject to continuous development ever since, the conflicting task of providing excellent ride comfort and ride safety, while simultaneously meeting constructional constraints, has not yet been solved satisfactory.
A vehicle suspension system should provide maximum ride comfort and has to guarantee ride safety by keeping constraints on the road holding in order to assure the transmission of longitudinal and lateral forces between the tires and the road surface.
The dynamic behavior of conventional suspension systems is thereby primarily determined by the choice of the spring stiffness and the damping coefficient. In defining the spring and damper layout, a compromise between comfort, which requires a soft setup and safety, which

requires a well damped setup needs to be made. This is a conflicting task and the major challenge is to find the best compromise for every driving situation [15, 23]

As a result of the continuous suspension development, there are more than just passive suspensions on the market. Meanwhile there are semi-active suspension configurations that can vary their damping characteristics and the first active suspension systems, which are characterized by their ability to apply forces independent of the direction of the suspension travel and velocity, also have found their way into series production (e.g. Mercedes-Benz S-Klasse: Magic Body Control (MBC) [21] and the Audi A8: AI active suspension [20]).
The development and implementation of active suspension systems is greatly accelerated by means of simulation techniques. Mathematical suspension models can be utilized to simulate the effect of suspension setups on the vehicle's dynamic behavior. The required model complexity depends on the application and on the availability of measurement signals. Often quarter car models are already sufficient to design and simulate a local controller. Having decided on a vehicle model, control algorithms can be applied to enhance the comfort and/or safety of a vehicle. The final controller implementation usually follows either a modular or a full-vehicle approach. The resulting suspension systems ease the conflict between comfort and safety and allow optimal suspension settings for different driving situations and personal preferences.

With the expectation of autonomous vehicles coming in the near future, suspensions that isolate the passenger cabin from road irregularities while maintaining good tire-road contact will become even more relevant as they are now. To suppress motion sickness and make the journey in an autonomous vehicle as comfortable as possible, for passengers that do not necessarily have to pay attention to the surrounding anymore, it is important that the body of the vehicle moves like a flying carpet, suppressing the external forces acting on the passenger cabin [13, 8].

1-2 Conceptual formulation

This work is carried out parallel to the development and implementation of an innovative active damper unit, developed by ZF Friedrichshafen AG. The active suspension unit is designed as a single unit for each wheel to optimize the dynamic behavior of a vehicle. Designed as a single unit with all the essential components integrated into one damper, it aims to facilitate implementation.

Being a part of an already existing project, the prerequisites of this work were already defined at the beginning. The active damper units and test vehicle were already present, as well as a mathematical model of the active damper unit and a defined structure of the vehicle controller. This confined the problem description of this master thesis.

The task in this master thesis was to develop and implement a disturbance compensation controller for the new active damper unit. The controller should enhance the vehicle's dynamics and complement the already existent control algorithms (e.g. Skyhook). It should do so without the possibility to scan the upcoming road surface (no preview system). The project's test vehicle was available to test the control algorithm, as well as the vehicle controller and a mathematical model of the active damper unit. The vehicle controller is developed in `Matlab/Simulink` and the final implementation follows on a `dSpace` system.

1-3 Project layout

This work is divided into two parts.

The first part provides a theoretical background on active suspension systems in the form of a literature survey. It focuses on the purpose of a suspension, different suspension types and control techniques which can be found in previous studies on active suspensions. −This literature survey was separately graded and is not considered in the final assessment of this master thesis. It is provided here for convenience as it is referred to every now and then in the second part of this work.−

The second part of this work is the actual master thesis report. It introduces the project's outline at ZF Friedrichshafen AG in the second chapter and explains the working principle of the active damper unit and the already existing modular vehicle controller structure in chapter three and chapter four respectively. The new signal based disturbance compensation algorithm is presented in chapter five and the corresponding required signal conditioning is discussed in chapter six. The proposed disturbance compensation control algorithm is validated in chapter seven, by simulations on an augmented quarter car model, which includes a linear approximation of the active damper unit, before it is implemented in the project's test vehicle in chapter eight. Extensive real world tests are conducted and the results are evaluated by means of two performance criteria in chapter ten. Chapter nine describes the test facility and road test procedures. An adaptation logic is developed to enhance the controller's performance in chapter eleven. It considers the physical limits of the active damper units and combines the disturbance compensation algorithm with Skyhook control. The control algorithms in combination with the adaptation logic are tested and the results are discussed in chapter twelve.
The second last chapter summarizes the thesis and presents the conclusions.
To finalize, a recommendation on further research is given. Emphasized there are suggestions to continue the development and further improve the disturbance compensation controller.

Part I

Literature Survey

Chapter 2

Definition

The suspension of a vehicle represents the connection between the road surface and the vehicle's body. Consisting of tires, wheels, wheel carriers, brakes, steering system, springs and dampers it is responsible for the transfer of forces between the tires and the road surface in order to enable driving, steering and braking. It should guide the wheels in a precise way for predictable driving dynamics while keeping suspension deflections within constructional limits and it should also provide a maximum of comfort by isolating the vehicle's body from disturbances caused by road surface irregularities.

The traditional method of finding the desired dynamic driving behavior is to tune the force-displacement and force-velocity characteristics of the springs and dampers. Once a chassis layout has been determined most of the variables and design parameters in the suspension design process are fixed. In case of a passive suspension this results in fixed spring and damping characteristics, preliminary defining the dynamic driving characteristics of the vehicle [9].

In addition to a permanently-fixed approach, there exist other suspension systems which allow the force acting on the vehicle body to be dependent on more than just a single curve relating the suspension travel and the relative suspension velocity [22]. They enable to adjust the spring and/or damping characteristics depending on the driving situation.
To help distinguish between various suspension systems, they are categorized according to their response time, energy requirement and effective range [7, 16].
The first distinction that is made, is between active and passive systems. The active systems are subsequently divided into semi-active suspension systems and active suspension systems. Depending on their ability to carry the static weight of the vehicle's body, active suspension systems are finally categorized into fully-supporting systems and partly-supporting systems.
An overview of suspension systems categorized according to effective range, response time and energy consumption is given in Table 2-1 from G. Koch et al. [16] p.26. The difference between fully-supportive and partly-supportive suspension systems is illustrated in Figure 2-2 from R. H. Streiter [33] p.31.

Table 2-1: Classification of vertical dynamic suspension systems [16] p.26

Type	Principle	Effective range	Frequency range	Energy demand
Passive	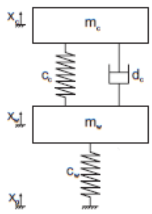	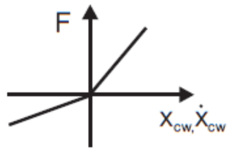	no actuators	0 W
Adaptive	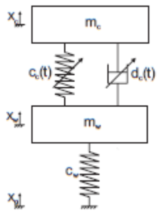	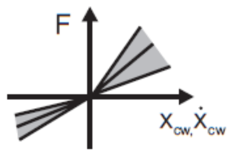	$< 1\,\mathrm{Hz}$	low
Semi-active	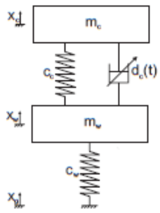	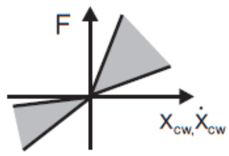	$0 - 40\,\mathrm{Hz}$	low
Slow active	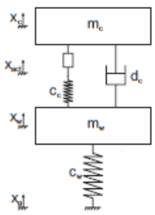	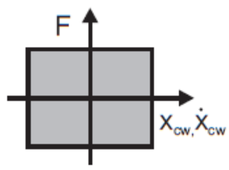	$0 - 5\,\mathrm{Hz}$	medium
Fully active	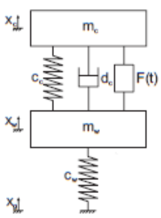	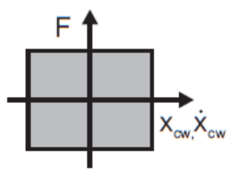	$0 - 30\,\mathrm{Hz}$	high

2-1 Passive suspension systems

Passive suspension systems neither require a controller nor do they require additional energy to function properly. The spring and damping characteristics of a passive suspension are fixed. Their properties are described by fixed force-displacement and force-velocity curves respectively. The springs are responsible for supporting the vehicle's weight and the spring stiffness is chosen such that the maximum suspension travel is sufficient even if the vehicle carries additional load and drives over a rough road [16].
Dampers dissipate the kinetic energy of the body and wheels, where the damping force depends on the relative damper velocity. If a constant force is applied to a damper with a linear force-velocity curve, the damper will shorten or elongate within its range of motion with a constant velocity depending on the direction of the force applied. This implies that a damper cannot support any static weight, e.g. the weight of the vehicle's body.

The direction of the force generated by a passive suspension is always defined by both the direction of the suspension travel and the relative suspension velocity. This is illustrated by the *effective range* in table 2-1. The effective range shows the four possible quadrants in which suspension forces can act. As illustrated in the table, a passive suspension is characterized by fixed force-displacement and force-velocity curves in two of these quadrants.
The force-displacement curve of a passive suspension is often designed to be linear in its operating range to ensure predictable driving dynamics with a progressive characteristic near the end of the range, whereas the rebound (hard) and compression (soft) stages of the damping are laid out asymmetric, resulting in a non linear force-velocity curve [22].

2-2 Adaptive suspension systems

Adaptive suspension systems can realize a variation of the spring and damper characteristics which helps to minimize body accelerations and wheel load fluctuations. They can account for the ride height and can compensate a change in the vehicle's load [27]. Most adaptive damping systems evaluate the displacement and acceleration of the vehicle's body to determine an actuation value based on threshold values [9].
Citroën was the first to develop an adaptive suspension system (Citroën Hydractive [9]). It was first offered on the 1989 Citroën XM, that uses a hydropneumatic suspension system to regulate the ride height. More recent systems apply airsprings to change the ride height of the vehicle. Porsche, for example, use airsprings in the Panamera and made the variation of the ride height velocity dependent in order to lower the center of gravity of the vehicle, which ensures a more sportive roadholding at higher speeds [16].
BMW introduced one of the earliest adaptive damping systems (BMW Electronic Damper Control (EDC)). Their system features three different damper settings. The active damper setting is chosen by a control unit which acts on the vertical acceleration of the body [9].
A change in the ride height by changing the pre-tension of the springs and/or a change in the damping characteristic effects the force-displacement and force-velocity curves in two quadrants of the effective range. The direction of the suspension force stays dependent on the suspension travel and relative suspension velocity.

2-3 Semi-active suspension systems

Suspension systems with a variable force-velocity curve are subdivided into the semi-active suspension category. As with passive and adaptive suspensions, the effective range of semi-active suspensions only covers two quadrants in the force-velocity diagram. Semi-active dampers can change the level of energy dissipation, but do not supply energy to the system [16]. Correspondingly, the direction of the force generated is always defined by the relative suspension velocity and the power demand is low.
High actuation bandwidths which allow to consider the movement of the wheels in addition to the motion of the vehicle's body distinguishes semi-active suspension systems from adaptive damping systems [9].
According to G. Koch et al. [16], there are three physical damping principles which can be distinguished. All of them allow fast adjustment of the damper characteristics.

1. *Adjustable hydraulic* dampers can vary the surface area of the openings through which the damping fluid flows. An adjustable damper is the Continuous Damping Control (CDC) damper developed by ZF Sachs. It has proportional damper valves that allow damping forces to be continuously varied between two (minimum and maximum) force-velocity curves (see Figure 2-1 from [5] p.3). These dampers provide fast reaction times and use a different valve for both the compression and rebound direction [9].

2. *Magnetorheological* dampers change their damping characteristics by applying a magnetic field, which causes magnetic particles in the damper fluid to form chains. This changes the viscosity of the fluid and as a direct result the damping without requiring adjustable proportional valves [9, 16].

3. *Electrorheological* dampers also change the viscosity of the damper fluid. The difference to magnetorheological dampers is that an electrical field is applied to the fluid instead of a magnetic field. Since there are no magnetic particles in the fluid, the abrasive effect is reduced which improves the durability [16].

These dampers are fast enough to enable feedback control strategies (rather than threshold control strategies) that enhance comfort and road holding.

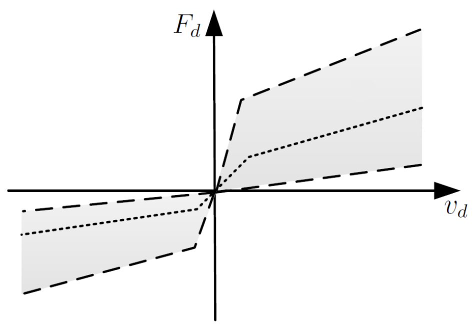

Figure 2-1: Example of the force characteristic of a passive damper (dotted line) and set of admissible semi-active damper forces (gray area) [5] p.3

2-4 Active suspension systems

In combination with the known passive spring and damper systems, additional hydraulic, electromagnetic and electromechanical units can be used to supply forces to a suspension. These suspension systems are called active suspensions . They can deliver forces independent of the relative motion of the suspension and their effective range covers all four quadrants of the force-displacement/force-velocity diagram.
Active suspensions that rely on the passive suspension characteristics at higher frequencies are classified as slow active suspension systems (actuation bandwidth typically $\approx$ 5 Hz). When the operating range of the active elements is fast enough (approximately two times the wheel eigenfrequency $\approx$ 25 Hz), the active systems cannot only influence the movement of the vehicle's body, also called sprung mass, but also the movement of wheels together with some parts of the suspension, called the unsprung mass. This however does come at the cost of high power demands and energy consumption [33].

Active suspensions can thus increase comfort and safety by controlling the forces between the sprung and unsprung masses in all four quadrants. When applied in a correct way, oscillations will be damped and ideally even get compensated before they have the chance to excite the passenger cabin at all.

Apart from the classification according to Table 2-1, active suspensions can furthermore be subdivided into fully-supportive and partly-supportive systems. In a partly-supportive suspension, the static weight of the sprung mass is, as before, supported by a spring parallel to the damper and/or active element in the suspension. In contrast, fully-supportive suspensions do not have a passive element to account for the weight of the sprung mass. This means that the active element has to account for the static weight, resulting in high power demands and energy consumption. Interpretations of fully-supportive, partly-supportive and non-supportive suspensions are schematically represented in Figure 2-2.

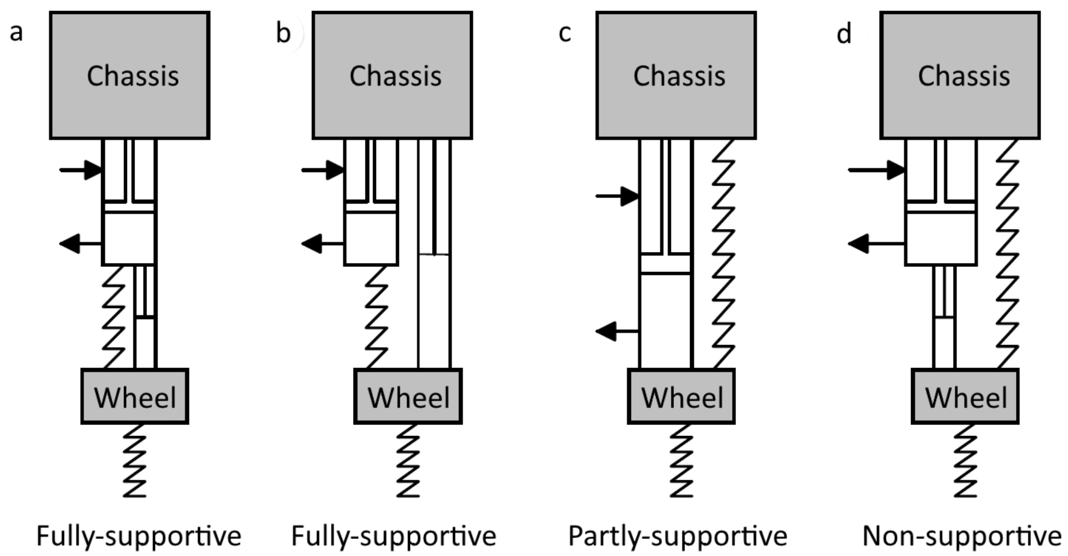

Figure 2-2: Possible layouts for active suspensions with conventional spring and damper units. **a** & **b**: Fully-supportive, **c**: Partly-supportive, **d**: Non-supportive [33] p.31

Depending on the layout, active suspensions have to fulfill the following requirements [27]:

- Support the static load of the sprung mass
- Accomplish a load independent dynamic behavior and ride height
- Decouple the sprung mass from high-frequency excitation
- Damp the sprung mass and reduce sprung mass accelerations
- Reduce roll and pitch movements
- Reduce fluctuations in the dynamic wheel load
- Guarantee a comfortable ride for the passengers

Active suspensions can also exclusively be represented by actuators, not using any passive elements whatsoever. An overview is of these suspension types is given in [9]. These systems however have not made it into series production yet due to immense power demands, high bandwidth demands and corresponding excessive costs [9]. An advantage of combining both conventional and active elements is, that in case of a system failure, the passive elements ensure that the vehicle is still drivable.

Chapter 3

Performance criteria and constructional limitations

Since all the external forces on a vehicle (with the exception of aerodynamic and inertial forces) are applied through the contact patch between the road surface and the tire, uninterrupted contact is the most important criterion for driving. If this contact between the road surface and the tire is interrupted, the transfer of longitudinal and lateral forces becomes impossible. Preventing this is a difficult task, because the road surface is not always straight, dry, adherent and free of bumps [9].
Knowing the limits of a suspension and using performance criteria to evaluate a suspension setup is therefore vital in the suspension design and fine-tuning process.

3-1 Roadway excitation

The input on a suspension is represented by the road surface irregularities.
Road surface irregularities in general take the form of excitations with varying amplitude and wavelength with random offsets. These typical irregularities can be seen as random vertical excitations, which are often approximated by Gaussian distributions (also called normal distributions). The mathematical properties of normal distributions are well known and are exploited in suspension design to help define design criteria [9, 22].
Furthermore, according to the Chassis Handbook [9], road surface irregularities in the range from $0 - 30$ Hz represent the most intensive source of input energy to the vehicle. This bounds the frequency spectrum of interest and helps when evaluating measurement data from real measurements.

3-2 System performance

To derive system requirements on a suspension, a measure for both comfort and safety has to be defined. This measure can be user-defined as long as it allows to objectively compare the effect of different suspension settings on the comfort and safety performance of the vehicle.

3-2-1 Comfort

As a measure for comfort, the vertical acceleration of the sprung mass can be considered. Often however, since a human body can be considered as a complicated mass/spring system with different eigenfrequencies, this vertical acceleration is not directly used as a measure for comfort. Accelerations transmitted to the passengers through the seat, backrest, feet and hands all have a different effect on human comfort and health. Therefore these accelerations have to be distinguished by their point of application and their direction. This has been researched (see for example [35]) and it turns out, that the human body is especially sensitive to vertical accelerations that are transmitted through the seats within the range from $4-8$ Hz. Eigenfrequencies within this sensitive range should therefore be avoided when designing the suspension of a vehicle [9, 19, 22].
To account for this sensitive vertical mechanical vibration range, the comfort index $||\ddot{z}_{c,comf}||_{rms}$ is often considered. This comfort measure results from the root mean square value (RMS-value) of the vertical acceleration after filtering with the ISO comfort filter given in [12].
The RMS-value of a signal $q(t)$ is defined as

$$||q(t)||_{rms} = \sqrt{\frac{1}{T}\int_0^T q^2(t)\,dt} \quad \text{, where } T \text{ is the period of the measured signal.} \tag{3-1}$$

Other sources (e.g. G. Koch et al. [17]) use the VDI norm given in [35] as a measure on the vertical acceleration to evaluate the effect on the human body. Both Verein Deutscher Ingenieure (VDI) and International Standard Organisation (ISO) recommend their own guidelines. Although similar, this shows that different norms can be used as long as they fulfill the requirements of the user's case.

3-2-2 Safety

The deviation from the wheel load around the average wheel load ($F_{stat}\,[N]$) is often used as measure for safety. For the signal $q(t)$, the average or mean signal value is defined as

$$\bar{q} = \frac{1}{T}\int_0^T q(t)\,dt. \tag{3-2}$$

And the deviation around the mean of the signal $q(t)$ is

$$\sigma_q = \sqrt{\frac{1}{T}\int_0^T \left(q(t)-\bar{q}\,\right)^2 dt}. \tag{3-3}$$

For a signal, such as the road excitation profile that can be approximated by a Gaussian Distribution, the deviation always has a certain specific form, called the standard deviation of the signal.
When the function $q(t)$ is represented by the wheel load $F_z(t)$ and the dynamic wheel load

$F_{dyn}(t)$ is equal to $F_z(t) - F_{stat} = F_z(t) - \bar{F}_z$, (3-3) is rewritten as

$$\sigma_{F_z} = \sqrt{\frac{1}{T}\int_0^T \left(F_z(t) - \bar{F}_z\right)^2 dt} \tag{3-4}$$

$$= \sqrt{\frac{1}{T}\int_0^T F_{dyn}^2(t)\,dt} \tag{3-5}$$

which is equal to $||F_{dyn}(t)||_{rms}$.

For a Gaussian distribution, these calculations result in a straight line that crosses the mean value of the signal and has a slope dependent on the standard deviation as illustrated in Figure 3-1 from M. Mitschke et al. [22], p.337. This graphical representation makes it possible to

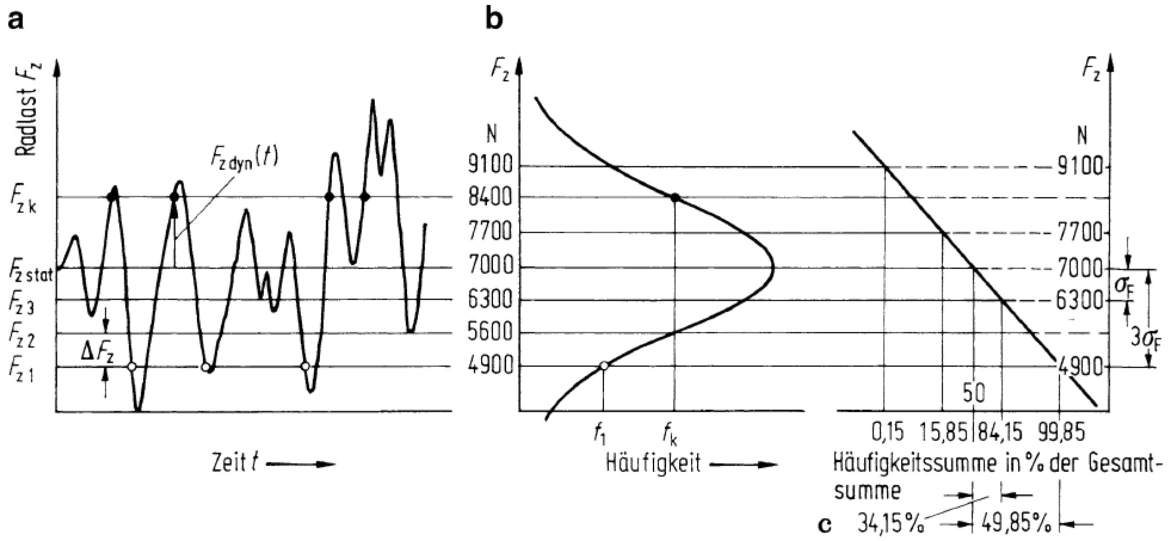

Figure 3-1: **a** Wheel load $F_z(t)\,[N]$ vs time [s] of an illustrative measurement signal with a Gaussian distribution. **b** Wheel load occurrence curve for a signal with a Gaussian distribution. **c** Representation of the wheel load occurrence in percentage ($x-$axis) on a standard deviation $y-$axis scale [22] p.337

directly read off the mean and standard deviation of a signal that can be approximated by a Gaussian distribution. The probability that the value of the signal $q(t)$ lies within $\bar{q} + \lambda\sigma_q$ and $\bar{q} - \lambda\sigma_q$, with $\lambda \in \mathbb{N}$ and the probability that the value lies outside this range is tabulated in so called normal distribution tables, see for example [4, 22, 26] and can also be seen in the figure.

The absolute value of $||F_{dyn}||_{rms}$ affects the driving dynamics differently, depending on the static wheel load F_{stat}. This effect is taken into account by dividing the standard deviation of the wheel load through the static wheel load

$$\frac{\sigma_F}{F_{stat}} = \frac{||F_{dyn}||_{rms}}{F_{stat}}. \tag{3-6}$$

To ensure safe driving, the following constraint on the dynamic wheel load is often applied by suspension designers [22]

$$||F_{dyn}||_{rms} \leq \frac{F_{stat}}{3}. \tag{3-7}$$

The effect of the constraint in (3-7) together with the probabilities found in Figure 3-1 are clarified in the following illustrative example from [22] p.353.

> For a vehicle with $||F_{dyn}||_{rms} = 1000\,N$ and $F_{stat} = 3000\,N$, the normal wheel load F_z is equal to zero when $F_{stat} - \lambda \cdot ||F_{dyn}||_{rms} = 0$, which is the case for $\lambda = 3$. From the normal distribution it follows that in $0.3\,\%/2 = 0.15\,\%$ of the time this occurs, meaning that the wheel lifts of from the road surface once every $1/0.0015 = 667$ wheel load peaks. For a vehicle with a wheel eigenfrequency of 15 Hz, this happens once every 44 seconds, or in other words every 889 meters when the vehicle drives at $72\,km/h = 20\,m/s$.
> Suppose now that $||F_{dyn}||_{rms}$ increases to $1500\,N$, then λ reduces to 2 and the wheel already lifts of every 58 meters.

Considering that a vehicle has four wheels this constraint practically guaranties constant road contact.

3-3 Conventional suspension limitations

An undamped and unsprung suspension would need to be rigid to support the weight of the vehicle's body. Driving over road irregularities, with such a suspension, would result in a virtual direct transmission of the induced forces to the body (slightly filtered by the tires [27]). High peaks in the acceleration and dynamic wheel load would be the result.
Adding a spring to the suspension to account for the weight of the vehicle's body would result in the desired degree of freedom allowing the wheels to move with respect to the body. This would reduce the peaks in the acceleration. The lag of damping however, would result in continuous movement of the passengers cabin and fluctuations in the dynamic wheel load.
Adding a damper to the system will subsequently damp the oscillations and reduce the fluctuations in the dynamic wheel load.

3-3-1 Trade-off

Concentrating on passive springs and dampers and especially on their spring and damping constant, $c_c\,[N/m]$ and $d_c\,[Ns/m]$ respectively, it becomes clear that a suspension layout is not as trivial as described above. Where a comfortable suspension setting requires soft springs and damping, a safety orientated setting requires a firm suspension setup to push the wheels onto the road. The firmer damping will reduce wheel load fluctuations, but leads to higher vertical accelerations of the vehicle's body [22].
The effect of different spring- and damper settings is illustrated in Figure 3-2, S. Spirk et al. [31] p.169.

The figure clearly shows, that optimal comfort and maximum safety cannot be reached at the same time by a passive suspension configuration. Variation of the damping coefficient offers some margin to adapt between a more safety or more comfort oriented dynamic behavior, but the potential range of variation (semi-active curve in the figure) in comfort is small due the fact that the spring stiffness cannot variate.
Alternating both the damping and spring stiffness makes it possible to adapt between safety

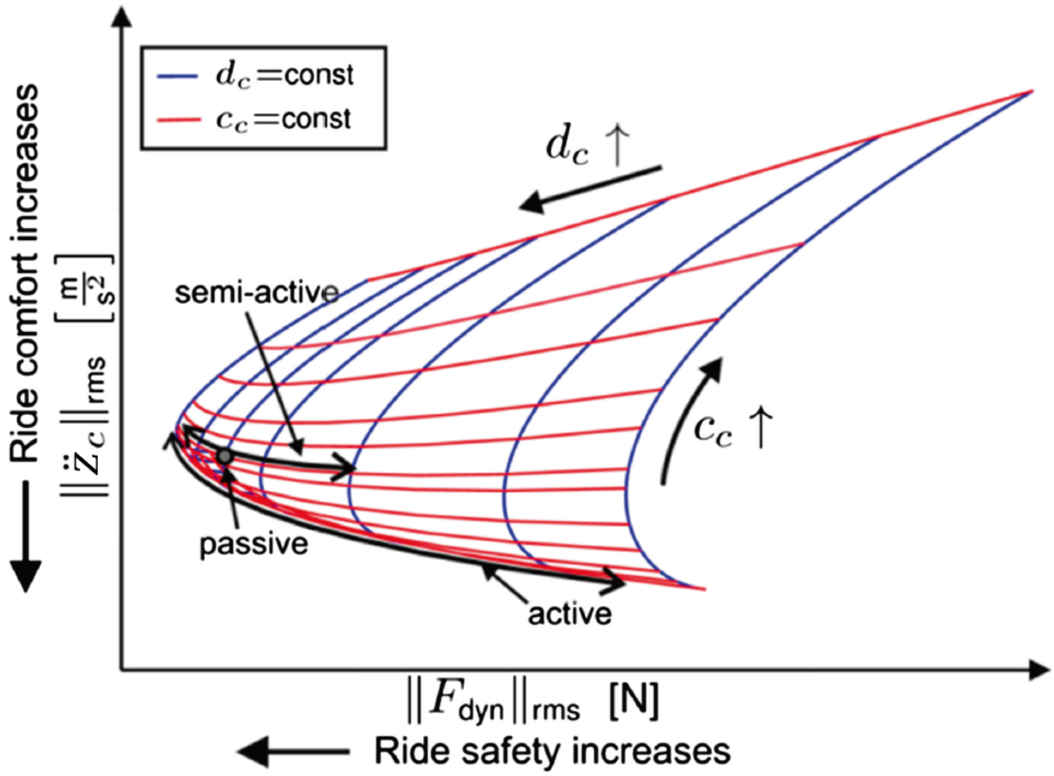

Figure 3-2: Vehicle suspension conflict diagram [31] p.169

and comfort oriented vehicle dynamics (active curve in the figure). When reacting fast enough upon changing conditions this theoretically allows to select the optimal setting for every dynamic driving situation. The optimal points together form the so called Pareto optimal curve [31].

A suspension setup that moves along the optimal Pareto curve is theoretically realizable with a fully active suspension. Due to the high demands that such a suspension has to fulfill however, there are only a hand full of series-production vehicles that actually have an active suspension (e.g. [20] and [21]). High bandwidth demands in combination with high force demands require powerful actuators, which leads to high production costs, energy consumption and other problems such as reliability and acoustics. Mathematical models are used to understand these problems, get an insight into the dynamic behavior of suspension systems and to find the essential requirements.

Chapter 4

Model

To get a feeling for the dynamic behavior and to be able to simulate the main characteristics of a suspension it is not needed to use very complex vehicle models. Simple models consisting of nothing more than rigid masses, linear springs and dampers already can reveal elemental characteristics of a suspension. Important is that essential characteristics, e.g. bandwidth and force limits of active elements, when present, are accounted for by the model and that the user is aware of the simplifications made. When considering only one corner (quarter) of a vehicle, which often already is sufficient to design a local controller, these suspension models reduce to so called quarter car models. To account for heave, roll and pitch motions of the vehicle's body however, half car (roll *or* pitch) or full car (heave, roll *and* pitch) models should be considered as illustrated in Figure 4-1 from M. Fleps-Dezasse [5] p.61.

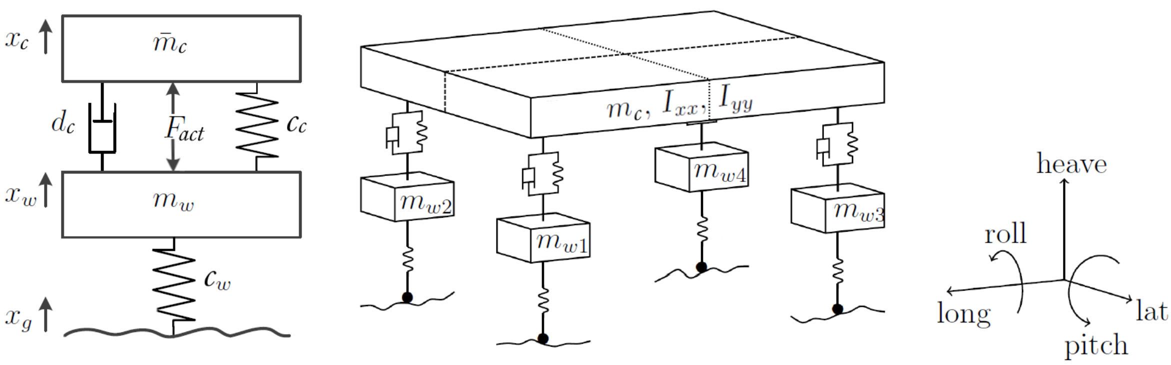

Figure 4-1: Left: Quarter car model. Middle: Full car model. Middle cut along dashed line leaving the left, or right half of the car: Pitch model. Middle cut along dotted line leaving the front, or rear of the car: Roll model. Right: Coordinate system [5] p.61

4-1 Eigenfrequencies

In the frequency range below approximately two times the eigenfrequency of the wheel (≈ 25 Hz), the vertical motion of wheels and body can be modeled by quarter car models. Above 25 Hz, constructional elements of the suspension and the chassis have to be considered as they are excited around their eigenfrequency. This means, they cannot be considered rigid anymore. This high frequency excitation also affects the passengers and not only by means of vibrations, but also by noise [22] p.528.

The eigenfrequency f_c of the body m_c is determined by the suspension spring stiffness c_c.

$$f_c = \frac{1}{2\pi}\sqrt{\frac{c_c}{m_c}} \quad \text{Hz.} \tag{4-1}$$

A change in the suspension spring stiffness therefore changes the eigenfrequency of the body. The eigenfrequency f_w of the unsprung mass m_w is unaffected by the suspension spring stiffness. This follows from the relatively low (negligible) suspension spring stiffness, when compared to the tire stiffness c_w [9, 22, 27].

$$f_w = \frac{1}{2\pi}\sqrt{\frac{c_w + c_c}{m_w}} \approx \frac{1}{2\pi}\sqrt{\frac{c_w}{m_w}} \quad \text{Hz.} \tag{4-2}$$

This effect is illustrated in Figure 4-2.

A stiffer damping reduces resonance peaks of both sprung mass and wheels, however compromises comfort at other excitation frequencies [27]. This effect is illustrated in Figure 4-3.
As a measure for the suspension's damping, the damping ratio D_c is defined as the damping of the suspension divided by the critical damping. For a damper with a constant damping stiffness (d_c), the damping ratio is

$$D_c = \frac{d_c}{2\sqrt{c_c\, m_c}}. \tag{4-3}$$

Correspondingly the damping ratio of the wheels is [22, 9]

$$D_w = \frac{d_c}{2\sqrt{(c_w + c_c)\, m_w}}. \tag{4-4}$$

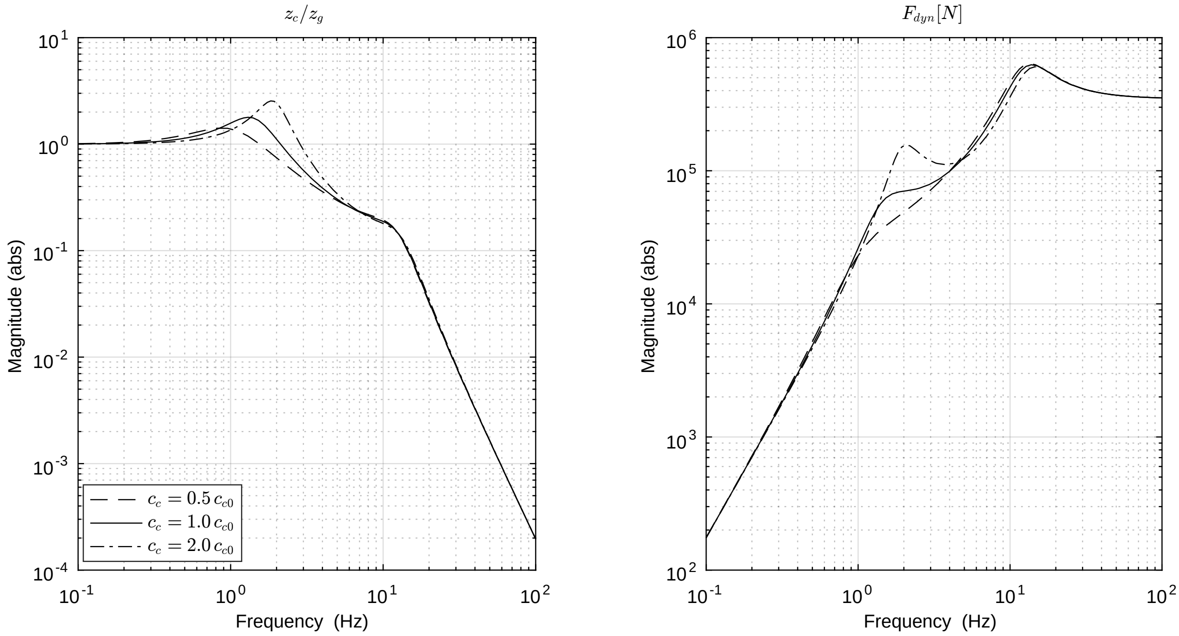

Figure 4-2: Effect of varying the suspension's spring stiffness, illustrated by means of the road z_g to body z_c transmissibility (left) and the dynamic wheel load F_{dyn} (right). Changing the stiffness of the suspension springs affects the eigenfrequency of the sprung mass. The eigenfrequency of the wheels remains unchanged. A change in the spring stiffness does not only affect the movement of the vehicle body, but also affects the dynamic wheel load.

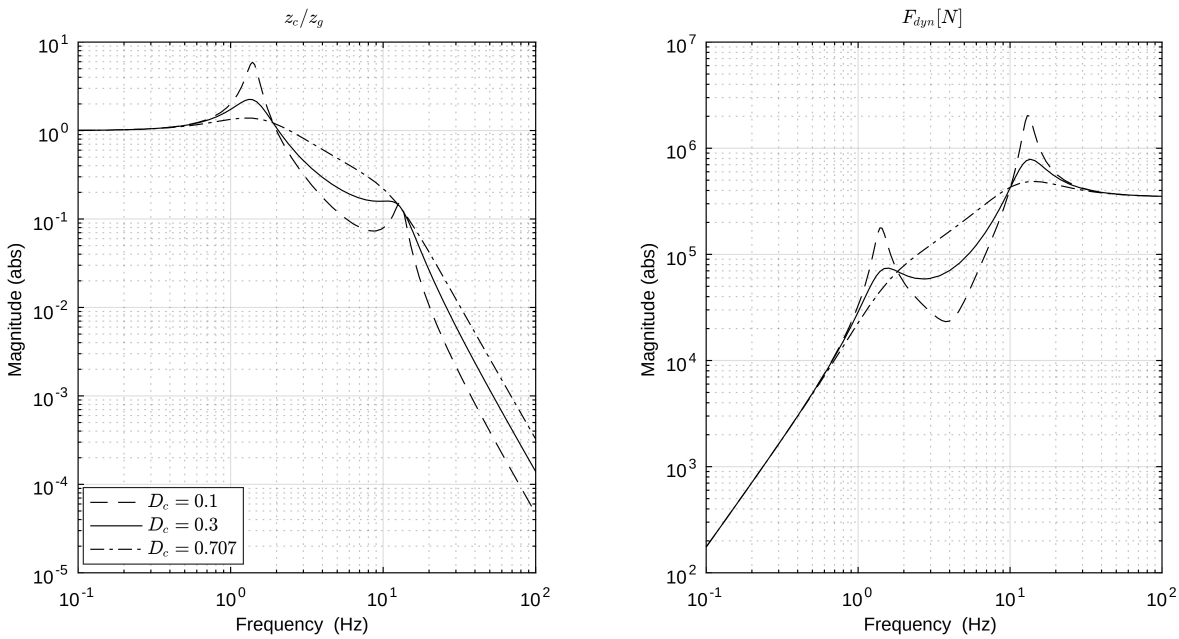

Figure 4-3: Effect of varying the suspension's damping ratio, illustrated by means of the road z_g to body z_c transmissibility (left) and the dynamic wheel load F_{dyn} (right). Increasing the suspension's damping reduces the resonance peaks of sprung mass and wheels, but compromises the dynamic behavior between those resonance peaks. The same holds for the fluctuations in the dynamic wheel load.

4-2 Schematic representation

Considering the frequency range below 25 Hz, quarter car models are also a valid way to represent the elemental behavior of a suspension. This frequency upper boundary represents no limit when developing an active suspension, since the frequency range of interest for suspension control is below this frequency [16]. Also M. Fleps-Dezasse [5] p.15 does not consider this upper boundary as a limit since "the control design should focus on the rejection of road disturbances as well as driver-induced disturbances. These two disturbances have distinct frequency ranges, meaning that the relevant frequency range of road disturbances is $0.5-20$ Hz, while the relevant frequency range of driver-induced disturbances is $0.1-3.0$ Hz".

4-2-1 Passive

A quarter car model that applies to a passenger vehicle and represents a passive suspension is shown on the left in Figure 4-4 from S. Spirk et al. [31] p.170 if the control force vanishes ($F_{act}(t) = 0$). To optimally represent the vehicle by the model ,the values for the sprung and unsprung mass of a quarter of the vehicle's body have to be identified for the vehicle in question. The same holds for the damping and spring characteristics which for a first approximation can be taken constant.
Often the tire stiffness and damping are unknown as they depend on many factors such as tire pressure and temperature. According to [9], tire stiffness can be approximated to be linear in the tire operating range. It can be approximated once the eigenfrequency and the mass of the unsprung mass are known. The tire damping can be approximated to be $50-100$ Ns/m. Other sources in literature however neglect the tire damping since "the tire damping compared to the suspension damping for a vehicle with a properly working damper hardly plays a role and can be neglected" M. Mitschke et al. [22] p.370.

A state-space representation of the differential equations (13-1) and (13-2) describing the quarter car model given in Figure 4-4a, with $F_{act}(t) = 0$ is given by (13-3) and (4-8). The state vector is introduced as $\underline{x} = \begin{bmatrix} z_c & \dot{z}_c & z_w & \dot{z}_w \end{bmatrix}^T$ and the input u is equal to the vertical road position z_g. The output $y = C\underline{x}$ in this example gives the position of the sprung mass.

$$m_c\ddot{z}_c = -c_c(z_c - z_w) - d_c(\dot{z}_c - \dot{z}_w), \tag{4-5}$$
$$m_w\ddot{z}_w = c_c(z_c - z_w) + d_c(\dot{z}_c - \dot{z}_w) - c_w(z_w - z_g) \tag{4-6}$$

$$\dot{\underline{x}} = \begin{bmatrix} 0 & 1 & 0 & 0 \\ -\frac{c_c}{m_c} & -\frac{d_c}{m_c} & \frac{c_c}{m_c} & \frac{d_c}{m_c} \\ 0 & 0 & 0 & 1 \\ \frac{c_c}{m_w} & \frac{d_c}{m_w} & -\frac{c_c+c_w}{m_w} & -\frac{d_c}{m_w} \end{bmatrix} \underline{x} + \begin{bmatrix} 0 \\ 0 \\ 0 \\ \frac{c_w}{m_w} \end{bmatrix} u \tag{4-7}$$

$$y = \begin{bmatrix} 1 & 0 & 0 & 0 \end{bmatrix} \underline{x} \tag{4-8}$$

This state-space model was actually used to generate the plots on the left in Figures 4-2 and 4-3 by changing the spring and damping constants according to (4-1) and (4-3) respectively.

4-2-2 Semi-active and active

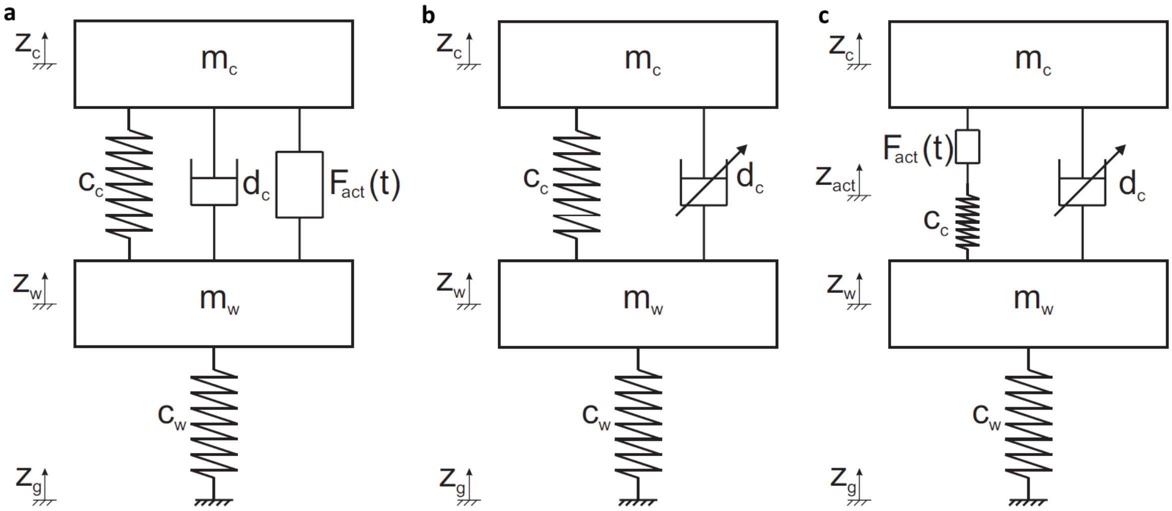

Figure 4-4: **a** Active partly-supportive suspension **b** Semi-active suspension **c** Active fully-supportive suspension [31] p.170

In Chapter 2, Figure 2-2, different suspension layouts were already introduced. These layouts can also be considered as quarter car models. The quarter car model in Figure 2-2b actually is, apart from an adjustable damper, the same as the quarter car model in 4-4c. The model in 4-4c is a schematic representation of the suspension behind MBC system from Mercedes-Benz. Although this system is active and even fully-supporting the weight of the vehicle's body, some literature sources e.g. [16, 25, 31] refer to it as a hybrid suspension system. This "hybrid suspension system" actively changes the ride height and spring displacement up to a frequency of 5 Hz and relies on the passive spring and semi-active damper characteristics to account for the higher frequencies. It allows to compensate for roll and pitch motions of the vehicle's body and increases the comfort for the passengers. In case of a system failure the vehicle will still be drivable due to the passive spring and damper elements [27].

Describing vehicle suspensions by means of quarter car models allows to mathematically describe suspensions in the form of matrices. This is a straightforward and clear method that enables to utilize well known analytical methods. Once the quarter car model including all the major suspension parts is described by matrices, not only the dynamic behavior can be simulated, but the effect of active interventions in case of active elements can be investigated as well. Designing and optimizing controllers is greatly simplified by this method.

For more accurate simulation results and ultimately control input calculations, the major non-linear effects such as hysteresis phenomena, a progressive spring characteristic, or nonlinear force-velocity curve of a semi-active damper with an asymmetric behavior in the compression and rebound direction as well as frequency-dependent characteristics of the tire have to be identified [25]. For a quarter car model this so called parameter identification process can be performed on a test rig, representing one corner of the vehicle.
Since the impact of hysteresis on control system performance can be significant, the availability of control-oriented simplified models of hysteresis is desired [24]. E. Pellegrini [24] proposes a hysteresis model for a continuously variable hydraulic damper and gives an overview of sev-

eral hysteresis models that have been proposed over the years. Using or not using a model to account for hysteresis phenomena again depends on the desired model complexity. In G. Koch et al. [16] a constant friction force in the suspension strut is included in the model to account for the hysteresis. Accurate models describing the dynamics of the suspension actuators allow to account for these dynamics when designing a controller. Inverting the actuator dynamics within a controller can lead to faster acceleration times, improving the bandwidth of a system.

Keeping in mind, that a quarter car model is a simplification of the real system, it is important that the controller is designed robust enough, such that the simplifications made have an insignificant impact on the final system.

Chapter 5

Control structures

There are different ways in which a vehicle can be described and in which a controller structure can be defined. This chapter gives an overview of common controller structures used in the automotive industry. There are controller structures with a modular approach, trying to divide a complex system into small-size peaces. And there are full-vehicle control approaches that consider the system as a whole. The latter is not considered here in detail, since it is not relevant for the subsequent master thesis. The interested reader is referred to [10, 33, 34] and references. Control algorithms, e.g. Skyhook, are discussed in Chapter 7.

5-1 Aktakon

T. Hestermeyer [10] describes two modular controller structures.

1. Active Body Control: Aktakon
    - translates to Aktive Aufbau Kontrolle (Aktakon) in German
    - refers to a controller structure and not to the Active Body Control (ABC) [9, 30] from Mercedes-Benz. ABC is an earlier development of the MBC from Mercedes-Benz and basically is MBC without preview
2. Additive Modular Modal Body Control: Ammakon
    - translates to Additive Modular Modale Aufbau Kontrolle (Ammakon) in German

The latter controller structure being an enhancement of the Aktakon method is applied in his research to a vehicle model with an advanced ABC suspension system.

In the eighties, it was Mercedes-Benz that developed Aktakon as the first comprehensive controller structure for an active suspension system. This controller structure has been modified and adapted ever since to meet practical requirements. According to T. Hestemeyer [10], R. H. Streiter [33] and references, the original Aktakon method is captured by the following four points.

1. Clarity

    - controller structure and control parameters should enable the engineers to optimize (fine-tune) the controller during test drives
    - requires transparent control parameters that affect defined parts of the vehicle dynamics
    - control parameters should represent known physical quantities e.g. spring stiffness and damping ratio

2. Modularity

    - a modular controller structure having separate controller modules for different controlling task should decouple controller functions from one another
    - transformation to modal coordinates
    - independent control of pitch, roll and heave

3. Extensibility

    - extensibility of the system should ensure convenient adaptation to different requirements and hardware
    - separate actuator controller
    - all controller modules should function on their own to allow optimization of different control functions during test drives

4. Transferability

    - transferability should enable the system to be driven by a force *or* displacement controlled system e.g. active suspension forces *or* suspension travel

These four points however are not always applicable in practice. It is for example not always possible to decouple controller structures and thereby ensure full modularity of the controller. Sometimes it is even desired to have a certain connection between controllers to find an overall optimum rather than individual optima that, when working together, can be far from optimal. The last point regarding transferability between force and displacement dependent systems also is redundant and results in an unnecessary complicated controller structure. This is the reason why the Aktakon controller structure has been modified over time. The basic idea behind this method however remained [10, 33].

The main motivation behind the above mentioned requirements is to have a structured controller with different control levels resulting in a structured hierarchy with high-level and low-level controllers. Typical for the Aktakon strategy is a complete separation between the vehicle's body and the active suspension system. They are only linked by the active forces between the suspension and the vehicle body as illustrated in Figure 5-1 from [10] p.86. This effectively means, that the connection between the suspension and the vehicle body is represented by an active element such as a hydraulic cylinder. Passive suspension elements (conventional springs and dampers) are not considered in the Aktakon method.

In the "Body" (Figure 5-1) all measured signals are transferred by transformation matrices into global modal vehicle quantities. These are lead through different control blocks (modules),

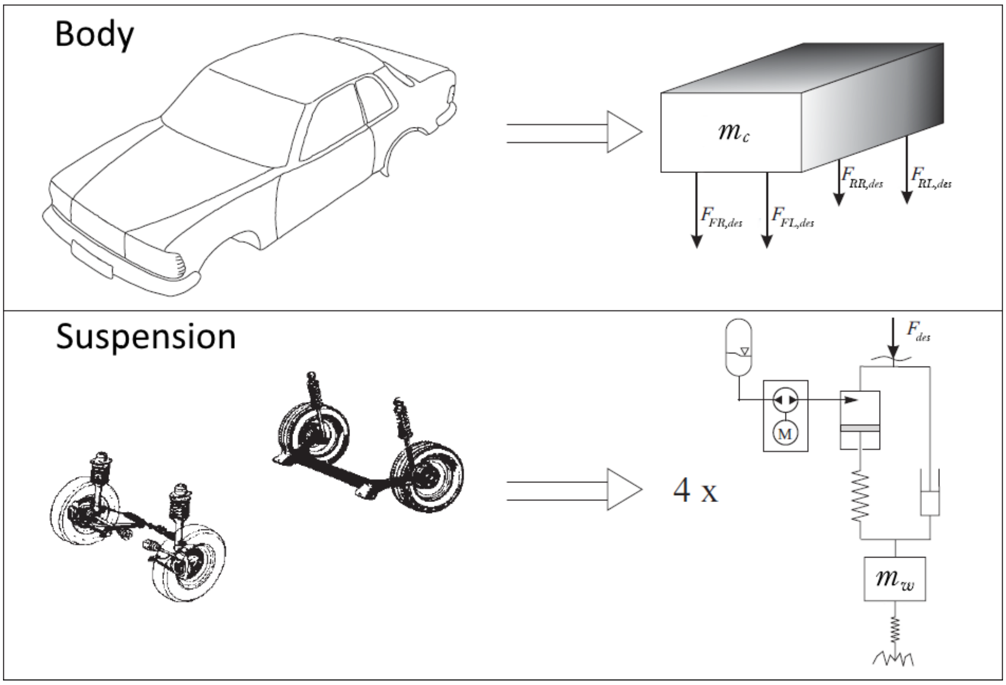

Figure 5-1: Schematic representation of the Aktakon control strategy [10] p.86

that each have their own optimized controller algorithm that calculates the desired forces and moments. The resulting desired forces and moments from all control modules are then added and by a second modal transformation subsequently transferred into the desired local forces for each actuator at each corner of the vehicle. The subordinate actuator controllers then calculate the required actions to deliver the desired actuator force at the end of the control chain.

For this to work, the Aktakon strategy assumes perfect actuators with unlimited dynamical properties. In reality however, actuators are only able to produce the desired forces up to a certain frequency. A cut-off frequency of 10 Hz already is very optimistic for a real active suspension system. Above this frequency, the excitations from the road come faster than the active suspension elements can react and the damper can be considered as a stiff column filled with oil. The driving comfort is compromised by the then direct rigid connection between sprung and unsprung mass. Due to this, the following effect is observed for vehicles with an active suspension system controlled according to the Aktakon strategy [10].

1. At low frequencies, the system behaves as desired
2. At medium frequencies, the desired- and passive dynamics of the system mix
3. At high frequencies, the system behaves as if the suspension is rigid

This shows, that a complete separation of the vehicle body and actuator dynamics does not hold in practice. The passive vehicle dynamics together with the actuator dynamics should be considered in the controller design to overcome this problem. This is in essence the biggest problem of the Aktakon controller strategy and motivates the introduction of a new controller strategy called Ammakon.

5-2 Ammakon

The vehicle's body plays a central roll in the Ammakon control structure concept. A variety of forces act on this body and together they determine the passive dynamic behavior. Other than the Aktakon strategy, the Ammakon strategy incorporates this passive dynamic behavior and *adds* additional active actuator forces to it, to realize the desired dynamic performance. In essence, this is the main difference to the Aktakon strategy.
The modular structure and controller hierarchy are preserved in the Ammakon strategy and applying additional forces to the passive system still allows a separation of the controller structure in vehicle and actuator dynamics (see Figure 5-2 from [10] p.91). Due to this, a change in the hardware structure (e.g. different actuators) is, as with the Aktakon strategy easily implemented without the need to completely rebuild the controller. In T. Hestermeyer [10] it is noted, that a change of the hardware structure might result in a change of the passive dynamics (see second criteria below). This has to be accounted for in the vehicle model.

The objective when constructing a controller according to the Ammakon controller structure is a separation of the control modules such that the following two criteria hold.

1. The bandwidth of the actuators must be known and the desired active forces should be controllable up till a known cut-off frequency
2. The model of the vehicle's body, under consideration of the actuator dynamics, should be modeled such that it holds for the complete frequency range and especially in the range where the actuators do not function anymore.
   The actuator dynamics are incorporated into the model of the vehicle's body by means of low-pass filters.

These two criteria require to design vehicle controllers under consideration of the actuator dynamics. When constructed with this in mind, the desired actuator forces tends to zero when the frequency approaches the cut-off frequency of the actuators. Since the model "knows" this limitation, the controller still can be active in the full frequency range. The mixed range, where the active and passive dynamics blend together furthermore exists as before with the Aktakon controller strategy, now however, this does not lead to uncontrollable desired forces and rigid suspension characteristics anymore [10].

E. Schäfer [27] uses a controller according to the Ammakon controller structure (see Figure 5-3). She starts by investigating the dynamics of the actuators and finds that the intended bandwidth of 10 Hz is to optimistic. The actuators "only" manage to realize a bandwidth of 5 Hz due to additional damping in the actuator system caused by tube connections between constructional elements in the vehicle. Nevertheless, a controller with a modular structure that takes this information into account is designed and in the end, an improvement of the vehicle's dynamics is achieved.
As motivation for the modular strategy, [27] refers to the clear and transparent nature of the method. When identifying system parameters for a real system this is a great advantage and it makes it possible to design controllers using quarter car models. E. Schäfer takes notice of the fact that "a separation of the controller in different modules eases the design and test phase. Single modules can be tested and implemented to the real system one after the other" [27] p.83.

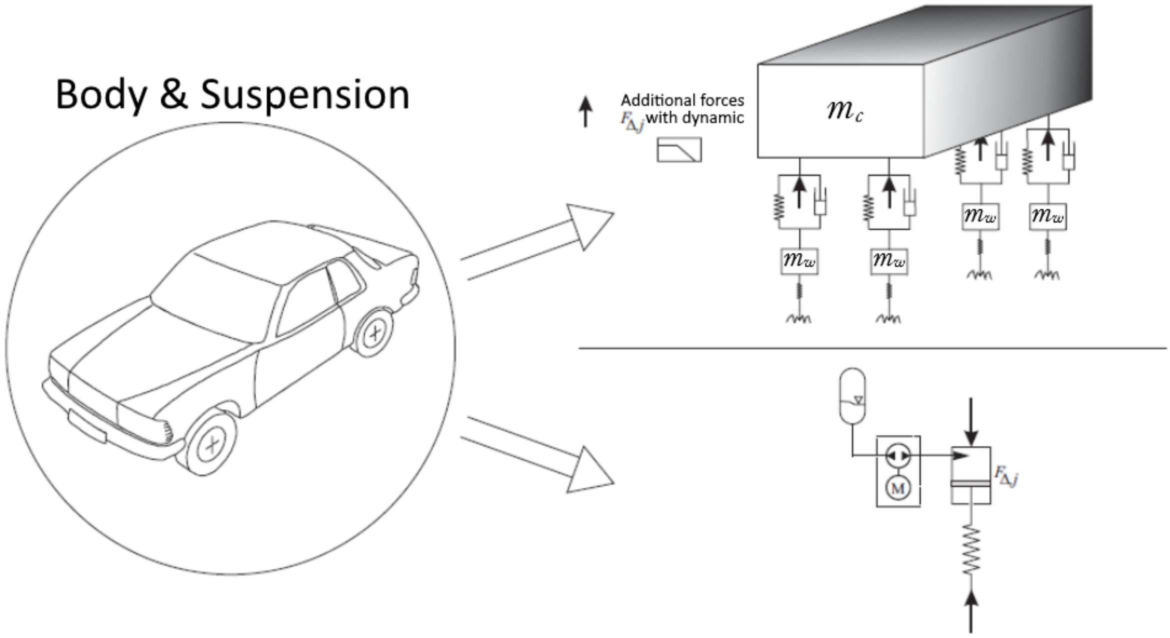

Figure 5-2: Schematic representation of the Ammakon control strategy [10] p.91

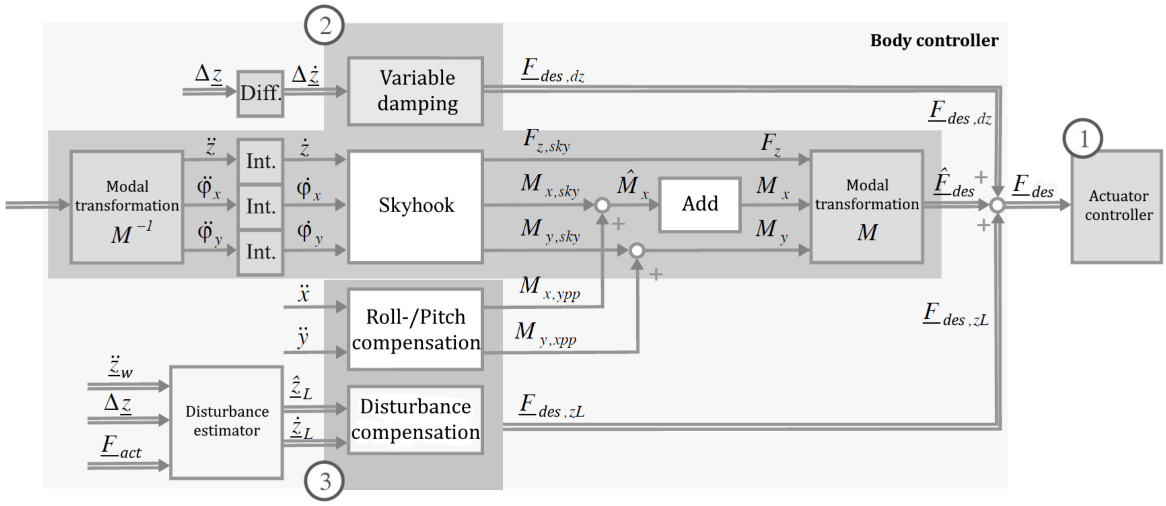

Figure 5-3: Schematic representation of the control strategy used in [27]. ① Actuator controller. ② Modal body controller units also accounting for passive dynamics. ③ Additional modal controllers with disturbance compensation for optimal performance. [27] p.84

5-3 Full-vehicle control structure

The advantages of the modular control approach indirectly reveal the problem of a full-vehicle model approach. In his conclusion to different control approaches, R. H. Streiter [33] mentions the problematic parameter identification all researches have to deal with, when using a full model approach. Control parameters not having a physical meaning anymore, often results in a trial and error optimization procedure with unclear problem specifications.

An advantage of a full model approach when performed correctly would be a globally optimized system. A full model approach generally also results in a more robust controller. Modeling errors in subsystems do not directly effect the desired actuator actions and connections between separate control modules do not accidentally get lost, something which can happen when one designs a controller according to a modular structure approach [5, 33].

Chapter 6

System states

As previously discussed, active suspensions offer the potential to enhance vehicle dynamics. To exploit this potential, there exist control algorithms that improve the ride comfort and safety. The general requirement for these algorithms to work is accurate information of the system states and inputs. Only when certain quantities e.g. vertical wheel acceleration are known, these algorithms can calculate the required active forces to improve the dynamical behavior of the system.

6-1 State estimation

Often not all the required system states and inputs can be measured directly, or the equipment to measure these is too expensive for series-production applications. Therefore so called state observers are often applied to estimate the unknown quantities using the available sensor signals. A state observer is represented by a mathematical model describing the real system e.g. quarter car model of a quarter car test rig. This model then runs parallel (on a computer) to the real system and receives the same input information. Since for a vehicle not all the desired signals are measurable e.g. road excitation, and the mathematical model does not exactly match the real system, the calculated states usually deviate from the real vehicle states. To compensate for these deviations, a state observer compares the estimated model states with the available measured quantities resulting in an estimation error which is corrected by an appropriate correction term, the so called observer gain. This is then used by the state observer to rectify the mathematical model. Since the mathematical model does not only estimate the measured states, but also the unknown states, these are indirectly corrected as well [7, 14].

6-1-1 Linear observer

An observer for the linear system

$$\begin{aligned} \dot{x} &= Ax + Bu, \\ y &= Cx + Du \end{aligned} \tag{6-1}$$

is

$$\begin{aligned} \dot{\hat{x}} &= A\hat{x} + Bu + L(y - \hat{y}), \\ \hat{y} &= C\hat{x} + Du \end{aligned} \tag{6-2}$$

that is specified by choosing an observer gain L. The observer gain should be chosen such that the estimation error $\tilde{x} = x - \hat{x}$ converges to zero quickly. The error dynamics follow from

$$\begin{aligned} \dot{\tilde{x}} &= \dot{x} - \dot{\hat{x}} \\ &= Ax + Bu - \left(A\hat{x} + Bu + L(y - \hat{y})\right) \\ &= A\tilde{x} - L(Cx + Du - C\hat{x} - Du) \\ &= (A - LC)\tilde{x} \end{aligned} \tag{6-3}$$

thus they are described by $\dot{\tilde{x}} = (A - LC)\tilde{x}$. Hence L should render $(A - LC)$ to be stable (real part of the eigenvalues $Re(\lambda) < 0$) such that $\lim_{t\to\infty} \tilde{x}(t) = 0$.
For observable (A, C) the eigenvalues of $(A-LC)$ can be placed arbitrarily in $\mathbb{C}$ as long as they are located symmetrically with respect to the real axis. If (A, C) only is detectable (meaning that the unobservable eigenvalues have $Re(\lambda) < 0$), then the eigenvalues of $(A - LC)$ cannot be placed arbitrarily, but it is still guaranteed that the estimation error goes to zero when $(A-LC)$ is chosen such that all the remaining eigenvalues also have a negative real part [14]. More about system stability, observability and detectability can be found in T. Keviczky [14].

To design a proper state observer, apart from appropriate system equations and observer gain, the measured quantities (and therefore sensor configuration) has to be chosen such that the system is observable. In case (A, C) is observable, E. Schäfer et al. [28] recommend to place the eigenvalues of the state observer in such a way that the state observer is two to three times faster than the wheel dynamics. Making the observer dynamics even faster will make the state observer sensitive to measurement noise. Moreover, large observer gains can adversely influence robustness [14].

6-1-2 Kalman filter

To account for the model uncertainty and measurement noise, model and measurement noise can be added to the linear system in (6-1) describing the system dynamics. When the noise is represented by white-noise with variances Q and R respectively, one can try to find the minimum-error variance estimates of the system states. This problem is defined as the well-known Kalman filter problem and is explained by M. Verhaegen et al. [36].

Assuming discrete system equations, the state-space representation together with model uncertainty $w(k)$ and measurement noise $v(k)$ is given by [36]

$$\begin{aligned} x(k+1) &= A_d x(k) + B_d u(k) + w(k), \quad w(k) \sim (0, Q), \\ y(k) &= C_d x(k) + D_d u(k) + v(k), \quad v(k) \sim (0, R). \end{aligned} \tag{6-4}$$

The Kalman filter is a member of the class of observers used to reconstruct missing system information from measured quantities in a state-space model. It is a computational scheme to reconstruct the state of a given state-space model in a statistically optimal manner, which is generally expressed as the minimum variance of the state-reconstruction error conditioned on the acquired measurements [36].

Kalman filters can be extended, such that not only the states are estimated, but model parameters (e.g. sprung mass m_c) get estimated as well. In case the vehicle mass changes when the vehicle gets loaded or unloaded, the corresponding parameters in the mathematical model will be readjusted to account for this change. These so called extended Kalman filters perform an online system identification and try to find the optimal system parameter values. The extended Kalman filter enables the application of linear Kalman filtering to nonlinear systems by linearizing the corresponding model in every time step. The system matrices are determined by a linearization of the nonlinear system equations for each time update around the actual estimated system state [15].
More details about Kalman filtering and the extended Kalman filter can be found in [7, 15, 36] and references.

6-1-3 Conventional filter

System states can also be derived using conventional low-pass and high-pass filters, denoted by $H_{LP}(s)$ and $H_{HP}(s)$ respectively. Integration and/or differentiation of available measurement signals and possibly combining them can lead to the desired state quantities. G. Koch et al. [16] and N. Pletschen et al. [25] use signal-based filtering to find estimates of the missing states. They also mention the inevitable phase shifts that occur when applying frequency filters in real-time applications. To overcome this problem, they use a combination of low-pass and high-pass filters with the same time constant ($T_{LP} = T_{HP}$) resulting in so called complementary filters. A complementary filter uses the property that low-pass and high-pass filters with the same time constant are each others counterpart.

$$H_{(LP+HP)}(s) = H_{LP}(s) + H_{HP}(s) = 1 \tag{6-5}$$

The combined signal resulting from a complementary filter shows neither a change in magnitude nor a phase shift [25]. This is illustrated in Figure 6-1.

M. Fleps-Dezasse [5] notes that complex methods are often seen in theoretical studies, but only rarely occur in practical applications. Moreover, he mentions that the relatively good performance of the common methods based on conventional filtering used in the industry, result in a high entry barrier for other control algorithms that come with significantly higher cost and effort. G. Koch [15] furthermore mentions that conventional filter based estimation concepts are frequently preferred over Kalman filtering in production cars, because "the full state information is seldom necessary for the applied suspension control techniques" [15] p.73.

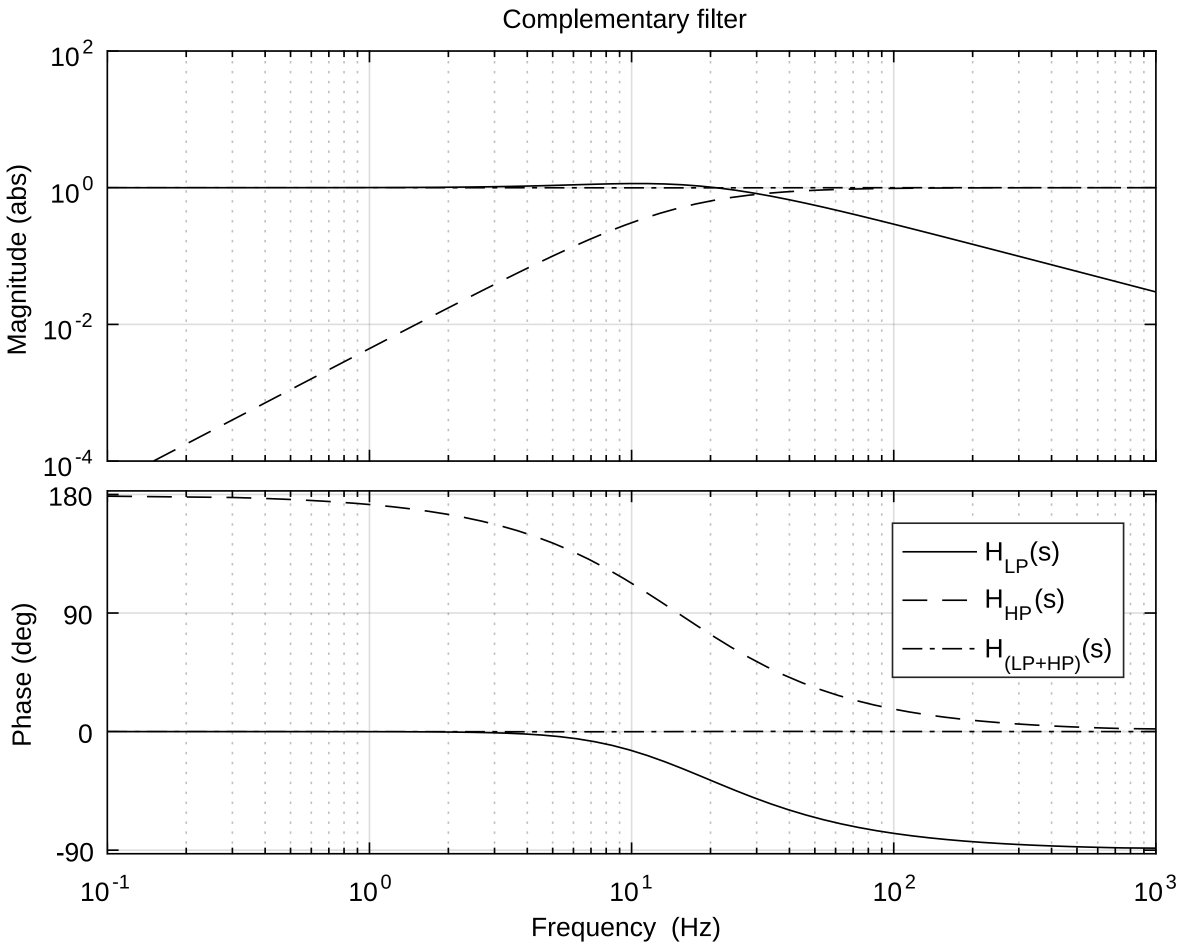

Figure 6-1: Example of a complementary filter. The phase and magnitude distortion caused by single frequency filters is canceled out in a complementary filter. This allows to create a desired signal from two different measurement signals without unwanted side effects.

6-2 Estimation approaches

M. Fröhlich [7] develops a sensor and observer concept for a semi-active suspension system that results in a reliable estimation of the required system states for his controller. In his study, extra attention is paid to robustness and applicability for series-production.
He investigates different Kalman filter and conventional filter techniques to find the best compromise between the quality of the estimated states and the required computation time. Simulations on a quarter car model show that conventional filters require the lowest computational power, but result in significantly worse estimates than the ones resulting from the more complicated Kalman filtering approaches. In the final evaluation however, he assesses the concepts according to estimation quality *and* series applicability and concludes that the best compromise between estimation quality and computational effort lies in a combination of both techniques.
Using conventional filters to account for the sensor noise and offsets, he manages to reduce the extended Kalman filter complexity and corresponding computation time without significantly reducing the estimation quality. Furthermore, he reduces the underlying quarter car model by ignoring the wheel dynamics and directly uses the measured vertical wheel acceleration at the wheel hub. Then he even goes one step further and switches from a model based Kalman filter to a signal based Kalman filter, directly writing down the relation between position, velocity and acceleration using measurement data from the sprung and un-sprung mass. This results in linear system equations with no vehicle parameters whatsoever, reducing the extended Kalman filter to a linear Kalman filter (for more details the reader is referred to [7] chapter 7).

G. Koch et al. [17] apply the parallel Kalman filter developed in the previous work [15] to estimate the relative damper velocity and dynamic wheel load for a hybrid suspension system. He uses the sensor setup from a production vehicle consisting of acceleration sensors for body and wheel and a displacement sensor that measures the suspension travel.
The use of a single Kalman filter results in an overall minimized variance of the estimation errors, meaning that not all required quantities can be estimated with maximum accuracy. Separation of the required quantities in multiple parallel Kalman filters, leads to estimates with maximum quality, which motivates his introduction of the parallel Kalman filters.
To keep the number of parallel Kalman filters small to facilitate the implementation, not all required signals are separated. This finally results in three parallel Kalman filters. The first Kalman filter provides estimations of the signals $\dot{z}_c$, $z_w - z_g$ and F_{dyn}. The second one $\dot{z}_w$ and $z_c - z_w$ and the third one is necessary for the estimation of the road excitation z_g, which is used later on in his study in a disturbance feed forward component of the suspension controller. To improve the robustness, the influence of deviation of the vehicle mass is considered by means of extended Kalman filtering.
The estimator structure based on three parallel *linear* Kalman filters that also take into account the *nonlinearity* of the damper is according to G. Koch [15] well implementable and computationally simple. Since the suspension model also takes the nonlinearity of the damper into account, the standard linear Kalman filter algorithm cannot be applied directly. Instead of using an extended Kalman filter, decomposing the nonlinear system and defining an augmented input, assuming the damper force as fictitious input signal, results in a linear system representation that serves as basis for his Kalman filter design. Since the damper force is unknown, it is estimated from the estimated damper velocity and damper characteristics from

the previous sampling instant.
In his research, a full model extended Kalman filter is used as benchmark to validate the performance of the parallel Kalman filter approach. The performance of the estimators is analyzed and compared in simulations and experiments using a quarter car test rig.

G. Koch et al. [15, 16] use conventional frequency filters to estimate the same systems states for the same setup as in [17]. Employing complementary filters to prevent phase delay results in the desired quantities and the estimated dynamic wheel load is calculated as follows

$$F_{dyn} = m_c \ddot{z}_c + m_w \ddot{z}_w. \tag{6-6}$$

Due to a generally varying vehicle mass m_c, they recommend to refine this estimation by an online estimation of the vehicle mass and refer back to the extended Kalman filter approach from M. Fröhlich [7]. As advantage of the conventional filtering approach, they emphasize the simple filter based estimation concept and realistic implementability compared to the complex Kalman filter algorithms.

E. Schäfer et al. [28] develops a conventional frequency filter to estimate the vertical position of the tire contact patch. This quantity is needed for their controller approach which they implement and test in a real vehicle. For their controller, the estimation quality achieved with the relatively simple filter is sufficient to improve the dynamics of the vehicle.

Chapter 7

Control methods

This chapter finally gives an overview of existing control methods that are applied to vehicles with an active suspension and aim to enhance comfort and/or safety. Since most control methods do not explicitly mention the actuator limitations of the corresponding active suspension system, A. Unger [34] rightfully notes, that the desired forces by the control methods should be limited to the force range of the actuators.

7-1 Skyhook

The Skyhook strategy attempts to decouple the vehicle's body from road surface irregularities. It is used to minimize the motion of the vehicle's body and simulates the vehicle, as if a damper were mounted between the vehicle's body and a traveling hook attached to a fixed inertial coordinate system: the sky [9]. This principle is illustrated on a quarter car model in Figure 7-1 from [9] p.530. The virtual damper results in a virtual force as soon as the vehicle's body has a relative velocity with respect to the fixed point in the sky. The resulting virtual damping force then damps the motion of the vehicle's body.

Since the virtual Skyhook damper does not really exist, the suspension has to compensate for it. The Chassis Handbook [9] gives the following equations to calculate the required Skyhook damping. It has to be noted that these equations base on local quantities which result from a transformation of the modal full-vehicle quantities onto the quarter car model.

$$F_{sky} = d_{SH}\,\dot{z}_c = d_c\,(\dot{z}_c - \dot{z}_w) \tag{7-1}$$

$$d_c = d_{SH}\,\frac{\dot{z}_c}{\dot{z}_c - \dot{z}_w} \tag{7-2}$$

In case of a semi-active suspension, which can only dissipate energy (see effective range, table 2-1 Chapter 2), the following constraints hold. Where P_{sky} is the mechanical power of the Skyhook damper [22].

$$P_{sky} = F_{sky}\,(\dot{z}_c - \dot{z}_w) = d_{SH}\,\dot{z}_c\,(\dot{z}_c - \dot{z}_w) \geq 0 \qquad \text{for} \quad \dot{z}_c\,(\dot{z}_c - \dot{z}_w) \geq 0 \tag{7-3}$$

$$P_{sky} = 0 \qquad \text{for} \quad \dot{z}_c\,(\dot{z}_c - \dot{z}_w) \leq 0 \tag{7-4}$$

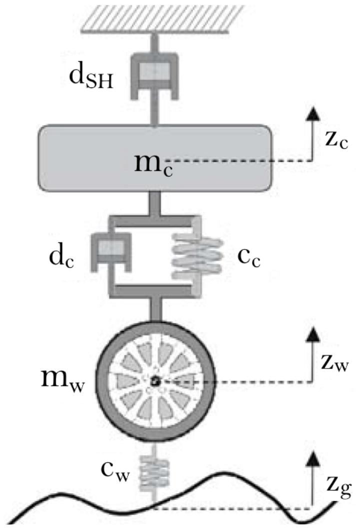

Figure 7-1: Schematic representation of the Skyhook principle, illustrated on a quarter car model [9] p.530

To fulfill these constraints, the compression and rebound damping of the Skyhook damper are either increased or reduced to zero, depending on the direction of the vehicle's body.

In case of an active suspension system, the desired Skyhook force from (7-1) can directly be applied and there is no necessity to change the damping characteristic (depending on the suspension layout). The Skyhook damping ratio can be chosen constant [34].

H. Li et al. [18] p.845 emphasize that "it is important to realize that the absolute velocity of the vehicle is practically very difficult to measure directly and must therefore be derived from a measurement of acceleration, which is fed through an integrator in order to derive the absolute velocity " which they estimate by means of both Kalman filtering and complementary filters to compare different methods.

N. Hohenbichler et al. [11] also note, that appropriate filtering is required before implementing the Skyhook control method in a real system. Instead of filtering and integrating the acceleration signal $\ddot{z}_c$ with a high-pass integration filter. They filter the desired force F_{sky} by means of a filter that distinguishes unwanted excitation from road inclines/declines. Without filtering the integrated signal, the desired suspension travel would be unrealistic (e.g. vehicle would try to drive through a mountain instead of driving over it). In their research it is suggested to add an "intuitive" high-pass filter to (7-1) resulting in

$$F_{sky}(s) = d_{SH}\, H_{HP}(s)\, s\, Z_c(s) \tag{7-5}$$

in the Laplace domain.
This however can lead to instability of the system when the cut-off frequency of the high-pass filter is close to the eigenfrequency of the system, leading to an undamped system in the resonance frequency range. To prevent possible stability issues they add a complementary low-pass filter (see Section 6-1-3) that calculates a passive damping force.

$$F_{sky}(s) = d_{SH} \cdot \Big(H_{HP}(s)\, s\, Z_c(s) + H_{LP}(s)\big(s\, Z_c(s) - s\, Z_w(s)\big)\Big) \tag{7-6}$$

Using the complementary filter properties (6-5), this finally results in

$$F_{sky}(s) = d_{SH} \cdot \Big(s\, Z_c(s) - H_{LP}(s)\, s\, Z_w(s)\Big). \tag{7-7}$$

The Skyhook principle is well known and commonly applied in series-production vehicles that have an active, or semi-active suspension system. The ABC control algorithm from Mercedes-Benz for example uses a Skyhook principle together with lateral (roll dynamics) and longitudinal (pitch dynamics) acceleration intervention control to help reduce the motion of the vehicle's body [9].

7-2 Groundhook

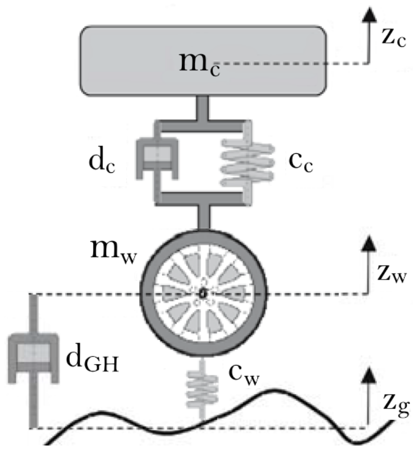

Figure 7-2: Schematic representation of the Groundhook principle, illustrated on a quarter car model [9] p.530

The Groundhook strategy is similar to the Skyhook strategy, but simulates the vehicle as if a damper were mounted between the vehicle's wheels and the ground. This principle is illustrated in Figure 7-2 from [9] p.530. The wheel damping is correspondingly calculated based on the excitation of the road [9].

$$F_{GH} = d_{GH}\,(\dot{z}_w - \dot{z}_g) \tag{7-8}$$

$$F_{damper} = -d_c\,(\dot{z}_c - \dot{z}_w) \tag{7-9}$$

These equations give the required damping to compensate for the non existing Groundhook damper [9]

$$d_c = d_{GH}\,\frac{\dot{z}_w - \dot{z}_g}{\dot{z}_w - \dot{z}_c}. \tag{7-10}$$

As for the Skyhook principle, the way the Groundhook principle is applied depends on the type of suspension (active, or semi-active).

The Skyhook control method attempts to maximize comfort whereas the Groundhook control method reduces the wheel load fluctuations and increases safety. Combining both methods has the potential to increase both comfort and safety [34].

7-3 Adaptive controller

G. Koch et al. [16, 17] develop an adaptive control logic that optimizes comfort without compromising the dynamic wheel load fluctuations for a hybrid suspension system. Instead of an additional Groundhook controller as suggested by A. Unger [34], an adaptation logic is used that adapts the control signal according to the estimated driving situation.
From the measured suspension deflection and the estimated dynamic wheel load (see Section 6-2) two real parameters q_{susp} and $q_{F_{dyn}}$ are calculated which indicate if the vehicles' driving state is critical. If a parameter q_i approaches a pre-defined bound, it indicates that the corresponding criterion tends to be violated.
For an uncritical driving state ($q_i \approx 0$) the natural frequency f_c and damping ratio D_c (see (4-1) and (4-3) respectively) are set according to the most comfortable setting, which is previously calculated by an offline nonlinear reference model of the system. The reference model calculates the comfort optimal setting and its corresponding natural frequency and damping ratio (along the Pareto front, see Chapter 3) such that the bounds are not violated for different road irregularities.
If the dynamic wheel load increases, $q_{F_{dyn}}$ rises. If the suspension travel becomes critical, q_{susp} rises. For both cases, the control logic changes the natural frequency and damping ratio according to the pre-calculated optimal values, such that the corresponding bound is not violated anymore. Details to this adaptation law for both cases can be found in [16] and [17].

7-4 Disturbance compensation

S. Spirk et al. [32] develop a disturbance compensation controller that uses road profile information to minimize the dynamic wheel load fluctuations. They introduce two concepts for the road profile acquisition. The first one uses a laser-sensor to sample the road profile right beneath the front of the car. The second concept uses the measured wheel disturbance at the front wheels and estimates the corresponding road profile with help of a discrete Kalman filter before sending this information to the rear axle of the car. The latter enhances road holding of the rear wheels without the need of additional sensors when driving along a straight road, which especially is an advantage for rear wheel and all wheel drive vehicles.

The desired forces that compensate for the road excitation are calculated by means of a simple quarter car model with an active element represented by an additional actuator (see Figure 4-4a). The differential equation describing the wheel dynamics is

$$m_w \ddot{z}_w = c_c(z_c - z_w) + d_c(\dot{z}_c - \dot{z}_w) - c_w(z_w - z_g) - F_{act}(t). \tag{7-11}$$

Neglecting actuator dynamics and physical limits, the force between the wheel and the sprung mass is

$$F_{cw}(t) = F_{act}(t) - c_c(z_c - z_w) - d_c(\dot{z}_c - \dot{z}_w) \quad \text{leaving} \tag{7-12}$$

$$m_w \ddot{z}_w = \underbrace{-c_w(z_w - z_g)}_{F_{dyn}} - F_{cw}(t). \tag{7-13}$$

Therefore, $F_{dyn} = m_w \ddot{z}_w + F_{cw}(t) = 0$ to compensate for the induced wheel load fluctuation ($F_{dyn} = 0$). To satisfy this equation, the vertical wheel displacement should be equal to the vertical road position: $z_w = z_g$. Since only the wheel acceleration can directly be influenced, $\ddot{z}_w$ should be equal to $\ddot{z}_g$. From this it follows that

$$F_{cw}(t) = -m_w \ddot{z}_g. \tag{7-14}$$

Moreover, since F_{cw} represents the force between sprung and un-sprung mass

$$m_c \ddot{z}_c = F_{cw}(t) \quad \rightarrow \quad \ddot{z}_c = -\frac{m_w}{m_c} \ddot{z}_g. \tag{7-15}$$

This indicates a linear relationship between the road excitation and the vertical acceleration of the vehicle's body. Due to this amplification gain, [32] implement the desired force (7-14) after filtering with a low-pass filter to reduce the control input at high frequency excitation. Furthermore, [32] explicitly present this method as a low-level control method without feedback control to complement global control strategies. Accordingly they test the controller on a quarter car test rig (with a semi-active and with a hybrid suspension) in addition to a Skyhook algorithm and also in addition to a Groundhook strategy. An improvement in comfort and/or safety is achieved with both road profile acquisition methods [32].

E. Schäfer et al. [28] develop a disturbance compensation controller for an active suspension system. Their target vehicle is an off-road utility vehicle weighing twelve tons with a high center of gravity, resulting in extreme roll, heave and pitch movement of the passenger cabin. The disturbance compensation algorithm aims to minimize the heave and pitch movement of the vehicle's body. The used active suspension system is a conventional passive system, were the conventional dampers are replaced with a hydraulic actuators resulting in a partly supporting suspension system.

An observer estimates the vertical position and velocity of the contact patch between the tires and the road ($\hat{z}_L$ and $\dot{\hat{z}}_L$ respectively). The missing vehicle states for the disturbance compensation controller are estimated by an observer which uses the following measurement data.

- Actuator force, calculated from measured cylinder pressure in the hydraulic actuator
- Vertical acceleration at the vehicle's axis
- Suspension travel

The mathematical vehicle model used for the observer is represented by a half car (roll) model that considers the forces and moments acting on the rigid axle of the vehicle. The damping and spring stiffness of the tires are considered constant. Furthermore, since part of the road profile excitation is filtered by the tires, they filter the road excitation with a ”contact patch filter” represented by a first order low-pass filter in the vehicle model.

To reduce the motion of the vehicle's body, the disturbance compensation controller should ”lift” the wheels, or press the wheels onto the road to follow the road surface, depending on the road excitation. The required actuator force to do so is calculated as follows

$$F_{act} = -c_c(z_c - z_w) - d_c(\dot{z}_c - \dot{z}_w) \approx c_c\, \hat{z}_L + d_c\, \dot{\hat{z}}_L. \tag{7-16}$$

Here it is assumed, that the induced forces due to road irregularities are fully compensated, meaning that the vehicle's body does not move.

In simulations E. Schäfer et al. [28] show that a considerable reduction of the vehicle's motion can be achieved. From the simulations it furthermore follows, that the part of the desired force F_{act} resulting from the damping term is small and has no considerable effect on the vehicle dynamics. Nevertheless, two tune parameters are introduced to optimize the controller: K_{zL} and K_{zLd} resulting in

$$F_{act} = K_{zL}\, \hat{z}_L + K_{zLd}\, \dot{\hat{z}}_L. \tag{7-17}$$

The starting parameters are set to $K_{zL} = c_c$ and $K_{zLd} = d_c$. The optimized controller further reduces the simulated body motion.

E. Schäfer et al. [29] finally implement this disturbance controller into the target vehicle and validate the simulation results in test drives. An overview of their complete controller structure is given in Figure 5-3 from [27]. The disturbance compensation controller achieves a considerable reduction of the vehicle cabins motion [29].

Part II

Master Thesis

Chapter 8

Vehicle description

The project vehicle is a VW Touran of the latest generation. It is a five-door MPV based on Volkswagen's MQB platform, with a McPherson strut front suspension and a twits-beam rear axle. The original suspension dampers are replaced by active damper units, such that is features an active suspension. The VW Touran is chosen as project vehicle, since it also serves other projects within the company. This does not only offer the possibility to show potential customers multiple new developments with one demo car, but it also means that the vehicle's (software) architecture is familiar, which greatly simplifies implementation of new hardware and software.
Here it has to be noted, that the target group of the sMotion active suspension system more likely are high end series-production cars, rather than middle class family cars. This is due to initial relatively high system costs and corresponding customer demands.

Figure 8-1: Project vehicle. VW Touran

8-1 Vehicle data

The most relevant vehicle data are listed in Table 8-1.

Table 8-1: Data Volkswagen Touran 2015 [2]. *Measured quantities.

Driveline	1.4L 4-Cylinder in-line Front/lateral Turbo charged 110 kW/150 HP 250 Nm at 1500 rpm Gasoline Front wheel drive 6-Speed manual gearbox
Dimensions	Exterior (LxWxH) 4527x1829x1674 mm Wheel base 2786 mm Wheel track (Front/Rear) 1561/1534 mm Ground clearance 156 mm
Weight	Unloaded weight 1454 kg Actual weight* 1792 kg Max. weight 2050 kg Unsprung mass front axis* 139 kg Unsprung mass rear axis* 112.5 kg
Suspension	Front McPherson Rear Twist-Beam Spring front* 32668 N/m Spring rear* 37873 N/m

Especially relevant for simulation purposes are the sprung and unsprung masses. The weight of the sprung mass is $1792 - 139 - 112.5 = 1540.5$ kg and the weight of the unsprung mass at each corner is equal to the unsprung mass of the front/rear axis divided by two (69.50 kg and 56.25 kg for the front and rear unsprung masses respectively). Furthermore, it should be noted here, that the anti-roll bars have been removed. Since the wheels (left and right) are no longer connected by the anti-roll bar, the front wheels are decoupled. The rear wheels are still connected to each other by the twist-beam axis, but are now less sensitive to one sided disturbances. This allows the active suspension units to control each wheel individually, without influencing the wheel across (front), or with a minimal effect on the wheel across (rear). Active interruptions even can account for the anti-roll bar without having the negative coupling effect.

Since anti-roll bars partly determine the vehicle's dynamical behavior and drive safety, removing them could lead to unsafe situations in case of a failure in the active system. This has been investigated for the project vehicle. It turns out, that upon a shutdown of the system, the vehicle still has an under steering behavior, which is considered as safe, without the anti-roll bars. The lack of anti-roll bars therefore does not compromise the safety.

8-2 Sensor configuration

The standard series sensor configuration of the project vehicle is augmented such that it features

- four wheel acceleration sensors (one at each wheel mount),
- four body acceleration sensors (one at each wheel dome),
- and four displacement sensors that measure the relative suspension displacement.

The sensors used are all regular series-production sensors found in passenger cars.

The measured relative suspension displacement at the front axle directly relates to the relative spring and damper displacement. Due to the different suspension layout of the rear axis, the measured relative suspension displacement has to be multiplied with the geometric factor 0.86 to correspond to the relative spring and damper displacement at the rear axle.

8-3 System architecture

Apart from the vehicle's sensor configuration, also the system architecture has been augmented to facilitate the active suspension units. The system is augmented with

- four ECUs, for the motor pump units (MPUs),
- two ECUs, for the CDC valves (eight CDC valves in total),
- one `dSPACE` Micro-Autobox II (MAB), for the vehicle control software,
- one DC/DC-Converter 12V/48V, for the electric motors,
- one Energy Storage 48V battery, supply for the electric motors.

A schematic picture of the system architecture is given in Figure 8-2. The two ECUs for the electric motors at the front are located under the front seats. All the other components, except for the active damper units, are integrated in the vehicle's luggage compartment. The system architecture concept for series production will deviate from this. It will have local micro-computers at each damper unit (one master, three slaves), to facilitate implementation and modularity. Apart from an additional 48V supply and DC/DC converter (which might even be redundant, since some new (especially hybrid/electric) cars already feature a 48V on-board supply), there will be no need to package additional system components.

Whereas the CDC and MPU ECUs are initialized once for every corresponding system component, the software on the MAB is easily updated by connecting it to a computer. The MAB furthermore enables to monitor/record system data when a computer is connected. This serves development purposes. System states can be monitored/recorded online during test drives and control parameters can be changed as well. This allows to change the behavior of the active system by one mouse click, without the need to rebuild the system. To do so, `dSPACE ControlDesk` computer software is used in this project. For more information about the `dSPACE ControlDesk` software, the reader is referred to the `dSPACE` website [3].

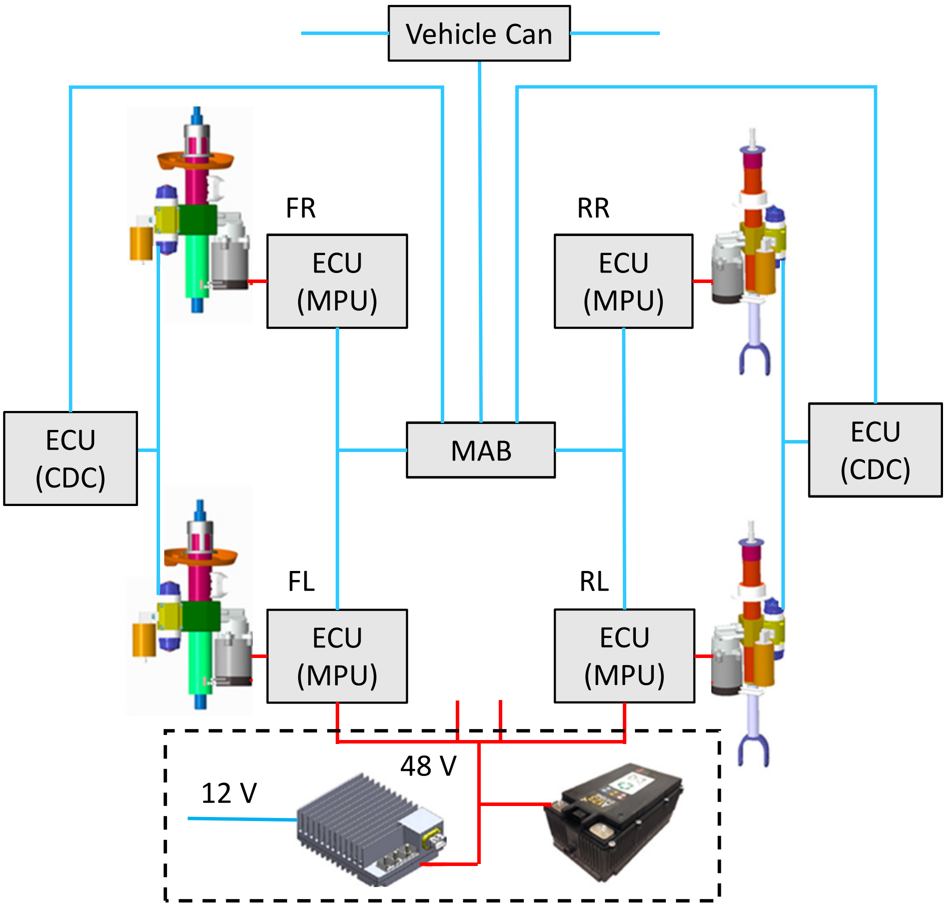

Figure 8-2: Schematic representation of the project vehicle system architecture, showing the additional components in the test vehicle required for the active suspension system.

8-4 Tablet

For demonstration purposes, the vehicle also has its own WiFi network with a tablet connected to it. The tablet allows to change predefined system parameters and activate demo programs. The tablet's functions are limited and predefined, such that potential customers can explore the possibilities of the active suspension system without compromising their safety.

Chapter 9

Actuator

This chapter explains the working principle of the active damper unit. It also introduces a non-linear actuator model of the active damper unit, based on characteristic maps, and a linearization of this model. The non-linear model (specified to each unit in the vehicle) is used in the test vehicle to control the active damper units. The linear model is derived from this non-linear model by linearizing it around a fixed operation point. The linear model is used for simulation purposes and allows to asses system dynamics.

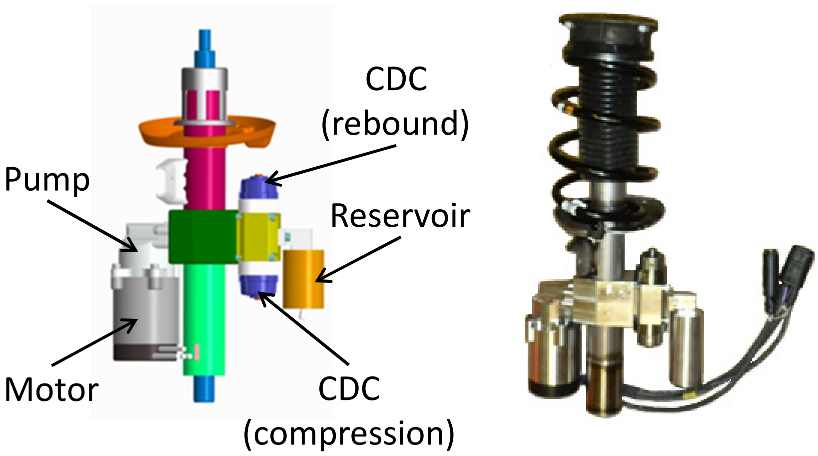

Figure 9-1: Left: CAD-model of the active damper unit (front). Right: picture of the corresponding (front) active damper unit including the suspension spring and connection wires, such as it is in the project vehicle

9-1 Active damper unit

The original suspension dampers are replaced by active damper units. A CAD-model of the active (front) damper unit is shown on the left side of Figure 9-1 and a picture of the complete

unit, as it is build into the test vehicle, is shown on the right.
These units each consist of a hydraulic cylinder, two CDC-valves, an accumulator (or reservoir) and a gear pump, which is driven by an electric motor. Due to the vehicle's suspension configuration, the layout of the front and rear active damper units is not the same. The McPherson front suspension requires the hydraulic cylinders to have a piston shaft throughout the whole cylinder, whereas the rear suspension units are regular cylinders as illustrated schematically in Figure 9-2. The continuous piston shaft is needed in the front suspension units, since the McPherson strut also has to account for forces other than the ones in the damping direction and partly has to help guide the wheel. A piston shaft throughout the cylinder gives the suspension strut the required additional stability and prevents the cylinder from buckling under transverse loads. As a result of the continuous piston shaft, the piston surface areas at each side are equal. This is not the case for the rear suspension units.

9-2 Working principle

The active damper unit is based on the Continuous Damping Control (CDC) damper, developed by ZF Friedrichshafen AG. Integrated into a damper, CDC valves allow the damping to be continuously variable between two (a minimum and a maximum) characteristic force-velocity curves by controlling the current i_{CDC}. The shape of these characteristic curves can be changed by adjusting, or replacing components in the CDC valve. In case of a system shutdown ($i_{CDC} = 0\,A$), the force-velocity curve is configured such, that driving is not compromised.

Each damper unit has two CDC valves to separately control the compression and rebound stages. More about changing the damping characteristics by adjustment and tuning of CDC valves can be found in the Chassis Handbook [9].

The dynamic behavior of a CDC damper is furthermore strongly influenced by the various elasticities in the damper itself. Together with the valve switching times (usually just a few milliseconds), this can result in noticeable delays in the damper's response time. A damper with a low overall elasticity is therefore required, when it has to feature a good dynamic response [9].
In the project's modular active damper units, the semi-active damping systems are each augmented with one gear pump. The resulting system is an active suspension system, which is not only capable of controlling the damping ratio, but it can also regulate the volume flow independently of the relative damper velocity. This enables to actively control the damping forces and expands the effective range (see Section 2-1) from two to four quadrants. The units are furthermore constructed such that all components are rigidly connected to each other. This minimizes the overall elasticity of the damping units. The resulting overall response time of the active damper units is approximated to be $12-25$ ms, depending on the system's operating point (high pressure and high CDC currents result in faster response times, whereas low pressure and open valves lead to longer response times). Due to communication latency and allowable phase shifts however, the actual realizable cut-off frequency of the active damper units is limited to approximately $3-5$ Hz.

9-2-1 Hydraulic architecture

The working principle of the active damper units is illustrated schematically by the hydraulic actuator architecture in Figure 9-2. The arrows in the figure indicate the positive directions.

In case of the rear active suspension units, the piston rod at one side of the cylinder, causes the top and bottom chamber to be different. This leads to a volume difference when the piston moves. The accumulator in the system compensates for this difference. Although the surface area on both sides of the piston are equal for the front suspension units, the accumulator is still required to account for leakage and internal system pressure. Moreover, the accumulator reduces pressure peaks in the system that occur when the cylinder moves rapidly.
The pressure inside the accumulator is 8 bar. For the rear suspension, this means that there is a resulting force (accumulator pressure minus air pressure multiplied with the difference in piston surface area) that pushes the damper out. This force is approximately 115 N and adds to the static spring load.

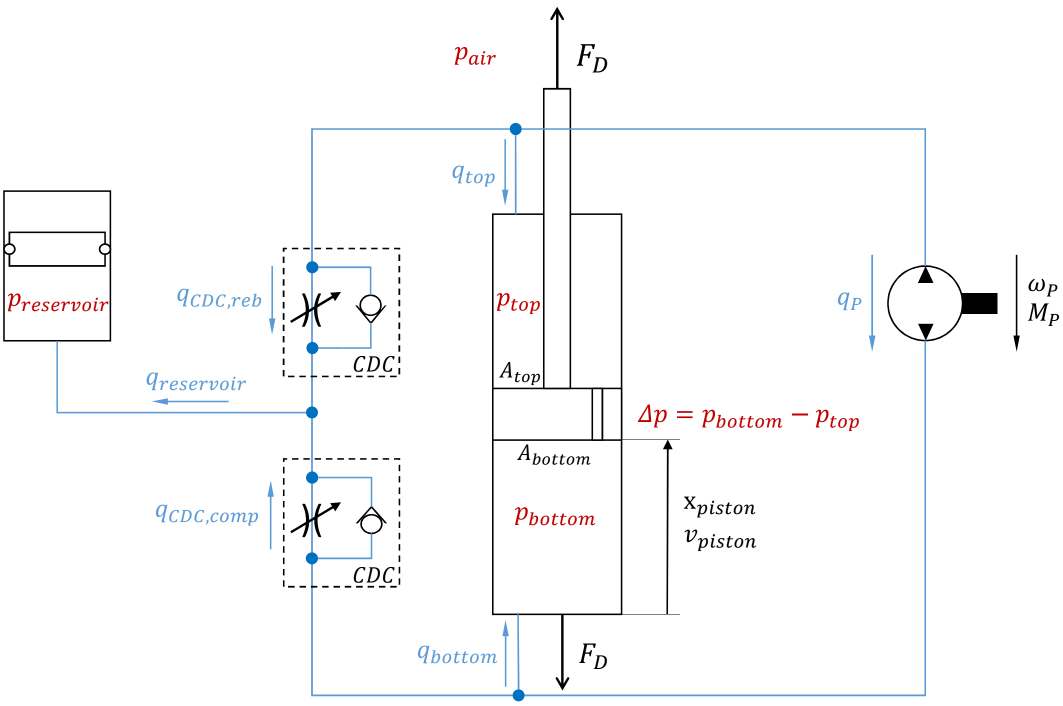

Figure 9-2: Hydraulic architecture of the active damper unit. Positive directions indicated by the arrows in the figure

9-2-2 Gear pump

The pump in the system is a gear pump that can reverse its pumping direction and can also act as a generator. The latter has not yet been utilized and is not part of this research. The required energy for the pumps is supplied by the 48V on-board power supply.

By compensating for a volume flow q, as a result of a relative damper velocity, or instead even generating a volume flow, the pump makes it possible to generate forces independent of

the relative damper velocity v_{piston}.
The volume flow generated by the pump q_P depends on the pump's displacement volume V_0 and the rotational pump speed ω_P. This can be approximated ideally (without considering leakage) as a linear relationship:

$$q_P = \frac{\omega_P}{2\pi} \cdot V_0. \tag{9-1}$$

To simplify (9-1), $V_P = V_0/2\pi$ is introduced and

$$q_P = \omega_P \cdot V_P. \tag{9-2}$$

The rotational pump speed is limited at approximately 6000 rpm. Higher rotational speeds are possible, but at the same time reduce the torque as the pump's power output-limit is approached.

9-2-3 CDC valves

The CDC valve is a continuously variable valve developed by ZF Friedrichshafen AG. Depending on the applied current i_{CDC}, the pressure required to induce a volume flow through the valve changes. This behavior can be approximated by

$$\begin{cases} i_{CDC} = 0\,A, & \text{Valve "open"} \\ 0 > i_{CDC} < i_{DCD,max}, & \text{Valve between "open" and "closed"} \\ i_{CDC} = i_{CDC,max}, & \text{Valve "closed"} \end{cases}$$

The maximal CDC current in the project's damper system is limited at 1400 mA. Higher CDC currents result in hydraulic pressures that cannot be supplied by the pump. If one would exceed this limit, the the power of the pump is not sufficient and the rotary speed of the pump will stall. The CDC valves and pump together can regulate the hydraulic resistance and the volume flow in the active damper units. This allows to control the pressure difference on both sides of the damper's piston ($\Delta_p = p_{bottom} - p_{top}$), which multiplied with the acting piston area, A_{top} or A_{bottom}, gives the active damping force F_D. The resulting characteristic curves and i_{CDC}-limit for the active damper unit system are illustrated in Figure 9-3).

9-3 Characteristic map

The characteristic map is generated from test rig measurements. In these measurements, the hydraulic damper unit (without suspension spring) was rigidly mounted and the resulting force at the damper's top mount was recorded for different CDC valve currents and rotational pump speeds. The resulting map relates the rotational speed of the pump ω_P (resulting in the volume flow q_P) and the applied current to the CDC valves i_{CDC}, with the resulting actuator force F_D (or pressure difference Δ_p). This map enables to predict the actuator force F_D that will result from a certain ω_P and i_{CDC} and vice verse.
Only one quadrant of the full four-quadrant operating range is depicted in the characteristic map of Figure 9-3. A line of operation is indicated to illustrate a possible pump-to-CDC-to-force relation.

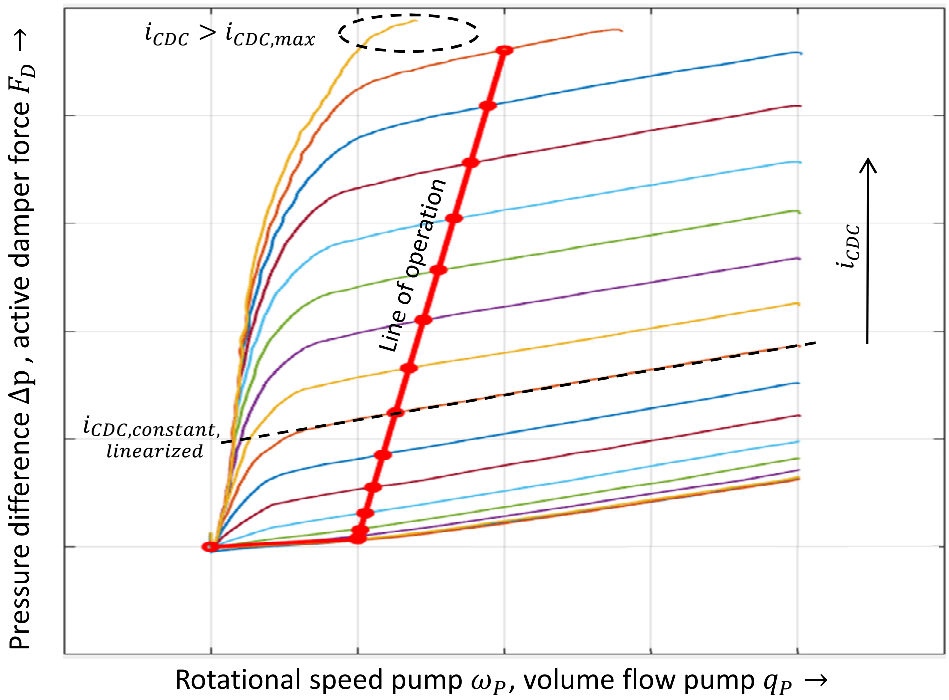

Figure 9-3: Characteristic map of the actuator, relating the rotational speed of the pump ω_P with the applied CDC current i_{CDC} and the resulting actuator force F_D. If $i_{CDC} > i_{max}$, the power limit of the pump is reached and the rotational pump speed stalls. Line of operation indicated.

From the figure it follows, that there is a steep force incline at low volume flows upon minor changes in the applied CDC current. This operation area has to be avoided for smooth and accurate force control.

9-4 Actuator control structure

The characteristic map from Figure 9-3 is fundamental for the active damper unit controller, which is shown in Figure 9-4. The figure schematically describes the structure of the actuator controller which is implemented for each individual active damper unit. Using the desired damping force F_{des} and the actual pump revolution speed ω_P, the controller selects the required operating point with a corresponding CDC current i_{CDC} and motor speed $\omega_{P,des}$ along a predefined line of operation within the characteristic map. The resulting desired motor speed and pressure difference Δ_p are subsequently used as input into a pump model, which accounts for the pump's dynamics and the oil temperature T_{oil}.
The desired rebound and compression CDC settings are sent to the corresponding CDC valve. In the present version, the desired CDC settings are just selected, without considering the CDC valve dynamics. An inverse CDC valve model has however been developed and shows an increase in the CDC valve performance by compensating for its dynamics. This modification has not however been used in this research and will first be implemented in further research. Finally, the control signals are sent to the individual ECUs, which transfer the signals into the desired actions.

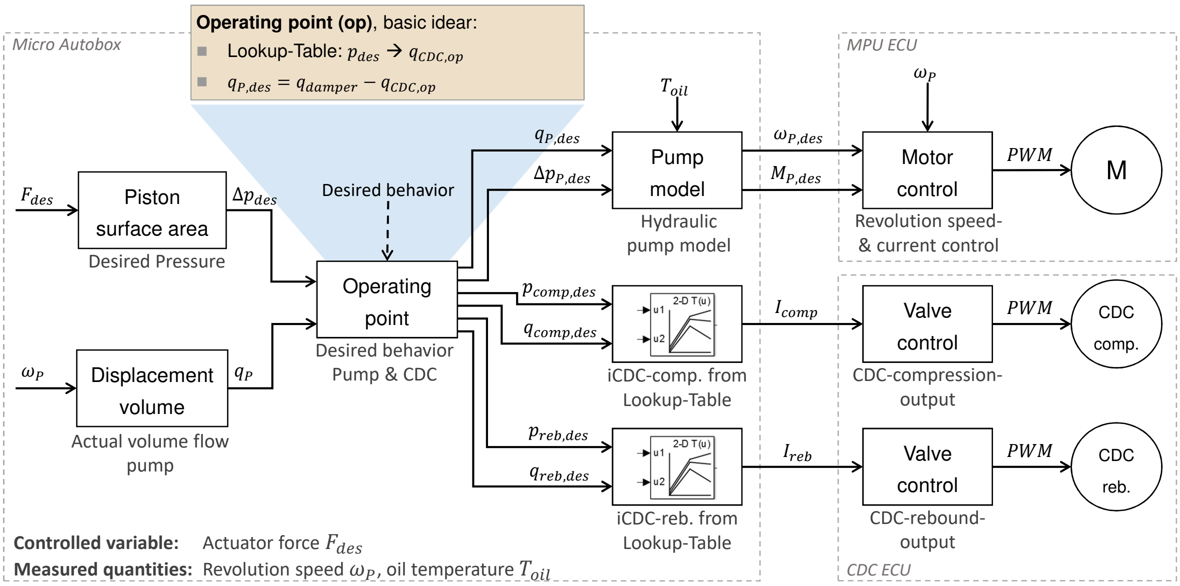

Figure 9-4: Schematic representation of the active damper unit controller based on characteristic maps.

9-5 Linear actuator model

A linearization of the actuator controller (extended with wheel dynamics) is given in Figure 9-5. For convenience, a list of the symbols used in the figure and their corresponding description is given in Table 9-1.
The linear model assumes constant oil properties (oil capacity C, C=constant) and is linearized around a fixed point in the characteristic map. This point is characterized by the gradient of the CDC curve in the fixed operating point ($i_{CDC} = constant$, which is represented by K_{CDC}. See Figure 9-3).
Furthermore, wheel dynamics are added to the linear model to be able to incorporate the effect of induced volume flows resulting from relative damper velocities. The vertical position of the wheel is represented by z_w, the vertical velocity by $\dot{z}_w$, the vertical acceleration by $\ddot{z}_w$ and the vertical position of the road surface by z_g in the figure. The effect of the wheel's damping is neglected (also see [9]) and the wheel's spring stiffness c_w is considered constant. This model extension allows to make first quantitative statements regarding the wheel's stability when the wheel is excited by the active damper unit and serves simulation purposes in this research.
It has to be noted here, that no distinction is made in the linear model between the rebound and compression stages and the piston's surface area correspondingly is assumed constant as $A = (A_{top} + A_{bottom})/2$.

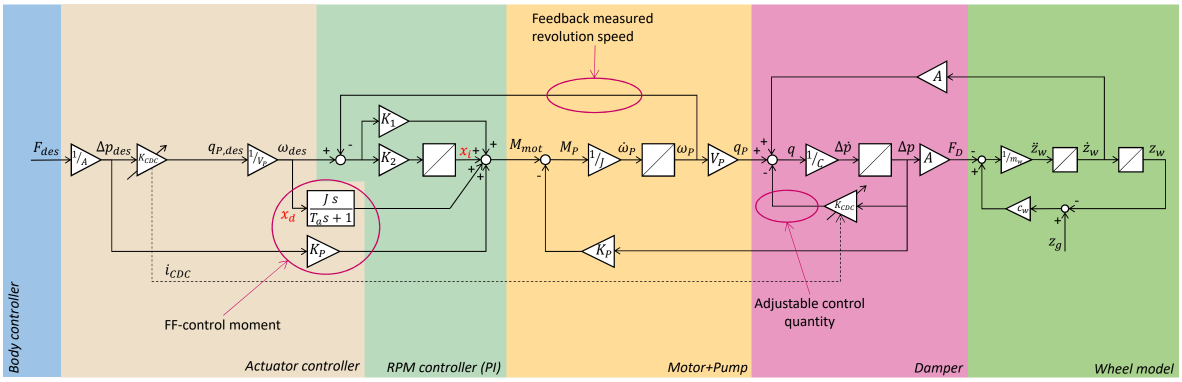

Figure 9-5: Linear actuator model, extended with wheel dynamics

9-5-1 Linear actuator model structure

The linear model in Figure 9-5 is divided into the sections:

- Body controller
  - Incorporates active control modules e.g. Skyhook and roll-compensation and results in desired active suspension forces F_{des}.
- Actuator controller
  - Calculates an initial feed forward motor moment from the desired forces. The proportional term K_p directly brings the pump into action as soon as a change in the required force is detected.
  - The time constant $T_a = 1/(f_a \cdot 2\pi)$ of the feed forward differentiation filter, with $f_a = 30$ Hz, is chosen such, that it can follow the wheel ($\approx$ two times the wheel's eigenfrequency), without amplifying to much noise when differentiating the signal.
- RPM controller
  - PI-controller that uses the desired rotational speed and the actual rotational speed to calculated the desired motor moment. The parameter values for the proportional term K_1 and integration term K_2 followed from system identification.
- Motor+Pump controller
  - Includes the inertia of the gear pump J and pressure difference Δp to calculate the resulting volume flow through the pump q_P.
- Damper model
  - Uses the oil capacity (proportional relation between volume flow and pressure change ($C = dV/dp = q/\Delta\dot{p}$)) and volume flows to calculate the pressure difference in the damper.
    Multiplied with the approximated piston area A, this gives the resulting damper force F_D.

- Wheel model
  - Includes wheel dynamics (z_w, $\dot{z}_w$, $\ddot{z}_w$) and allows to feedback a change in the relative damper velocity, which results in an additional volume flow according to $q = \dot{z}_w A$.

Table 9-1: List of symbols corresponding to the linear actuator model of Figure 9-5

Symbol/ System state	**Description**
F_{des}	Desired active damper force, resulting from the body control modules e.g. Skyhook and Roll compensation
A	Average piston surface $(A_{top} + A_{bottom})/2$
$\Delta_{p_{des}}$	Desired pressure difference as a result of the desired active damper force
K_P	Proportional term to include the effect of the pressure difference on both sides of the damper cylinder on the rotary pump speed
i_{CDC}	CDC current
K_{CDC}	Gradient of the CDC curve in the fixed operating point ($i_{CDC} = constant$)
$q_{P_{des}}$	Desired volume flow through the rotary gear pump
V_P	Pump displacement volume $V_0/2\pi$
ω_{des}	Desired pump rotary speed
x_d	Differentiation system state
J	Rotary gear pump inertia
T_a	Time constant of the differentiation filter
K_1	Proportional term of the PI controller
K_2	Integration term of the PI controller
x_i	Integration system state
M_{mot}	Motor torque of the electric motor
M_P	Resulting pump torque (including the pressure difference)
ω_P	Resulting rotary speed of the gear pump
q_P	Resulting volume flow through the pump
q	Resulting volume flow in the active damper (including the volume flow as a result of the relative damper velocity)
C	Oil capacity
Δ_p	Resulting pressure difference in the active damper
F_D	Resulting active damper unit force
m_w	Mass of the wheel in the wheel model
$\ddot{z}_w$	Vertical wheel acceleration
c_w	Linear spring constant of the tire

9-5-2 State-space representation

For simulation purposes, the linear model is translated into a state-space representation, which is suited for implementation in `Matlab`. To define the system matrices, first, the system states, system inputs and desired output are defined as

$$\underline{x} = \begin{bmatrix} x_d & x_i & \omega_P & \Delta p & z_w & \dot{z}_w \end{bmatrix}^T, \tag{9-3}$$

$$\underline{u} = \begin{bmatrix} F_{des} & z_g \end{bmatrix}^T, \tag{9-4}$$

$$y = F_D. \tag{9-5}$$

The differentiation and integration states are denoted by, x_d and x_i respectively (see Figure 9-5). With the desired actuator force F_{des} and road excitation z_g as input and the resulting actuator force F_D as output, the state-space representation of the system finally is

$$\dot{\underline{x}} = \underbrace{\begin{bmatrix} -\frac{1}{T_a} & 0 & 0 & 0 & 0 & 0 \\ 0 & 0 & -K_2 & 0 & 0 & 0 \\ -\frac{1}{T_a} & \frac{1}{J} & -\frac{K_P}{J} & 0 & 0 & 0 \\ 0 & 0 & \frac{V_P}{C} & -\frac{K_{CDC}}{C} & 0 & \frac{A}{C} \\ 0 & 0 & 0 & 0 & 0 & 1 \\ 0 & 0 & 0 & -A & -\frac{c_w}{m_w} & 0 \end{bmatrix}}_{A} \underline{x} + \underbrace{\begin{bmatrix} \frac{K_{CDC}}{A \cdot V_P \cdot T_a} & 0 \\ \frac{K_{CDC} K_2}{A \cdot V_P} & 0 \\ \frac{1}{J \cdot A}\left(\frac{K_{CDC} \cdot K_1}{V_P} + \frac{K_{CDC} \cdot J}{V_P \cdot T_a} + K_P\right) & 0 \\ 0 & 0 \\ 0 & 0 \\ 0 & \frac{c_w}{m_w} \end{bmatrix}}_{B} \underline{u}, \tag{9-6}$$

$$y = \underbrace{\begin{bmatrix} 0 & 0 & 0 & A & 0 & 0 \end{bmatrix}}_{C} \underline{x} + \underbrace{\begin{bmatrix} 0 & 0 \end{bmatrix}}_{D} \underline{u}. \tag{9-7}$$

Chapter 10

Control framework

The projects controller structure is arranged similar to the Aktakon control structure, where the controller is separated into vehicle and actuator dynamics. The system's measured input signals are filtered by means of signal conditioning. This initial filtering is necessary to process the measured signals. Conform to the Aktakon control structure, the measured quantities are furthermore transformed into modal quantities where necessary, before they enter the individual body control modules. The resulting modal output quantities from the different control modules are subsequently collected and transformed by an inverse modal transformation into the desired forces for each active damper unit.

10-1 Body controller

The body controller embodies single control modules, each having their own task, conform to the modular Aktakon approach. Already implemented in the body controller are the Skyhook algorithm, an algorithm to compensate for roll motions and an algorithm that decides how this roll compensation is distributed over the front and rear of the vehicle. Furthermore, a pitch compensation algorithm is foreseen, but not yet implemented. A schematic representation of the controller structure is given in Figure 10-1.

The roll compensation controller is needed to complement the Skyhook controller in long lasting corners and also acts on fast motions. Since dampers cannot support a load (and the Skyhook algorithm is based on a Skyhook*damper*), a vehicle with only a Skyhook algorithm to control the vehicle's body motion will start to roll in long lasting corners.
This becomes clear when one imagines a vehicle driving along a circle with a constant radius at a constant velocity. Since the conditions do not change, this can be considered as steady-state cornering. The resulting constant lateral acceleration a_y (centrifugal acceleration) will however cause the vehicle to roll and needs to be actively compensated for. As can be seen in Figure 10-1, the roll compensation controller uses this lateral acceleration of the vehicle's body a_{y_c} rather than a relative velocity with respect to a reference frame (Skyhook principle).

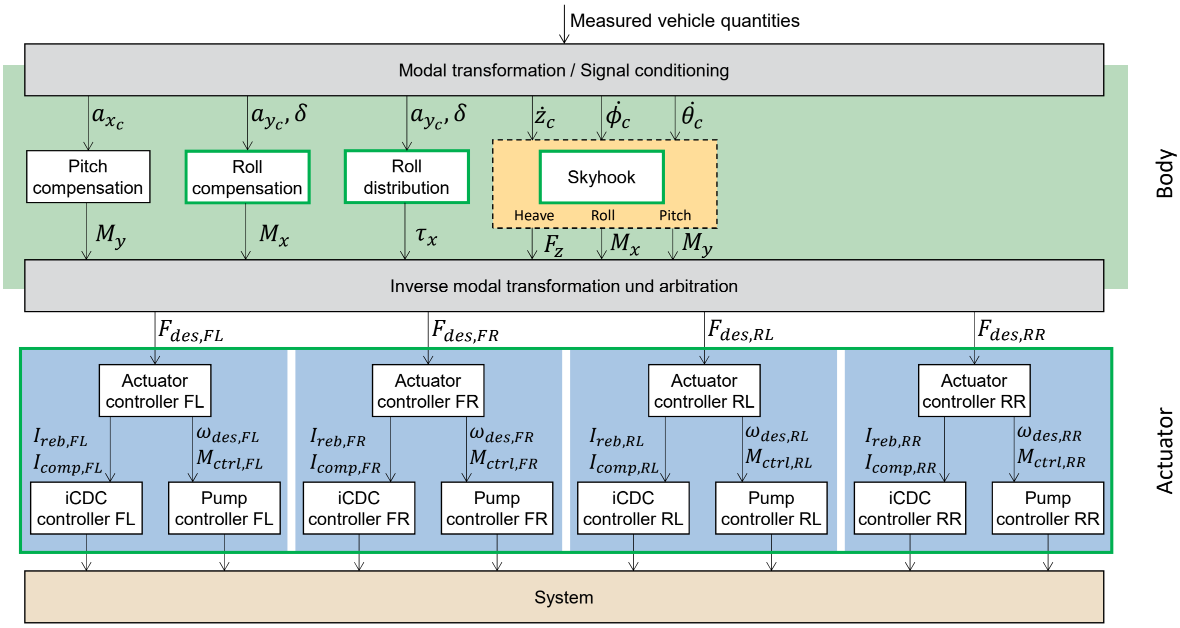

Figure 10-1: Predefined controller framework of the project according to the Ammakon principle

It also uses the steering wheel angle δ. The latter has to do with the underlying vehicle-bicycle model, which enhances the controller dynamics. This augmentation enables the roll compensation controller to act on the driver's input even before the lateral acceleration is present (driver's steering input $\delta \rightarrow$ lateral acceleration $a_{y_c} \rightarrow$ roll motion $\dot{\phi}_c$, ϕ_c).
The roll distribution algorithm finally enhances vehicle stability and gives the designers an extra degree of freedom in fine-tuning the vehicle's dynamic behavior.
Since the relevant frequency range of driver-induced inputs is $0.1 - 3.0$Hz (see [5]) and the control modules are force limited, the actuator dynamics are not compromised, despite the relatively simple Aktakon controller framework.

The actuator controllers in the lower half of Figure 10-1 are the ones from Section 9-4 and finally output the desired actuator forces at each individual corner.

Chapter 11

Disturbance compensation concept

The dynamic behavior of a system can be enhanced by disturbance compensation. If the disturbance on a system can be measured, or estimated, a controller can compensate for this disturbance with the aim to minimize its effect on the system. Considering a vehicle, the dynamic system response highly depends on the road induced disturbances. When the goal is to minimize the vertical body acceleration, then a disturbance compensation algorithm, that compensates for the road excitation, has great potential to improve the dynamic behavior.
Common comfort enhancing algorithms such as the Skyhook algorithm, react on the motion of the passenger cabin. This means that they only act, when a cabin motion already is induced. The disturbance compensation algorithm tries to minimize the induced forces before they reach the passenger's cabin.

11-1 Disturbance estimation

The previous literature survey describes different methods to estimate system states that cannot directly be measured. Many of the described estimation methods are based on model based observers and Kalman filters (see for example [7, 15, 17]). These estimation methods however, are all investigated in a theoretical context, or applied at test rigs in a controlled environment. Successful practical implementations of these techniques are not known at this time of writing.
An alternative approach is pursued by, for example, G. Koch et al. [16], N. Pletschen et al. [25] and E. Schäfer [27]. Their research show that conventional filtering techniques can be sufficient for the design of an disturbance compensation controller while facilitating implementation.
To facilitate implementation of active suspension control algorithms, G. Koch et al. [16] use conventional frequency filters to generate estimates of the same systems states as they did for a test setup with parallel Kalman filters in [15]. M. Fröhlich [7] furthermore investigates different state estimation techniques (e.g. model based, signal based, Kalman filters, observers and conventional filters) and assesses them according to estimation quality and applicability. The findings on this subject are described in the previous literature survey and let to the disturbance compensation algorithm development approach in this research.

11-2 Project facilities and aim

Aim of this research is to develop and *implement* a disturbance compensation controller in a vehicle. Since the final controller has to work under real conditions in an actual vehicle, it is decided to develop an control algorithm based on conventional frequency filters. This choice is supported by the above mentioned considerations and the absence of a test rig of the vehicle (or its suspension) in this project.
A validated model of the active suspension units was available at the beginning of this project (see Chapter 9). This model is extended and used for simulation purposes in this research.

The disturbance compensation concept introduced in this chapter and further developed in the rest of this research uses the findings from the previous literature survey as a foundation. The disturbance compensation controller as introduced by E. Schäfer [27], based on conventional filters, is considered for its simplicity and applicability. Rather than the model based controller from E. Schäfer however, a signal based controller motivated by the research of M. Fröhlich [7] is developed. This further simplifies the algorithm and an accurate model of the vehicle's suspension is no longer required. The absence of a test rig and corresponding system identification possibilities therefore do no longer pose a problem.

11-3 Concept study

Instead of using an estimation of the road z_g as model disturbance input, E. Schäfer [27] estimates the vertical position of the contact patch between the tire and the road z_t. The motivation to choose for the contact patch as input signal and the resulting disturbance compensation algorithm is briefly described in this section. Special attention is paid to this, since the introduced disturbance algorithm in this research followed from insights in Schäfers research.

11-3-1 Contact patch

E. Schäfer [27] approximates the contact patch as a small flat surface between the tire and the road. The area of this contact patch surface A_t follows from the wheel load F_z and tire pressure ρ_t according to

$$F_z = A_t \cdot \rho_t \quad \text{and} \tag{11-1}$$
$$A_t = l_t \cdot w_t. \tag{11-2}$$

Where l_t is the length of the contact patch and w_t represents the width of the tire. Due to elasticity of a tire, not all of the road excitation is transmitted to the vehicle. According to Schäfer, road disturbances with a wavelength smaller than twice the contact patch length are even widely absorbed by the tire. She approximates this behavior by a first order low-pass filter

$$H_{LP_1}(s) = \frac{z_t}{z_g} = \frac{1}{T_t \cdot s + 1}. \tag{11-3}$$

The filter's time constant T_t follows from the contact patch length and the vehicle velocity v.

$$T_t = \frac{1}{f_t \cdot 2\pi} = \frac{2 \cdot l_t}{v \cdot 2\pi} = \frac{l_t}{v \cdot \pi}. \tag{11-4}$$

Using this approximation, Schäfer is able to calculate a reliable approximation of the actual (filtered) road profile and develops an effective disturbance compensation algorithm based on this insight.
This implies, that one does not necessarily need to estimate the road profile to be able to compensate for its induced disturbance. This insight motivated to even go one step further in this research. Before going there however, Schäfers disturbance compensation approach is explained.

By means of a simplified wheel model, Schäfer estimates the vertical contact patch position z_t and velocity $\dot{z}_t$. The wheel model considered has a constant tire spring stiffness and a constant damping coefficient. Using Newton's second law of motion, Schäfer derives the required system equations and introduces a disturbance compensation algorithm. The equations, modified here to correspond to a quarter car model, for the wheel and contact patch dynamics are

$$m_w \ddot{z}_w = c_w(z_t - z_w) + d_w(\dot{z}_t - \dot{z}_w) + c_c(z_c - z_w) - F_{act}, \tag{11-5}$$

$$\dot{z}_t + \frac{c_w}{d_w} z_t = \frac{m_w}{d_w} \ddot{z}_w + \frac{c_w}{d_w} z_w + \dot{z}_w - \frac{c_c}{d_w}(z_c - z_w) + F_{act}. \tag{11-6}$$

Using these equations and introducing the following assumptions leads to the disturbance compensation algorithm defined by [27].

- $z_w \approx z_t$
- Vehicle's body stays still: $z_c = \dot{z}_c = \ddot{z}_c = 0$

Here, the second assumption is essential, since it decouples the wheel from the body by assuming that the vehicle's body stays still. Positions relative to a moving point (the vehicle's body without this assumption) reduce to positions with respect to a fixed point in space.
For the last assumption to hold, the resulting vertical forces on the vehicle's body F_c must be equal to zero.

$$F_c = c_c(z_w - z_c) + F_{act} = c_c(z_t - z_c) + F_{act} = c_c\, z_t + F_{act} \approx 0 \tag{11-7}$$

Knowing the position, velocity and acceleration of the wheel, or in this case, of the contact patch, now is enough to define a control algorithm. The actuator force should therefore compensate for the suspension springs. This principle is illustrated in Figure 11-1 from [27] p.127. Since the actuator used by E. Schäfer also represents the suspension's damper, she finally defines the required disturbance compensation force as

$$\begin{aligned} F_{act} &= K_s \cdot z_t + K_v \cdot \dot{z}_t, \quad \text{with initial values} \\ K_s &= -c_c \quad \text{and} \quad K_v = -d_c. \end{aligned} \tag{11-8}$$

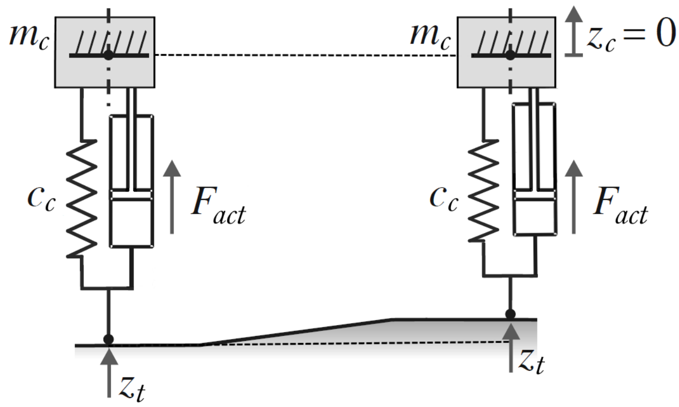

Figure 11-1: Disturbance compensation concept and assumptions according to Schäfer [27] p.127

11-3-2 Wheel

Without a sophisticated preview system that scans the road in front of the vehicle and allows to *act* upon upcoming disturbances, an active suspension system is confined to *react* on disturbances as soon as their induced effect is noticed. To get the most out of an active suspension system, it is therefore crucial to notice the disturbances on the system as close as possible to the source.
Since the wheels have direct contact to the road surface, they are the first to notice any change in the road profile. Transferred by the suspension, these changes result in movement of the vehicle's body.
If an active suspension system would be fast enough to compensate for the measured disturbance at the wheels, the disturbance would be eliminated before it even reaches the vehicle's body. This thought is in line with Schäfers second approximation.

The desired control disturbance compensation actuator force in (11-8) depends on the estimated tire contact patch. The velocity and position of this patch, $\dot{z}_t$ and z_t respectively, are calculated using the model equation (11-6). This equation uses the measurement quantities $\ddot{z}_w$ (wheel acceleration sensor), $z_c - z_w$ (displacement sensor) and F_{act} (pressure sensor), but all the other terms are estimates. When one abandons the vehicle model and uses the measured wheel acceleration instead, (11-8) can be written as

$$\begin{aligned} F_{act} &= K_s \cdot z_w + K_v \cdot \dot{z}_w, \quad \text{with initial values} \\ K_s &= -c_c \quad \text{and} \quad K_v = -d_c. \end{aligned} \tag{11-9}$$

Now the desired actuator force to compensate for the road induced disturbance depends on the wheel's vertical position and velocity. As with the contact patch, the wheel's velocity and position still cannot be measured directly, but they can be calculated by high-pass integration of the wheel acceleration signal. Where the high-pass term is needed to filter out offsets in the measured signal.

Chapter 12

Measurement data

The sensor output signals in the test vehicle are offset and noise afflicted. Before using them in a controller, they have to be conditioned to ensure correct and reliable controller performance. Depending on the sensor orientation, position, wiring connection and other factors, such as temperature and erosion, the offset and signal noise are different for each sensor at each moment in time. Therefore, it is not possible to apply one overall constant correction term that corrects the errors in the signals for all sensors of the same sort in the vehicle.

12-1 Signal conditioning

To dynamically remove signal offsets and reduce signal noise, the sensor signals should be filtered. By integration, differentiation and combining signals, it is furthermore possible to estimate quantities that are not measured directly.

12-1-1 Filters

Considering a signal offset and its properties, the appropriate filters can be chosen. Since an offset has a constant or low frequency behavior, high-pass filters can remove the offsets in sensors signals adequately. The cut-off frequency f_c of the high-pass filter needed for an offset free wheel acceleration sensor signal is determined from measurement data. In determining the required cut-off frequency, the aim is to let as much of the sensor's output signal through to retain as much of the signal information as possible, without risking a signal error induced by the offset.
To find the appropriate cut-off frequency, a first order high-pass filter $H_{HP_1}(s) = Ts/(Ts+1)$, with $T = 1/(f_c \cdot 2\pi)$ (see Figure 12-1), is implemented in `Simulink` to filter the measurement signal (see Figure 12-1). Observing the filter's output reveals how the cut-off frequency has to be adjusted. This method can be applied for different filters, it is straightforward and easy to implement.

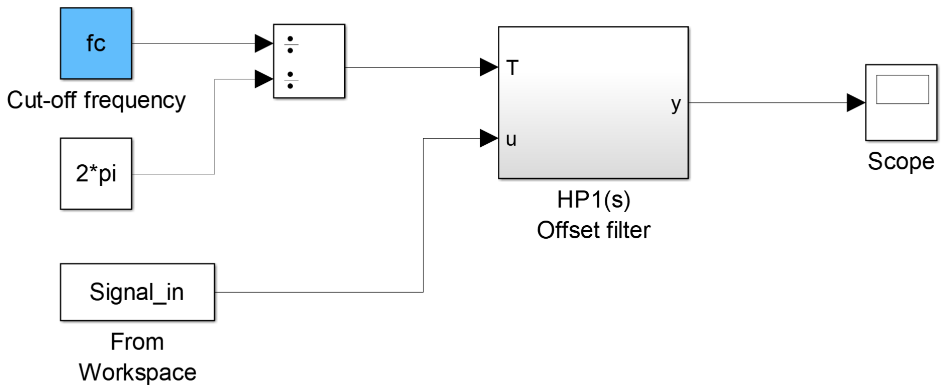

Figure 12-1: First order high-pass filter in `Simulink` to find the required cut-off frequency f_c to ensure an offset free signal y.

12-1-2 Final value theorem and DC gain

First order high-pass filters are able to remove the initial drift in a signal. The proposed disturbance compensation algorithm however, requires integration of the wheel acceleration signal to find the velocity and position of the wheel. Integrating the high-pass filtered offset free signal, might however again result in an offset. Multiple integration of an offset free signal can even lead to an increasing, unbounded offset, also denoted as signal drift. It is therefore interesting to know what happens with a signal over time, or expressed differently: assuming a signal $u(t)$, what happens to the signal as time approaches infinity ($\lim_{t\to\infty} u(t)$). To solve this problem, properties of the Laplace domain are utilized.

Knowing the Laplace transform of a function, an especially useful property of the Laplace domain can be utilized to calculate the final value of the function as time approaches infinity [6]. This property is known as the Final Value Theorem and it is defined as

$$\lim_{t\to\infty} y(t) = \lim_{s\to 0} sY(s), \tag{12-1}$$

where $Y(s)$ in this case is represented by the function of the first order high-pass filter $H_{HP_1}(s)$, which is used to remove the signal offset.
G. Franklin et al. [6] mention three possibilities for the final value of the function. It can be constant, undefined, or unbounded. If $Y(s)$ has any unstable poles in the right half of the s-plane, then $y(t)$ will grow and the limit will be unbounded. In case that there are two poles on the imaginary axis, then $y(t)$ will contain an undamped sinusoid and the limit final value will not be defined. Only if all poles are stable ($Re\{pole\} < 0$), $y(t)$ will go to zero. When all poles are in the left half s-plane except for on at $s = 0$, then the term corresponding to the pole at zero will result in a constant value: an offset. Accordingly, the final value theorem should be used on stable systems only.

The final value theorem can subsequently be used to find the DC gain of a system. The DC gain is the ratio of the output of a system to its input after all transients have decayed. To find the DC gain, the systems input (the measured sensor signal) is approximated as a step input signal $U(s) = 1/s$. The DC gain of the signal is then calculated using the final value theorem [6]. The steady-state output value of $Y(s) = G(s)U(s)$, where $G(s)$ is a transfer function (the high-pass filter) is then calculated as follows

$$\text{DC gain} = \lim_{s\to 0} s\, G(s)U(s) = \lim_{s\to 0} s\, G(s)\frac{1}{s} = \lim_{s\to 0} G(s). \tag{12-2}$$

12-2 Required filtering

Using the final value theorem to calculate the DC gain of the filtered sensor signals, it is possible to define the required filters that result in the desired offset free wheel velocity and wheel position signals. In this section, this method is applied to the measured wheel acceleration signal in the vehicle. Proceeded is as follows:

- it is verified, that the offset in the acceleration signal is indeed removed by the high-pass filter,
- additional filters are added to account for the signal integration and to find offset free estimates of the velocity and position.

For convenience, the time constants of the filters below are all denoted by T. Their values are actually determined using the scheme in Figure 12-1.

12-2-1 Required acceleration signal filtering

Filtering the measured vertical wheel acceleration with a first order high-pass filter $G(s) = H_{HP_1}(s)$, gives an offset free vertical wheel acceleration signal. This is verified by (12-3), where the suggested step input signal (representing the measured vertical wheel acceleration signal) is multiplied with a first order high-pass filter in the Laplace domain. The final value of this multiplication, or directly: the resulting DC gain of the first order high-pass filter is

$$\text{DC gain} = \lim_{s\to 0} H_{HP_1}(s) = \lim_{s\to 0} \frac{T\cdot s}{T\cdot s+1} = \frac{0}{1} = 0. \tag{12-3}$$

The resulting DC gain is equal to zero, meaning that the value of the signal will return to zero after all transients have decayed: the offset is reduced to zero.
According to the same reasoning, an offset free velocity signal and an offset free position signal are calculated next.

12-2-2 Required velocity signal filtering

To find the velocity signal, the acceleration signal has to be integrated. The integration step, which is equal to multiplication of the signal with $1/s$ in the Laplace domain, requires a second first order high-pass filter.

$$\begin{aligned}\text{DC gain} &= \lim_{s\to 0} H_{HP_1}(s)\cdot H_{HP_1}(s)\cdot\frac{1}{s}\\ &= \lim_{s\to 0} \frac{T\cdot s}{T\cdot s+1}\cdot\frac{T\cdot s}{T\cdot s+1}\cdot\frac{1}{s}\\ &= \lim_{s\to 0} \frac{T\cdot s}{T\cdot s+1}\cdot\frac{T}{T\cdot s+1} = \frac{0}{1}\cdot\frac{T}{1} = 0.\end{aligned} \tag{12-4}$$

12-2-3 Required position signal filtering

Following the same procedure, two times integration of the acceleration signal to find the position signal requires two additional first order high-pass filters, or equivalently: one additional second order high-pass filter.

$$\begin{aligned} \text{DC gain} &= \lim_{s\to 0} H_{HP_1}(s)\cdot H_{HP_2}(s)\cdot \frac{1}{s^2} \\ &= \lim_{s\to 0} \frac{T\cdot s}{T\cdot s+1}\cdot \frac{T^2\cdot s^2}{T^2\cdot s^2+2T\cdot s+1}\cdot\frac{1}{s^2} \\ &= \lim_{s\to 0} \frac{T\cdot s}{T\cdot s+1}\cdot \frac{T^2}{T^2\cdot s^2+2T\cdot s+1} = \frac{0}{1}\cdot\frac{T^2}{1} = 0. \end{aligned} \tag{12-5}$$

12-2-4 Matrix notation

To implement these filters into a mathematical model, which is later used for simulation purposes, it is required to find the matrix representation of these filters. Starting with the **acceleration** signal, the state-space notation is determined as follows

$$\frac{Z_{out}(s)}{Z_{in}(s)} = \frac{T\cdot s}{T\cdot s+1}, \tag{12-6}$$

$$(T\cdot s+1)Z_{out}(s) = T\cdot s\, Z_{in}(s), \tag{12-7}$$

$$T\,\dot{z}_{out} + z_{out} = T\,\dot{z}_{in}, \tag{12-8}$$

$$\dot{z}_{out} = -\frac{1}{T} z_{out} + \dot{z}_{in}. \tag{12-9}$$

If $\dot{z}_{in}$ is represented here by the wheel acceleration sensor signal $\ddot{z}_w$, then $\dot{z}_{out}$ will be the filtered offset free wheel acceleration $\ddot{z}_{w_1}$. This gives

$$\ddot{z}_{w_1} = -\frac{1}{T}\dot{z}_{w_1} + \ddot{z}_w, \tag{12-10}$$

or in matrix representation with the system state $x_1 = \dot{z}_{w_1}$

$$\dot{x}_1 = -\frac{1}{T}\, x_1 + \ddot{z}_w, \tag{12-11}$$

$$y_1 = \ddot{z}_{w_1} = -\frac{1}{T}\, x_1 + \ddot{z}_w. \tag{12-12}$$

To find an offset free signal for the **velocity**, the high-pass filtered acceleration $\ddot{z}_{w_1}$ signal is used as input. Using (12-6)-(12-9) for the second high-pass filter and substituting $\dot{z}_{in}$ by $\ddot{z}_{w_1}$ gives $\dot{z}_{out}$, which is equal to the filtered offset free wheel acceleration $\ddot{z}_{w_2}$ and enables a one time offset free integration step. This gives

$$\ddot{z}_{w_2} = -\frac{1}{T}\dot{z}_{w_2} + \ddot{z}_{w_1}, \tag{12-13}$$

or in matrix representation with the system state $x_2 = \dot{z}_{w_2}$

$$\dot{x}_2 = -\frac{1}{T}\, x_2 + \ddot{z}_{w_1}, \tag{12-14}$$

$$y_2 = \dot{z}_{w_2} = x_2. \tag{12-15}$$

Likewise, the offset free **position** signal is found by adding the required second order high-pass filter to the filtered acceleration signal.

$$\frac{Z_{out}(s)}{Z_{in}(s)} = \frac{T^2 \cdot s^2}{T^2 \cdot s^2 + 2T \cdot s + 1}, \tag{12-16}$$

$$(T^2 \cdot s^2 + 2T \cdot s + 1)Z_{out}(s) = T^2 \cdot s^2 \, Z_{in}(s), \tag{12-17}$$

$$T^2 \, \ddot{z}_{out} + 2T \, \dot{z}_{out} + z_{out} = T^2 \, \ddot{z}_{in}, \tag{12-18}$$

$$\ddot{z}_{out} = -\frac{1}{T^2} z_{out} - \frac{2}{T} \dot{z}_{out} + \ddot{z}_{in}. \tag{12-19}$$

Substituting the offset free wheel acceleration signal $\ddot{z}_{w_1}$ for $\ddot{z}_{in}$ gives $\ddot{z}_{out}$ as the filtered offset free wheel acceleration, denoted by $\ddot{z}_{w_3}$, and enables two offset free integration steps. This gives

$$\ddot{z}_{w_3} = -\frac{1}{T^2} z_{w_3} - \frac{2}{T} \dot{z}_{w_3} + \ddot{z}_{w_1}. \tag{12-20}$$

Introducing the state vector $\underline{x}_3 = \begin{bmatrix} z_{w_3} & \dot{z}_{w_3} \end{bmatrix}^T$ gives

$$\dot{\underline{x}}_3 = \begin{bmatrix} 0 & 1 \\ -\frac{1}{T^2} & -\frac{2}{T} \end{bmatrix} \underline{x}_3 + \begin{bmatrix} 0 \\ 1 \end{bmatrix} \ddot{z}_{w_1}, \tag{12-21}$$

$$y_3 = z_{w_3} = \begin{bmatrix} 1 & 0 \end{bmatrix} \underline{x}_3 + \begin{bmatrix} 0 \end{bmatrix} \ddot{z}_{w_1}. \tag{12-22}$$

12-2-5 Series interconnection

The three systems derived above are added together by series interconnection to form one single system. A series interconnection of different systems is obtained if the output of the first system enters a second system as an input [14]. In this case there are also two series interconnections, both using the output of the first system as input. The series interconnection for the systems

$$\begin{aligned} \dot{x}_1 &= f_1(x_1, u_1), \quad & y_1 &= h_1(x_1, u_1), \\ \dot{x}_2 &= f_2(x_2, u_2), \quad & y_2 &= h_2(x_2, u_2), \\ \dot{x}_3 &= f_3(x_3, u_3), \quad & y_3 &= h_3(x_3, u_3) \end{aligned}$$

is then described by

$$\begin{pmatrix} \dot{x}_1 \\ \dot{x}_2 \\ \dot{x}_3 \end{pmatrix} = \begin{pmatrix} f_1(x_1, u_1) \\ f_2(x_2, h_1(x_1, u_1)) \\ f_3(x_3, h_1(x_1, u_1)) \end{pmatrix}, \quad \begin{pmatrix} y_2 \\ y_3 \end{pmatrix} = \begin{pmatrix} h_2(x_2, h_1(x_1, u_1)) \\ h_3(x_3, h_1(x_1, u_1)) \end{pmatrix}. \tag{12-23}$$

With the linear systems

$$\begin{aligned} \dot{x}_1 &= A_1 x_1 + B_1 u_1, \quad & \dot{x}_2 &= A_2 x_2 + B_2 u_2, \quad & \dot{x}_3 &= A_3 x_3 + B_3 u_3 \\ y_1 &= C_1 x_1 + D_1 u_1, \quad & y_2 &= C_2 x_2 + D_2 u_2, \quad & y_3 &= C_3 x_3 + D_3 u_3 \end{aligned} \tag{12-24}$$

and $x = \begin{bmatrix} x_1 & x_2 & x_3 \end{bmatrix}^T$ this results in

$$\underline{\dot{x}} = \begin{bmatrix} A_1 & 0 & 0 \\ B_2C_1 & A_2 & 0 \\ B_3C_1 & 0 & A_3 \end{bmatrix} \underline{x} + \begin{bmatrix} B_1 \\ B_2D_1 \\ B_3D_1 \end{bmatrix} u_1, \tag{12-25}$$

$$\underline{y} = \begin{bmatrix} C_1 & 0 & 0 \\ D_2C_1 & C_2 & 0 \\ D_3C_1 & 0 & C_3 \end{bmatrix} \underline{x} + \begin{bmatrix} D_1 \\ D_2D_1 \\ D_3D_1 \end{bmatrix} u_1. \tag{12-26}$$

Implementing the system matrices finally gives

$$\underline{\dot{x}} = \begin{bmatrix} -\frac{1}{T} & 0 & 0 & 0 \\ -\frac{1}{T} & -\frac{1}{T} & 0 & 0 \\ 0 & 0 & 0 & 1 \\ -\frac{1}{T} & 0 & -\frac{1}{T^2} & -\frac{2}{T} \end{bmatrix} \begin{bmatrix} \dot{z}_{w1} \\ \dot{z}_{w2} \\ z_{w3} \\ \dot{z}_{w3} \end{bmatrix} + \begin{bmatrix} 1 \\ 1 \\ 0 \\ 1 \end{bmatrix} \ddot{z}_w, \tag{12-27}$$

$$\underline{y} = \begin{bmatrix} \ddot{z}_{w1} \\ \dot{z}_{w2} \\ z_{w3} \end{bmatrix} = \begin{bmatrix} -\frac{1}{T} & 0 & 0 & 0 \\ 0 & 1 & 0 & 0 \\ 0 & 0 & 1 & 0 \end{bmatrix} \begin{bmatrix} \dot{z}_{w1} \\ \dot{z}_{w2} \\ z_{w3} \\ \dot{z}_{w3} \end{bmatrix} + \begin{bmatrix} 1 \\ 0 \\ 0 \end{bmatrix} \ddot{z}_w. \tag{12-28}$$

These matrices are implemented into the simulation model, which is introduced in the next chapter, to account for the sensor signal dynamics in the system.

Chapter 13

Concept validation and evaluation

The wheel based disturbance compensation algorithm (11-9) assumes that the vehicle's body stays still ($z_c = \dot{z}_c = \ddot{z}_c = 0$). Since this is unlikely to happen, the forces resulting from (11-9) could also negatively affect the dynamic behavior of the vehicle. Compensating for the damping possibly even leads to undamped and unstable dynamics, which can lead to unsafe situations. Before implementing the proposed algorithm in the vehicle, it is therefore important to study its impact on the driving dynamics in a save environment.
In this chapter, the stability of the introduced disturbance compensation algorithm is investigated by means of simulations. These simulations are based on a quarter car model. This model initially assumes perfect conditions and constant linear damper/spring properties. This highly simplified model allows to get a first impression of the effect of the proposed disturbance compensation algorithm on the system. Then, the model is extended, such that it includes the appropriate signal conditioning and also accounts for the active damper unit dynamics. This model extension also leads to an adaptation and augmentation of the proposed disturbance compensation algorithm.

13-1 Stability check

The stability of the proposed disturbance compensation controller is initially investigated with help of the quarter car model given in Figure 13-1a. The equations of motion corresponding to this quarter car model are:

$$m_c\ddot{z}_c = -c_c(z_c - z_w) - d_c(\dot{z}_c - \dot{z}_w) + F_{act}, \tag{13-1}$$
$$m_w\ddot{z}_w = c_c(z_c - z_w) + d_c(\dot{z}_c - \dot{z}_w) - c_w(z_w - z_g) - F_{act}. \tag{13-2}$$

Introduction of the system state vector $\underline{x} = \begin{bmatrix} z_c & \dot{z}_c & z_w & \dot{z}_w \end{bmatrix}^T$ and implementing the desired disturbance compensation force (11-9) gives the following state-space representation of the system

$$\underline{\dot{x}} = \begin{bmatrix} 0 & 1 & 0 & 0 \\ -\frac{c_c}{m_c} & -\frac{d_c}{m_c} & \frac{c_c}{m_c} - \frac{K_s}{m_c} & \frac{d_c}{m_c} - \frac{K_v}{m_c} \\ 0 & 0 & 0 & 1 \\ \frac{c_c}{m_w} & \frac{d_c}{m_w} & -\frac{c_c+c_w}{m_w} + \frac{K_s}{m_w} & -\frac{d_c}{m_w} + \frac{K_v}{m_w} \end{bmatrix} \underline{x} + \begin{bmatrix} 0 \\ 0 \\ 0 \\ \frac{c_w}{m_w} \end{bmatrix} u, \tag{13-3}$$

$$y = C\,\underline{x} + D\,u, \tag{13-4}$$

where $u = z_w$ the input of the system and the desired output is determined by the C and D matrices.

The assumption that the vehicle's body initially is at rest ($z_c = 0$ and $\dot{z}_c = 0$) and the substitution of the disturbance control algorithm (11-9), with $K_s = -c_c$ and $K_v = -d_c$ gives

$$\begin{aligned} m_c\ddot{z}_c &= -c_c(z_c - z_w) - d_c(\dot{z}_c - \dot{z}_w) + K_s\,z_w + K_v\,\dot{z}_w \\ &= -c_c(z_c - z_w) - d_c(\dot{z}_c - \dot{z}_w) - c_c\,z_w - d_c\,\dot{z}_w \\ &= -c_c\,z_c - d_c\,\dot{z}_c \quad \text{initial conditions } (z_c = 0 \text{ and } \dot{z}_c = 0) \\ &= 0 \end{aligned} \tag{13-5}$$

$$\begin{aligned} m_w\ddot{z}_w &= c_c(z_c - z_w) + d_c(\dot{z}_c - \dot{z}_w) - c_w(z_w - z_g) - K_s\,z_w - K_v\,\dot{z}_w \\ &= c_c(z_c - z_w) + d_c(\dot{z}_c - \dot{z}_w) - c_w(z_w - z_g) + c_c\,z_w + d_c\,\dot{z}_w \\ &= c_c\,z_c + d_c\,\dot{z}_c - c_w(z_w - z_g) \quad \text{initial conditions } (z_c = 0 \text{ and } \dot{z}_c = 0) \\ &= -c_w(z_w - z_g) \end{aligned} \tag{13-6}$$

This shows, that the body and wheel would no longer be connected to each other (except for the static spring force), when such an ideal controller could be realized. This is illustrated in Figure 13-1b. The lag of damping results in undamped wheel dynamics (two poles on the imaginary axis) and the wheel will resonate as soon as it gets excited at its eigenfrequency (see Figure 13-2). Although this is an unrealistic situation, it is important to realize that the proposed disturbance control law can lead to an unstable system and thereby compromise the drive safety.

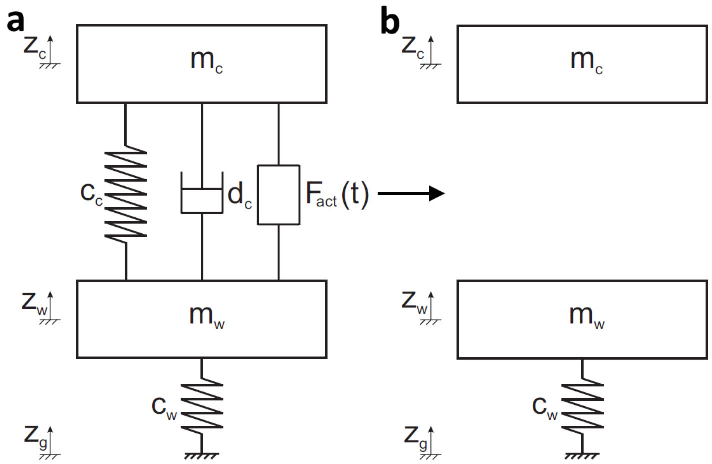

Figure 13-1: **a** Quarter car model used for the initial simulations. **b** Disturbance compensation resulting in undamped wheel dynamics, when the sensors and actuator are modeled to be ideal.

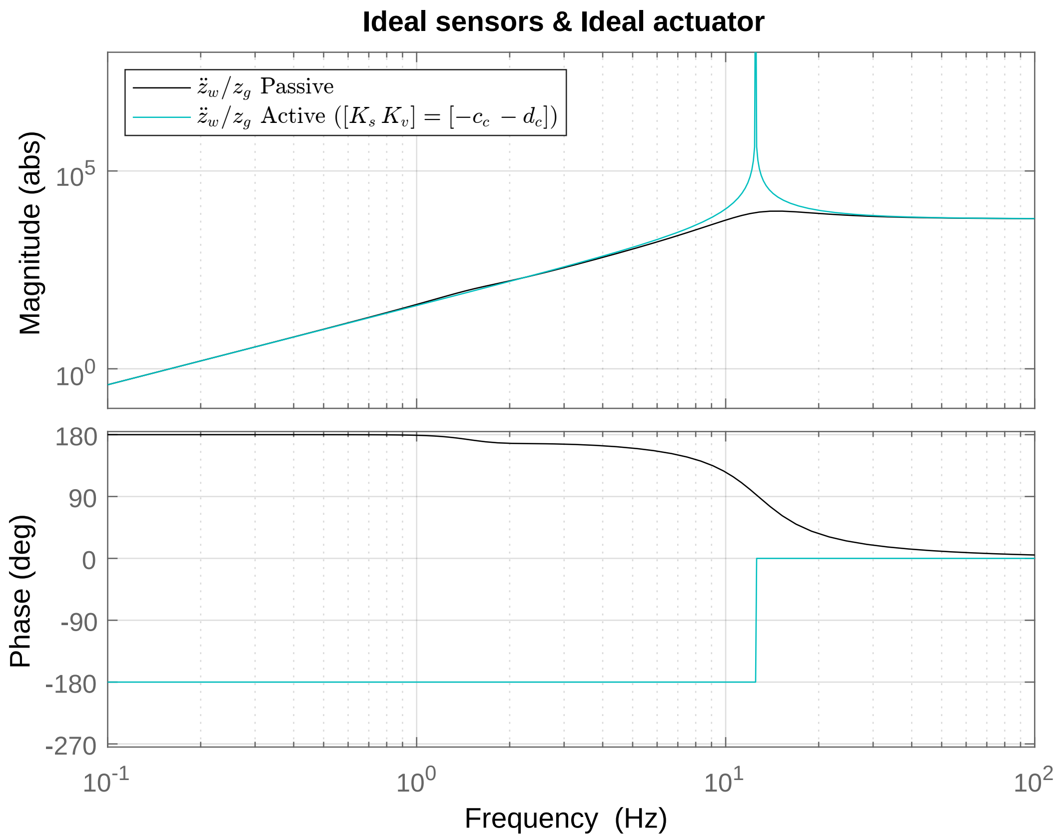

Figure 13-2: Instable wheel dynamics, when sensor and actuator are modeled to be ideal. Resonance peak at the wheel's eigenfrequency, undamped system poles at $\pm i\sqrt{c_w/m_w}$

13-1-1 Effect of sensor dynamics and actuator bandwidth

For more realistic simulations, it necessary to include the sensor and actuator dynamics into the model. The sensor dynamics follow from Section 12-2. The actuator dynamics are for a first approximation represented by a first order low-pass filter (see [27]) with a cut-off frequency of $f_c = 5$ Hz, that corresponds to the approximated system bandwidth.

$$\begin{aligned} H_{LP_1} &= \frac{1}{T_{act} \cdot s + 1}, \quad \text{where} \\ T_{act} &= \frac{1}{f_c \cdot 2\pi} = \frac{1}{5 \cdot 2\pi} \end{aligned} \tag{13-7}$$

Extending the model's state vector correspondingly to

$$\underline{x} = \begin{bmatrix} z_c & \dot{z}_c & z_w & \dot{z}_w & \dot{z}_{w_1} & \dot{z}_{w_2} & z_{w_3} & \dot{z}_{w_3} & F_{act} \end{bmatrix}^T$$

results in the following model, that considers the sensor and actuator dynamics

$$\dot{\underline{x}} = \begin{bmatrix} 0 & 1 & 0 & 0 & 0 & 0 & 0 & 0 & 0 \\ -\frac{c_c}{m_c} & -\frac{d_c}{m_c} & \frac{c_c}{m_c} & \frac{d_c}{m_c} & 0 & 0 & 0 & 0 & \frac{1}{m_c} \\ 0 & 0 & 0 & 1 & 0 & 0 & 0 & 0 & 0 \\ \frac{c_c}{m_w} & \frac{d_c}{m_w} & -\frac{c_c+c_w}{m_w} & -\frac{d_c}{m_w} & 0 & 0 & 0 & 0 & -\frac{1}{m_w} \\ \frac{c_c}{m_w} & \frac{d_c}{m_w} & -\frac{c_c+c_w}{m_w} & -\frac{d_c}{m_w} & -\frac{1}{T} & 0 & 0 & 0 & 0 \\ \frac{c_c}{m_w} & \frac{d_c}{m_w} & -\frac{c_c+c_w}{m_w} & -\frac{d_c}{m_w} & -\frac{1}{T} & -\frac{1}{T} & 0 & 0 & 0 \\ 0 & 0 & 0 & 0 & 0 & 0 & 0 & 1 & 0 \\ \frac{c_c}{m_w} & \frac{d_c}{m_w} & -\frac{c_c+c_w}{m_w} & -\frac{d_c}{m_w} & -\frac{1}{T} & 0 & -\frac{1}{T^2} & -\frac{2}{T} & 0 \\ 0 & 0 & 0 & 0 & 0 & \frac{K_v}{T_{act}} & \frac{K_s}{T_{act}} & 0 & -\frac{1}{T_{act}} \end{bmatrix} \underline{x} + \begin{bmatrix} 0 \\ 0 \\ 0 \\ \frac{c_w}{m_w} \\ \frac{c_w}{m_w} \\ \frac{c_w}{m_w} \\ 0 \\ \frac{c_w}{m_w} \\ 0 \end{bmatrix} u. \tag{13-8}$$

Where for the body's vertical acceleration $\ddot{z}_c$ the output is equal to

$$y = \begin{bmatrix} -\frac{c_c}{m_c} & -\frac{d_c}{m_c} & \frac{c_c}{m_c} & \frac{d_c}{m_c} & 0 & 0 & 0 & 0 & \frac{1}{m_c} \end{bmatrix} \underline{x} + 0\,u \tag{13-9}$$

and for the wheels' vertical acceleration $\ddot{z}_w$ the output is equal to

$$y = \begin{bmatrix} \frac{c_c}{m_w} & \frac{d_c}{m_w} & -\frac{c_c+c_w}{m_w} & -\frac{d_c}{m_w} & 0 & 0 & 0 & 0 & -\frac{1}{m_w} \end{bmatrix} \underline{x} + \frac{c_w}{m_w} u. \tag{13-10}$$

The additional sensor dynamics and actuator bandwidth result in a system that is no longer unstable. This follows from simulations and is illustrated in Figure 13-3.
Due to the limited actuator dynamics (relatively low cut-off frequency of $f_c = 5$Hz), this was to be expected around the wheel's eigenfrequency. It is now no longer possible to completely compensate for the suspension spring and damping in the system at higher frequencies.
Nevertheless, even though the input sensor dynamics compromise the control input signals and the actuator's bandwidth is limited, the disturbance compensation algorithm is able to reduce the motion of the vehicle's body around its eigenfrequency. Tuning the control parameters K_s and K_v (reducing them) furthermore improves the stability of the system, while still leading to a reduction of the vehicle's vertical body acceleration. The effect of the signal conditioning on the signals is plotted in Figure 13-4.

From these simulation results, it is concluded, that the proposed disturbance compensation algorithm (11-9) based on the measured vertical acceleration of the wheel shows the desired effect. This motivates to replace the passive damper in the mathematical model by the linear model description of the active damper unit derived in Section 9-5. This leads to a model that gives a more realistic approximation of the actual active suspension system.

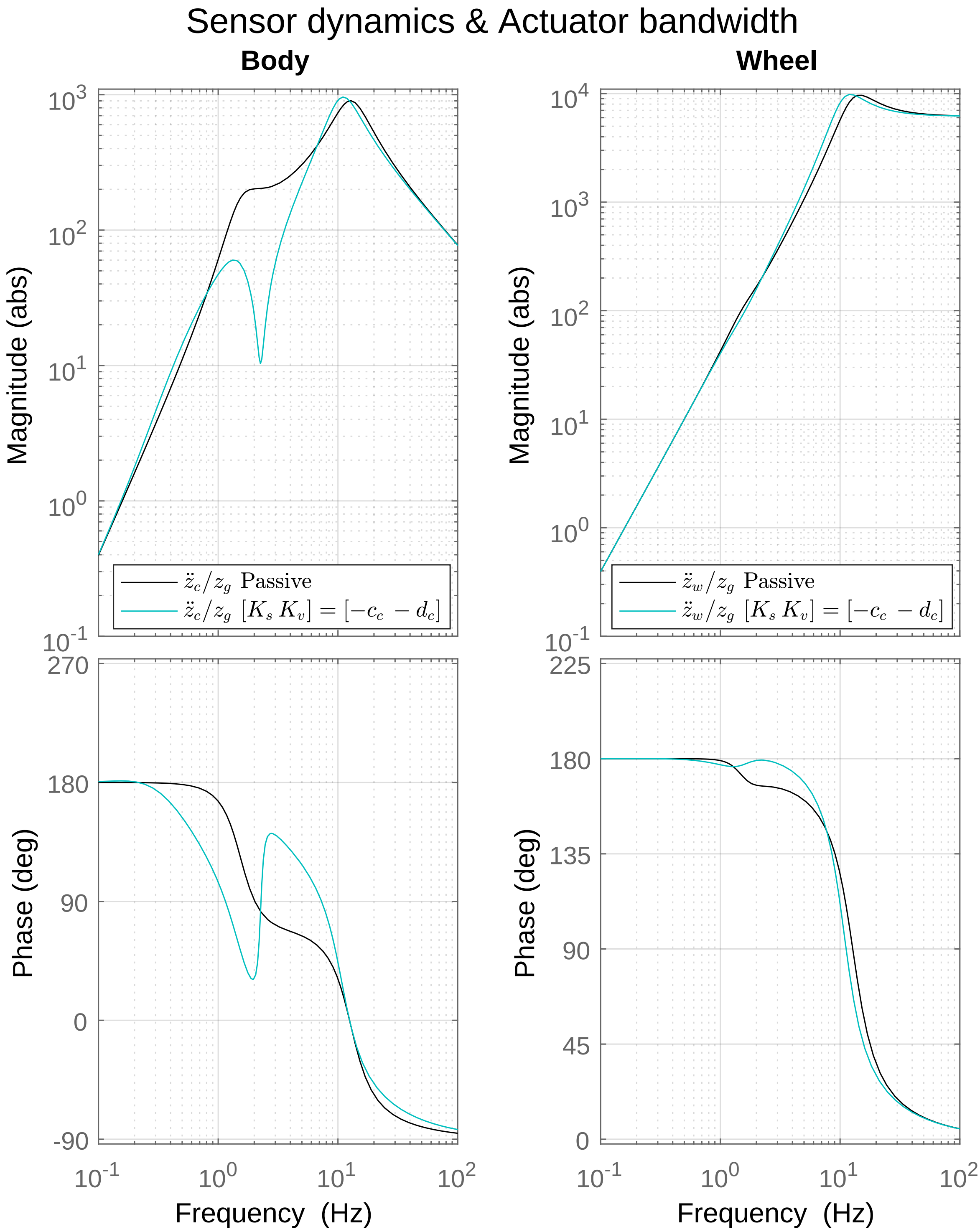

Figure 13-3: Frequency response of the system (13-8). Actuator dynamics, approximated by a low-pass filter stabilize the system around its wheel eigenfrequency. Body acceleration is reduced around the vehicle's body eigenfrequency, despite non-ideal sensors.

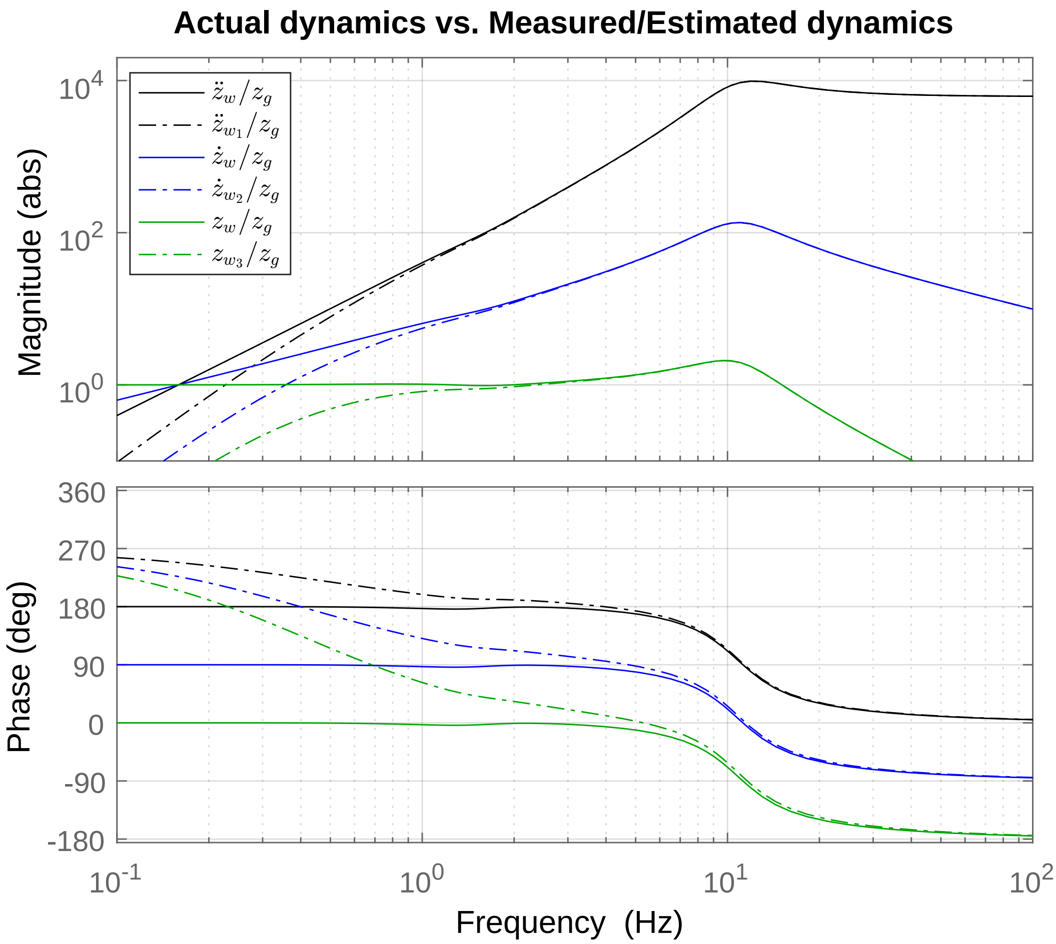

Figure 13-4: Effect of the signal conditioning on the signal dynamics compared to the unfiltered actual signal dynamics. $90°$ Phase shifts between the acceleration, velocity and position signals are illustrated by the phase plot.

13-2 Augmented disturbance compensation algorithm

Replacing the passive damper in the model (13-8) by the linear active damper model makes the system more realistic. At the same time, it also offers the opportunity to redefine the disturbance compensation algorithm (11-9).
Where the suspension spring compensation term K_s is added to the model as a tuning factor that is multiplied with the spring stiffness, the velocity dependent damping compensation (K_v) is implemented differently. Analog to this different implementation, an additional third term is introduced as well.

13-2-1 Velocity term

Preserving the wheel acceleration signal based control algorithm, the control parameter K_v is implemented differently. Instead of multiplying the wheel's vertical velocity with a damping factor, to results in a desired force to compensate for the system's damping, the wheel's vertical velocity is multiplied with the piston area of the damper. This results in a volume flow q, which after multiplication with the tuning factor K_v is subtracted from the desired volume flow in the active damper model. Physically, this means that an increase, or decrease of the volume in the hydraulic cylinder, caused by the vertical velocity of the wheel, is compensated for by pumping away the resulting change in volume. Dividing the required volume flow by the displacement volume of the pump (see Section 9-2-2), allows to determine the required rotary speed of the pump.

13-2-2 Acceleration term

Analog to this, an upcoming change in the hydraulic cylinder volume by movement of the wheel can be detected from the wheel's acceleration. Theoretically this enables faster compensation of changes in the damper's movement, since integration of a signal $1/s$ comes with a 90 degrees signal phase delay

$$\angle\frac{Numerator}{Denominator} = \angle tan\left(\frac{Im\{Numerator\}}{Re\{Numerator\}}\right) - \angle tan\left(\frac{Im\{Denominator\}}{Re\{Denominator\}}\right), \tag{13-11}$$

$$\angle\frac{1}{s} = \angle tan\left(\frac{0}{1}\right) - \angle tan\left(\frac{1}{0}\right) = 0^\circ - 90^\circ = -90^\circ. \tag{13-12}$$

This means, that an acceleration term, defined as K_a, will have 180° phase lead with respect to the position term K_s.

$$\text{acceleration } (K_a) \underset{-90^\circ}{\Longrightarrow} \text{velocity } (K_v) \underset{-90^\circ}{\Longrightarrow} \text{position } (K_s)$$

This effect can also be seen in Figure 13-4, where the wheel acceleration, velocity and position are plotted for the system given in (13-8). As a result of this behavior, the additional acceleration compensation term is expected to compensate for high frequency disturbance.

The acceleration compensation term K_a is implemented into the model according to the following reasoning:
Multiplication of the wheel's vertical acceleration with the area of the piston gives a change

in the volume flow ($\dot{q}$). Dividing this term by the displacement volume of the pump, results in a change in the pump rotational speed. Multiplying this with the inertia of the pump J and tuning parameter K_a results in the desired required motor torque, that increases or decreases the pump's rotational speed.

13-3 Augmented linear model

The resulting three disturbance compensation terms, are implemented into the linear model (see Figure 13-5). The initial wheel model is replaced by the quarter car model and the required sensor signal filters are also included. The resulting filtered signals are multiplied with the corresponding terms and fed back into the system.

Since the quarter car model also considers the vehicle's body, the volume flow resulting from the relative damper velocity is used, rather than the volume flow as a result of the wheel's velocity. At the same time, a Skyhook damper term K_{SH} is added to the model. This term allows to consider the system performance with both the disturbance compensation and Skyhook algorithm. The latter will tell, if the disturbance compensation algorithm can be used as an enhancement to the already existing control modules.

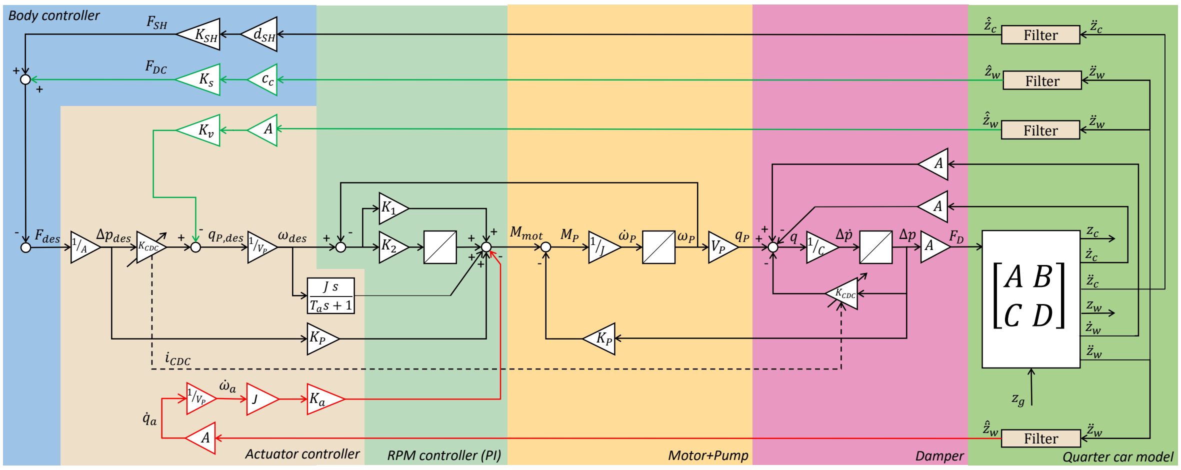

Figure 13-5: Augmented linear actuator model of the project. K_s, K_v and K_a parameters added for disturbance compensation. K_{SH} parameter added to simulate the Skyhook algorithm

The state-space representation of the augmented linear model is given in Appendix B. The effect of the more realistic damper model on the vehicle dynamics (with disturbance compensation and Skyhook control terms set to zero) is illustrated in Figure 13-6. This figure clearly shows the differences between the simple linear model with constant damping term and the augmented model. At the same time, although the passive damper is replaced by the linearized actuator model, the two models show similarity. From the figure it follows, that the inactive actuator behavior reduces the suspension's damping ratio, resulting in the peaks at the vehicle's body eigenfrequency and wheel's eigenfrequency (see damping ratio Section 4-1). A different passive CDC valve layout could change this.

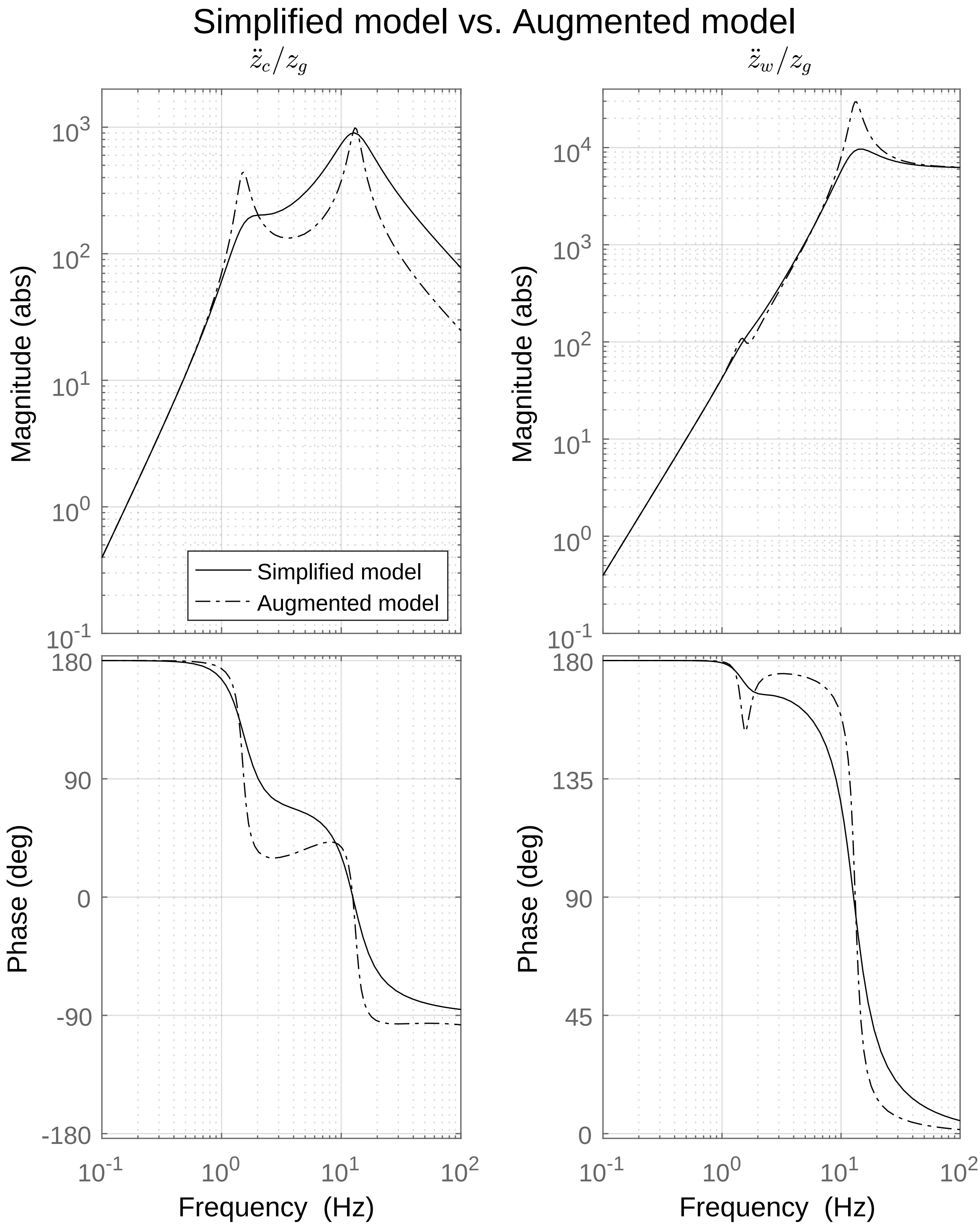

Figure 13-6: Initial quarter car model with linear spring and damper dynamics (simplified) and augmented model with actuator dynamics (augmented). Plot of the passive behavior (K_s, K_v, K_a and K_{SH} equal to zero)

13-4 Disturbance control setting

The effect of varying control parameters K_s, K_v and K_a can now be investigated on the augmented system. The result is shown in the Figures 13-7, 13-8 and 13-10. In each figure, the corresponding control parameter is varied from $0 - 1.2$ in 0.2 sized steps. Apart from stability limits, these figures also show the (frequency) range in which each control term has the greatest effect on the system.

13-4-1 Variation of position compensation term

The spring force compensation term K_s effects the system in the relatively low frequency range $1-8$ Hz. From the signal integration (see Subsection 13-2-2), this was to be expected. Varying the control parameter significantly affects the dynamics of the vehicle's body. Increasing K_s reduces the body's vertical acceleration. Since this term does not influence the system's damping, it hardly affects the system around the wheel's eigenfrequency and will not lead to stability issues there. As soon as K_s reaches values ≥ 1 however, its effect on the vehicle's body changes (extreme degradation of the body's acceleration and a sudden phase shift in the system) and the simulation results are not reliable anymore. This has to be considered in the real vehicle test. It is therefore not recommended to increase this control parameter above 0.8 for initial testing.

13-4-2 Variation of velocity compensation term

The damping force compensation term K_v effects the system in the medium to high frequency range $4 - 30$ Hz. The upper limit of 30 Hz is chosen here, since it corresponds to real road conditions (see Section 3-1). Since this term directly influences the system's damping, the stability around the wheel's eigenfrequency is compromised for high K_v values. In real conditions, this can lead to dangerous situations. It also means that this control parameter does not improve the vehicle's dynamics over its whole range. A compromise has to be found. A close up of the system's behavior at the wheel's eigenfrequency is shown in Figure 13-9. This figure shows, that compensating approximately sixty percent ($K_v = 0.6$) of the system's damping results in significantly increased acceleration around the wheel's eigenfrequency. This motivates to start the real vehicle tests with low K_v values, to prevent unsafe situations. Increasing the control parameter in small steps will tell where the limit is.

13-4-3 Variation of acceleration compensation term

Variation of the acceleration term K_a has a no considerable effect on the system's dynamics. It only influences the system at very high frequencies and is not expected to make any difference. Since the simulation model is an approximation of the real system, the acceleration compensation term will still be considered in the vehicle tests. If it turns out, that the effect of the control parameter is not noticeable, then it can be simply ignored by setting K_a to zero.

13-4-4 Combined control parameters

The system dynamics change ones more, as soon as the control parameters are combined. Combining them allows for a further enhancement of the system dynamics. A combination of K_s and K_v enables to reduce the vertical accelerations over almost the complete $0-30$ Hz frequency range. Only the wheel dynamics are compromised, but remain within boundaries, when K_v is kept small. The effect of K_a still only marginally affects the system and is therefore no longer considered in the simulations.

13-5 Disturbance compensation and Skyhook control

As stated in the beginning, disturbance compensation control can improve the general system behavior by complementing existing control algorithms. So far, the simulations have shown, that by only looking at the wheel, a part of the induced road disturbance can be filtered out by the disturbance compensation algorithm. The remainder of the disturbance is however still transmitted to the vehicle's body.

For further improvement of the system dynamics, the Skyhook algorithm is used to damp the motion of the vehicle's body. Since the disturbance compensation and Skyhook control algorithms act independent of each other, they can be considered as separate control modules and are easily added in the model. Simulations confirm, that combining both control methods enhances the controller performance. Figure 13-11 shows the effect of a favored control setting considering both the disturbance compensation and the Skyhook algorithms. The figure also shows the frequency ranges of both control strategies. The Skyhook algorithm greatly reduces the vertical acceleration of the vehicle's body around its eigenfrequency, whereas the disturbance compensation algorithm also reduces the motion a higher frequency accelerations. Together they complement each other.

The positive results of the simulations in this chapter motivate to implement the proposed disturbance controller into the test vehicle. The simulations not only show the stability limits of the system, but they also help understanding the effect of the different control parameters on the system. These insights will be useful for the implementation and testing of the controller in the real test vehicle.

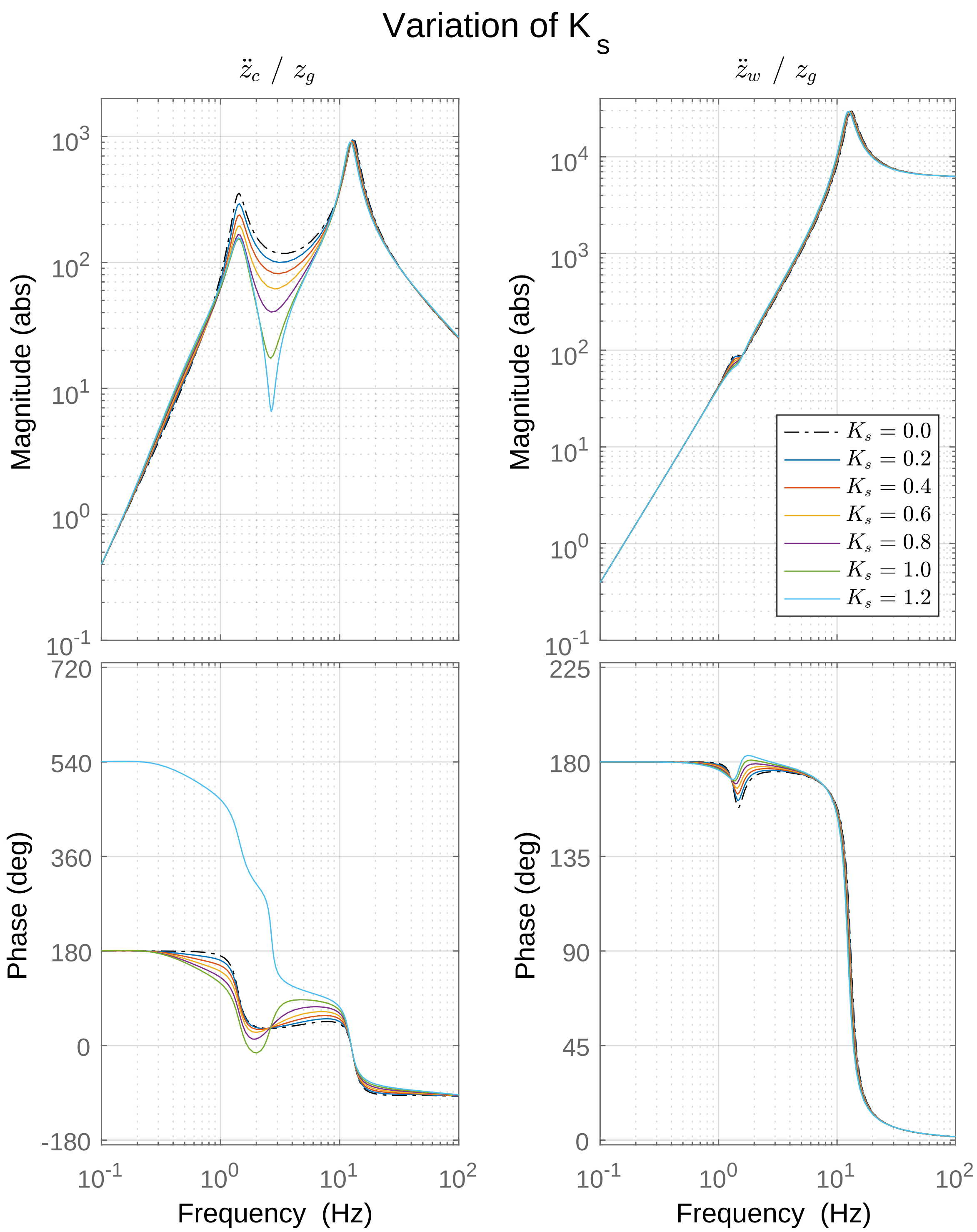

Figure 13-7: Effect of the spring compensation term K_s on the system. All other control parameters equal to zero.

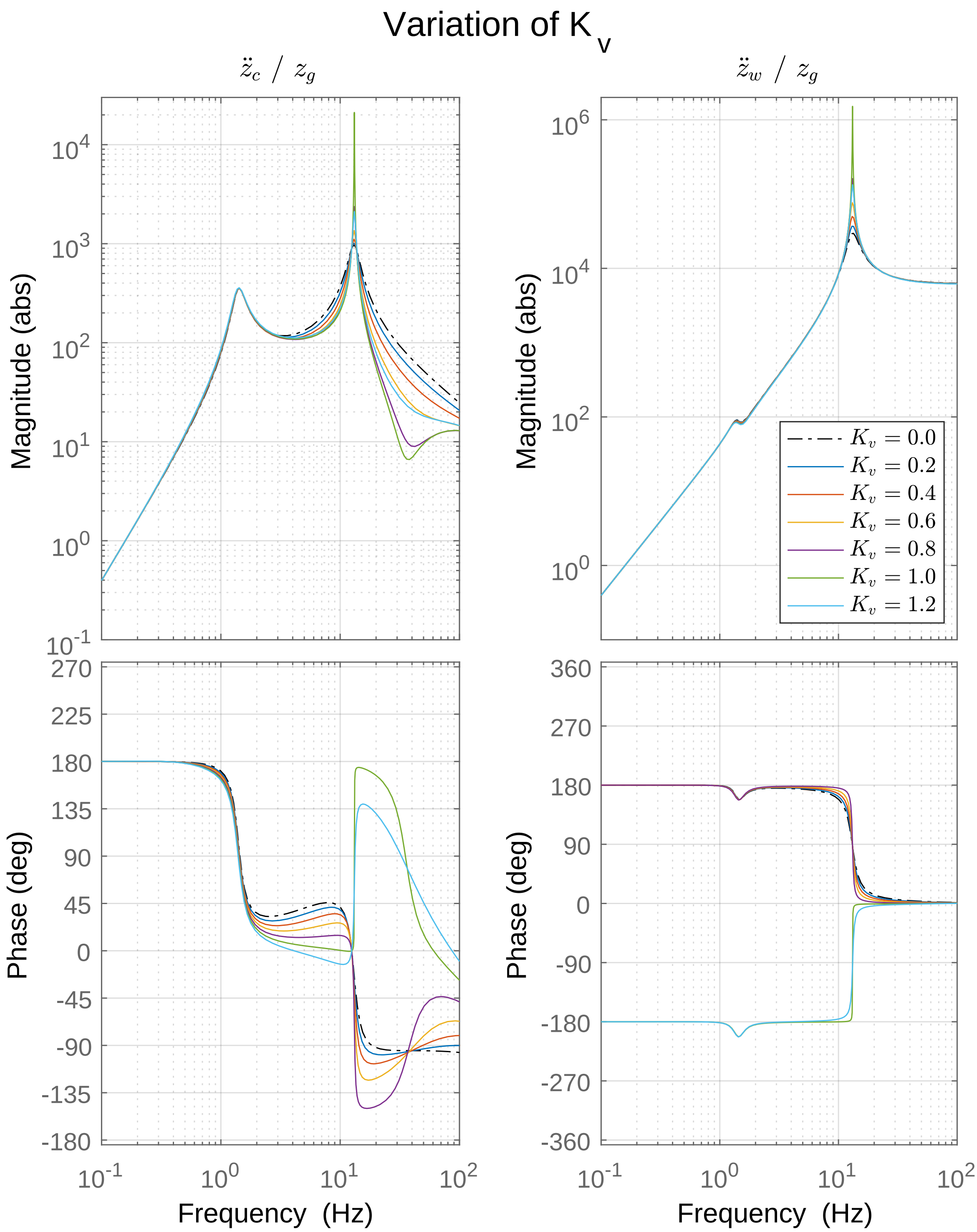

Figure 13-8: Effect of the damping compensation term K_v on the system. All other control parameters equal to zero. Compensating the damping results in high wheel accelerations, which can compromise safety.

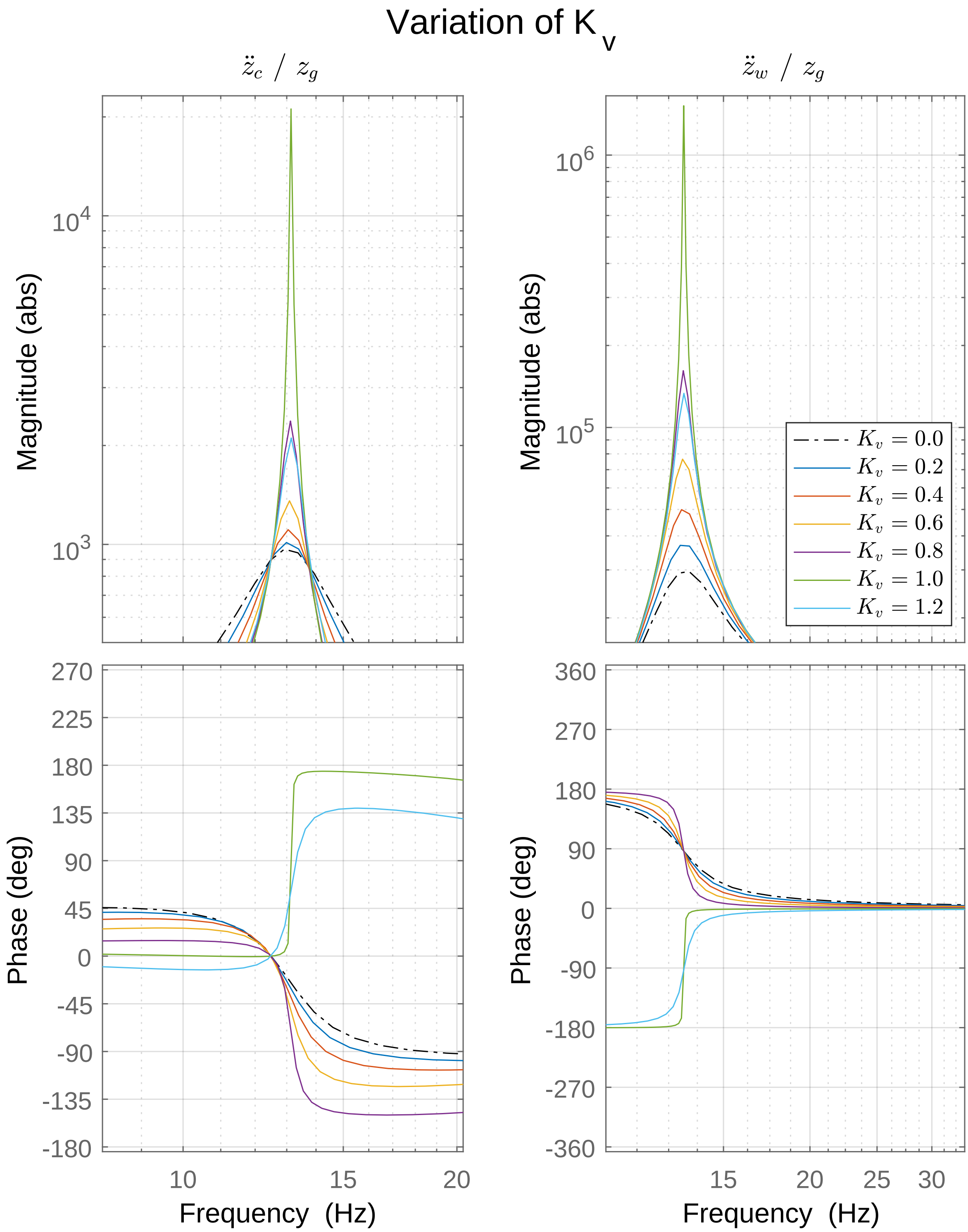

Figure 13-9: Close up around the wheel's eigenfrequency to illustrate the effect of K_v on the system.

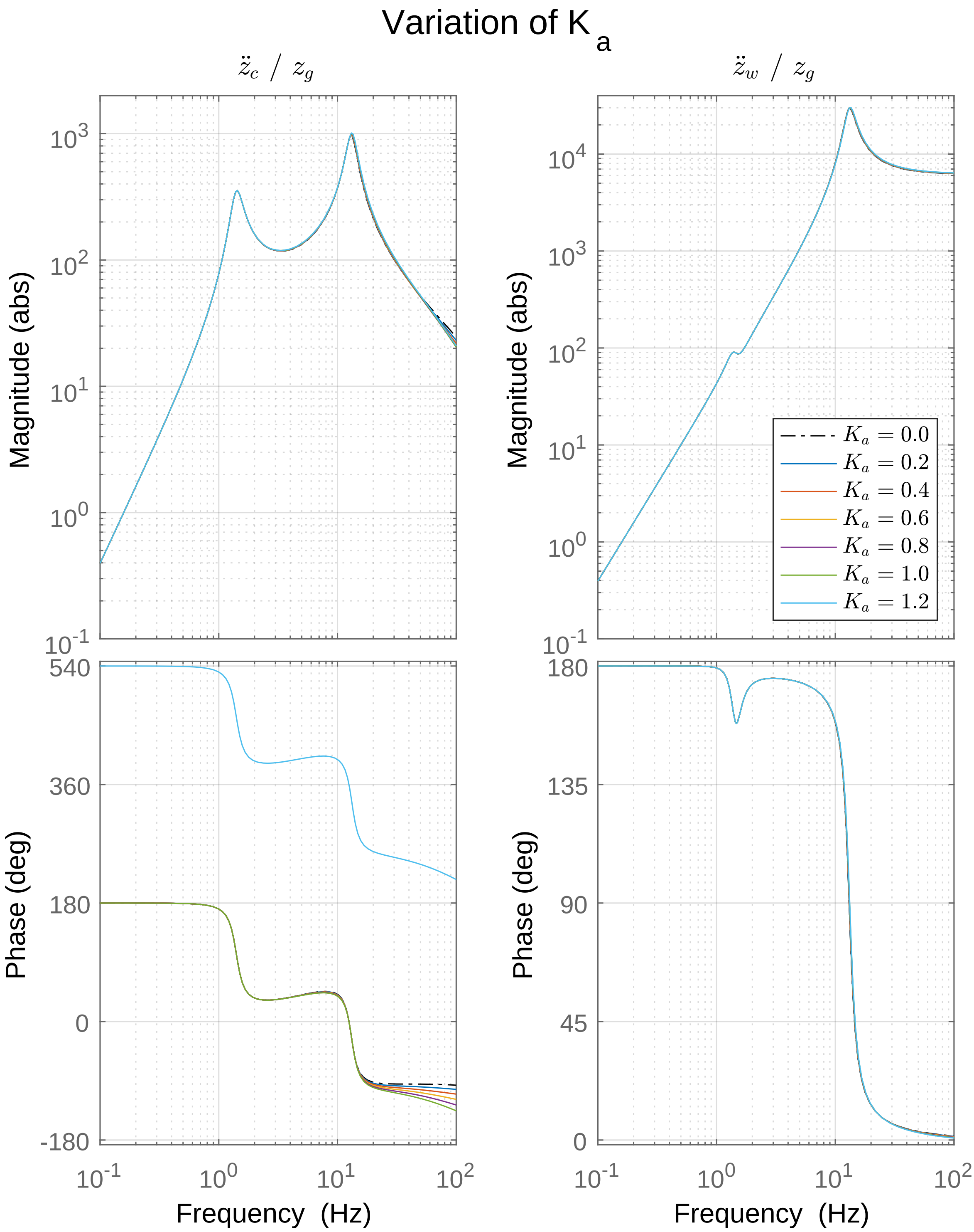

Figure 13-10: Effect of the acceleration compensation term K_a on the system. All other control parameters equal to zero. K_a only marginally influences the system dynamics.

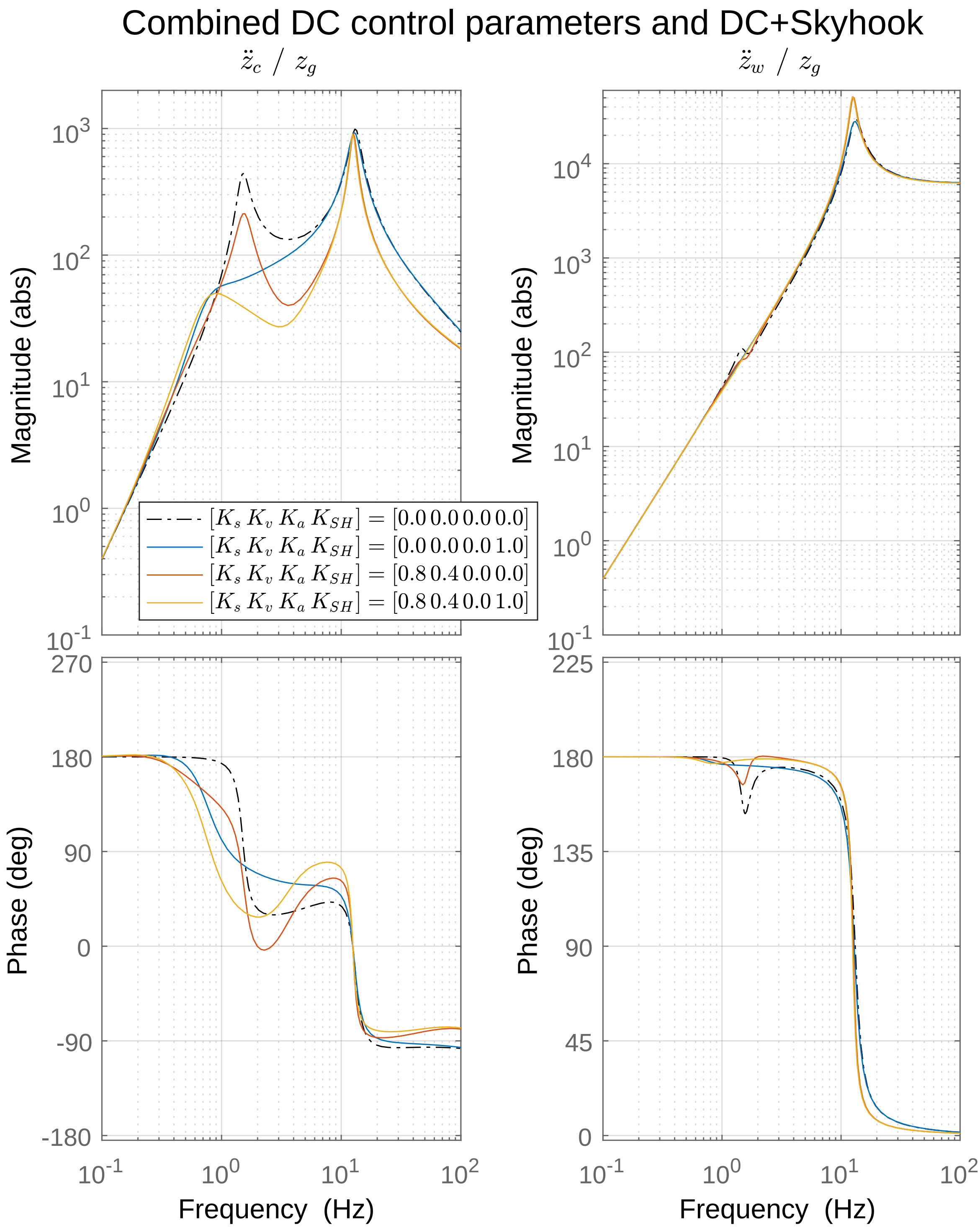

Figure 13-11: Combined test setups showing the effect of disturbance compensation, Skyhook and both control algorithms together.

Chapter 14

Implementation

Simulations show the desired disturbance compensation control effect on the system. The next step in the development is to test the control algorithm in the test vehicle. To do so, it is implemented in the already existing controller structure. Due to the modular structure of the vehicle controller, this is done without the need to rebuild the entire controller.

14-1 Augmented controller structure

A schematic picture of the augmented controller structure is given in Figure 14-1. First of all, the missing wheel acceleration, velocity and position were added to the original model. This was realized by extending the signal conditioning block, such that it also accounts for the required wheel signals. Then a module for the spring compensation term K_s was implemented additionally to the already existing control modules in the *body* controller. Since the output of this module is the required force for each wheel and all the other modules output modal quantities, the required disturbance spring compensation force is transformed into modal quantities such that it can be added to the other terms. Once added, the inverse modal transformation calculates the resulting desired forces for each active damper unit.

14-2 Augmented actuator controller

The velocity and acceleration compensation terms (K_v and K_a respectively) are implemented into the *actuator* controller to finally complement the augmented controller structure. The volume flow resulting from the velocity term is considered in the required volume flow calculation and the acceleration term influences the required pump torque and rotational pump speed. This new damper controller layout is represented schematically in Figure 14-2.

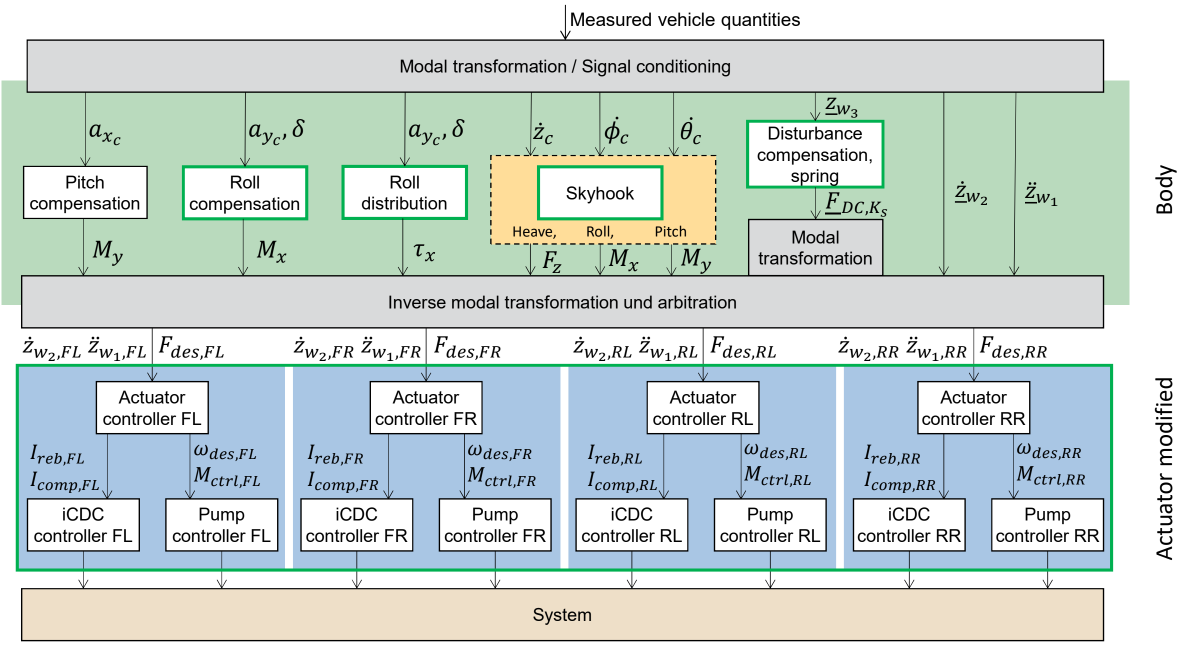

Figure 14-1: Augmented controlframework of the controller used in the project vehicle. Layout according to the Ammakon principle.

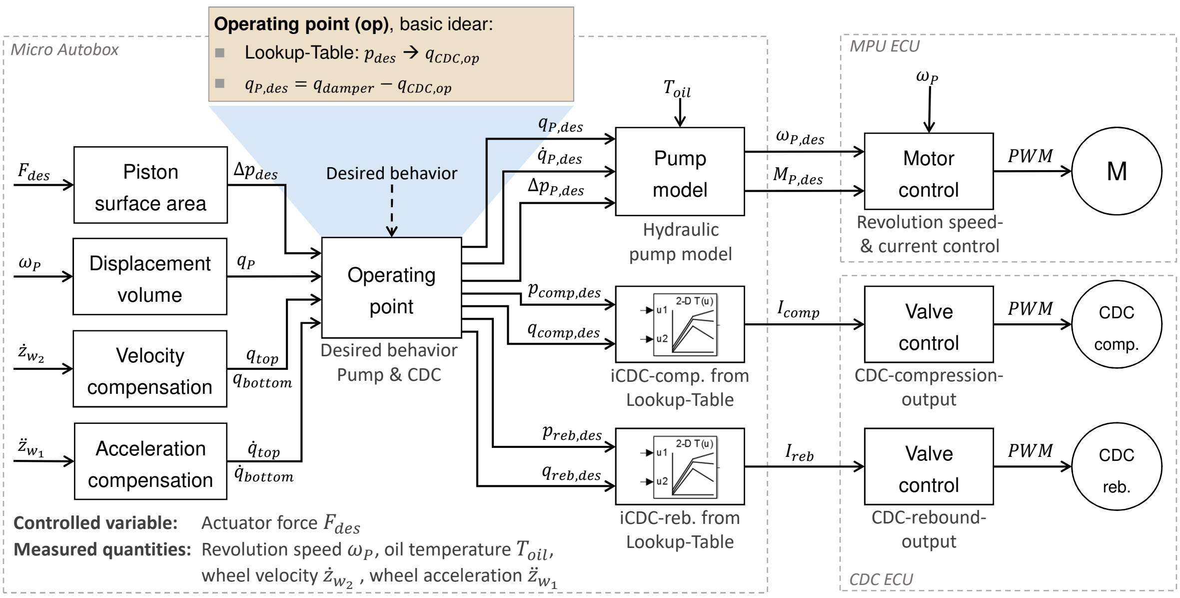

Figure 14-2: Augmented actuator controller. Wheels velocity and acceleration are added to the model as input as well as their corresponding disturbance compensation terms (K_a and K_v respectively).

Chapter 15

Test facility and road test preparation

The Automotive Testing Papenburg (ATP) test facility in Papenburg (Germany), was the test facility of choice to test the disturbance compensation controller for the first time. There, it is not only possible to test concept cars that are not allowed to drive on public roads, but the facility also offers a variety of road sections. These road sections feature different excitation profiles, which is ideally suited for vehicle testing.

This chapter lists the road sections used for testing the disturbance compensation controller. The road section information is extracted from the ATP website [1].

15-1 Road sections

The road sections chosen for testing are selected according to their road excitation profile. Important is to have a wide range of excitation profiles to cover the biggest spectrum. For the actual test drives, also the vehicle speed and starting and stopping points were defined to ensure repeatability.

The controller setup parameters for the tests are initially orientated according to the simulation results and are then varied with small steps for safety/stability reasons. Furthermore, an initial measurement with an inactive (also revered to as Soft Open, referring to the *open* CDC valves and correspondingly *soft* damping)) suspension setup is made at each road section and considered as a reference.

15-1-1 High Speed Oval (ORK)

The High Speed Oval (ORK), German: Ovalrundkurs, is the place to test vehicles at high speeds. It features an oval course with banked curves up to 49.7° which results in zero lateral force, up to 250 km/h, during cornering. The total course is 12.3 km long and has multiple drive lanes, which partly feature different road profiles.

The inner drive lane offers a straight, one kilometer long, asphalted road section with long-wave, equal-sided excitation (resulting in vehicle pitch motion) almost directly followed by a straight, 648 meter long, asphalted road section with long-wave, two way excitation (resulting in vehicle roll motion). Moreover, seen in the driving direction, the amplitude of both excitation profiles increases step-wise towards the end of each section.
The excitation profiles in these sections are laid out, such that a vehicle gets excited around its sprung mass eigenfrequency ($f_c \approx 1.2$ Hz, where $_c$ denotes car and not a cut-off frequency), when driving with a velocity of 80 km/h. Considering this, the test vehicle is driven at 80 km/h to test the disturbance compensation controller with low frequency excitation roadway input.

15-1-2 Durability Road (DLK)

The south section of the Durability Road (DLK), German: Dauerlaufkurs, is a 4.8 km long road with various special modules. These modules vary from manhole covers to replications of actual road sections found in Germany. The DLK is designed to offer all possible excitation profiles and extreme road inputs one can find on public roads. The track has two lanes (inner and outer lane) that both have a different road profile. The inner drive lane is used for testing the disturbance compensation controller since it offers the greater variety of modules and it allows others to overtake.
From experience and an initialization lap, it is decided to aim for a velocity of 80 km/h on the straight sections and a velocity of 60 km/h in the curves.

15-1-3 Rough Road (SWS)

The Rough Road (SWS), German: Schlechtwegstrecke, features four different drive lanes, each being straight and each having different excitation profiles. Except for the normal road (third) drive lane, the drive lanes offer rough to very rough road conditions.

Two of these lanes are considered to be relevant for the testing and validation of the the disturbance compensation controller.

1. Pavement lane, offering:
    - 300 meters cobblestone road surface followed by
    - 25 meters normal road (asphalt) and
    - 150 meters small set pavement
2. Concrete plates lane, offering:
    - concrete plate jolts downwards (increasing steps) shortly followed by
    - concrete plate jolts upwards (increasing steps)

The test vehicle is driven over the pavement lane with a velocity of 30 km/h. Driving faster is not realistic when considering the rough road conditions and could potentially damage the vehicle. The concrete plates lane is not so tough on the vehicle's suspension and can be driven over with a velocity of 60 km/h.

Chapter 16

Parametrisation and evaluation

This chapter introduces four performance criteria for the assessment of the disturbance compensation algorithm. The first three criteria are based on the vertical cabin acceleration and allows to assess the driving comfort. Each of these three criteria has its own frequency range (from low to high) to asses the effect of the three different disturbance compensation terms. The last criterion is based on the vertical wheel acceleration and is used to assess the condition of the road surface.
In this chapter, the measurement data from the test drives are subsequently evaluated by means of these criteria. In the evaluation process, different evaluation methods were considered to find the clearest representations of the measured quantities. Scatter and time domain plots are found to be the clearest and easiest to interpret. Although excitation frequencies play a great role, no new results were found using Fourier transformations to evaluate the measurement data. Since none of the measurements are exactly the same, it is furthermore hard to compare them in the frequency domain. The scatter plots enable to quantitatively assess the measurements, whereas the time domain plots are easy to interpret.

16-1 Performance criteria

From the previous simulations it follows, that the disturbance compensation control parameters (K_s, K_v and K_a) influence the vehicle dynamics in different frequency ranges. The effect of low frequency road excitation is mostly affected by K_s, whereas the higher frequency road excitation is influenced by K_v (and fractionally by K_a). To exploit these insights from the simulations, cabin criteria based on the measured body acceleration are defined in three different frequency ranges. This theoretically enables to optimize each control parameter in its ”own” frequency range.

16-1-1 Cabin criterion

The cabin criterion is composed from the vertical cabin accelerations from each corner, by leading them through different band-pass filters and subsequently adding the absolute values of the resulting signals. This is illustrated in Figure 16-1, with the frequency filters abbreviated as H_{BW_i}, with $i = 1, 2, 3$.

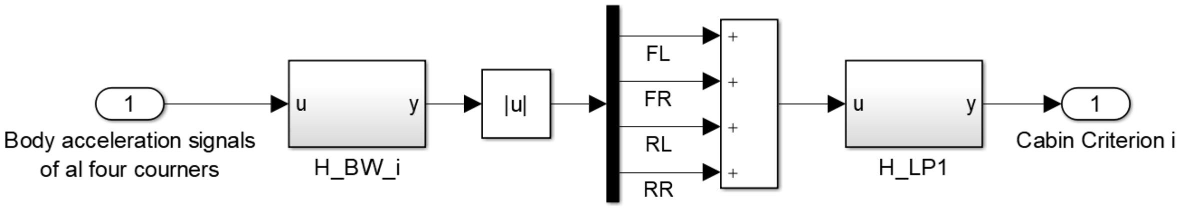

Figure 16-1: Schematic representation of the formula that calculates the cabin criterion.

The absolute value of the measured acceleration ensures, that positive and negative accelerations do not cancel each other out. The additional low-pass filter (H_{LP}) subsequently filters high fluctuation peaks. It has a cut-off frequency of 0.25 Hz.

The frequency ranges of the band-pass filters are

1. 0.4 – 3.0 Hz
    - 0.4 Hz is the lower frequency bound determined by the sensor signal quality (lowest frequency to still ensure a drift free signal)
    - 3.0 Hz limits the first bandwidth filter, such that it includes the vehicle's body eigenfrequency (≈ 1.2 Hz)
2. 3.0 – 10 Hz
    - medium frequency range
    - expected to cover the range above the vehicle's body eigenfrequency up to almost the wheel's eigenfrequency in which the actuator can still enhance the vehicle dynamics
3. 10 – 30 Hz
    - high frequency range
    - expected to include the fastest signal information and range in which the actuators are limited
    - upper limit defined by the relevant road excitation frequency range (see Section 3-1)

16-1-2 Road criterion and correlation

Initially, a criterion to assess the road quality was defined according to the same reasoning. Instead of all four available acceleration signals however, only the acceleration signals of the two front wheels are used. Since a vehicle primarily drives forward, the front wheels usually are the first to experience a change in the road profile. Defining a road criterion based on this, will therefore allow to react on changing conditions the fastest.

Although the modular active damping units can be controlled separately, only one road criterion for all four units is used to minimize the control parameters. This initially helps to explore the system's capabilities, without making the implementation unnecessary complicated. In a later development stage, this simplification can easily be adjusted.

Another simplification of the road criterion actually followed from the first measurement evaluations and could already partly be expected from the theoretical background, in which is stated, that road surfaces can be approximated by a Gaussian distribution (see Section 3-1).
This approximation, as it turns out, also holds in practice, since the acceleration signals of the two front wheels filtered by three different band-pass filters show an almost linear correlation of the resulting road criteria among the different frequency ranges. This holds for all road sections (ORK, DLK and SWS) as is illustrated by the scatter plots in Figure 16-3.
Here it has to be noted, that even though, not the road surface, but the wheel acceleration is measured, still the typical road surface characteristic emerges. This outcome supports the choice to use a signal based, instead of a model based controller, as it turns out that measuring the vertical wheel acceleration still allows to assess the state of the road surface. Neglecting the wheel dynamics by only considering a signal based approach, therefore does not compromises the road condition assessment according to the measurements.
The plotted data in Figure 16-3 is acquired from the test vehicle with, driving with an inactive suspension setup. From this correlation it finally is concluded, that there is no use in defining three different criteria indicating the state of the road surface. Instead, the high frequency range criterion is selected as road criterion for all further measurement evaluations. The $10-30$ Hz frequency range criterion is chosen for its fast (high frequency) signal information and the criterion is calculated according to Figure 16-2.

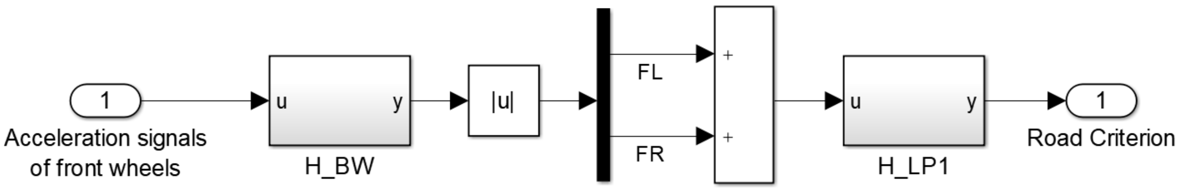

Figure 16-2: Schematic representation of the formula that calculates the road criterion.

16-1-3 Cabin criterion correlation

The vehicle body criteria resulting from the same test drives do not show a linear correlation among the different frequency ranges (see Figure 16-4). This is comprehensible as well. Low frequency excitation often leads to high amplitudes in the vehicle's body motion as it gets excited around its relatively low eigenfrequency. High frequency excitation on the other hand is primarily compensated by the tires and suspension. Furthermore, the relatively high mass of the vehicle's body prevents high frequency motion of the body itself.

16-2 Durability Road and Cobblestone

The left side of Figure 16-5 shows the cabin criteria at the different road sections in the defined frequency ranges for an inactive suspension setup plotted against the $10 - 30$ Hz road criterion. It shows the impact of the different road sections on the cabin. Whereas the smooth asphalted road surface with long sine wave excitation of the ORK leads to motion of the cabin in the $0.4 - 3.0$ Hz frequency range, it hardly has an effect on the vehicle's body in the higher frequency ranges. The rough Cobblestone road section on the other hand, has an effect on the body in all frequency ranges and especially effects the body in the medium to high frequency ranges. From the figure it furthermore follows, that the DLK and Cobblestone road sections already cover all the occurring road excitation profiles. The right side of Figure 16-5 shows that this also holds for a suspension setting with the disturbance compensation controller activated. As it turns out, this actually holds for all suspension settings, which motivates to confine the road test to the DLK and Cobblestone road sections only.

16-3 Suspension setup

Confining the road tests to the DLK and Cobblestone road sections and evaluating the road and cabin with the introduced criteria, gives the outline for the subsequent road testing. Table 16-1 lists some of the considered suspension setups considered in the tests. These particular setups are selected here, since they enable to clearly explain the effect of different control parameter settings. The measurement results are explained both objectively as well as subjectively in the next sections.

Table 16-1: Road test procedure

Setup	$\boldsymbol{K_s, K_v, K_a}$	**Commend**
Soft Open	$0.0, 0.0, 0.0$	Reference
Active, low DC	$0.5, 0.5, 0.0$	K_s and K_v equal
Active, optimal DC	$0.7, 0.3, 0.0$	From simulations promising setup
Active, relatively high DC	$0.7, 0.7, 0.0$	K_s and K_v equal, relatively aggressive setup
Active, high DC	$0.9, 0.9, 0.0$	K_s and K_v equal, aggressive setup

16-3-1 Objective results

The 3D-scatter plots in Figure 16-6 show the different outcomes as result of the different suspension settings in the three cabin criteria frequency ranges. In the lowest frequency range (cabin criterion $0.4 - 3.0$ Hz), all active disturbance compensation control settings result in a reduction of the body's vertical acceleration. In the higher frequency ranges, this behavior changes. According to Section 5-1 a change in the dynamic behavior was already to be expected. As soon as an active suspension unit is actively intervening in the vehicle dynamics, more or less distinct ranges in which the vehicle dynamics change occur:

- the low frequency range, where the system behaves as desired,

- a transitional phase, where the active and passive vehicle dynamics mix
- and a higher frequency range, where the system acts as if it were passive.

Although the graphs in the figure for the different suspension settings seem to agree to this principle, a close look tells that only the first characteristic really occurs. The higher frequency behavior is different. Instead of a transition to the inactive suspension behavior, the vehicle's vertical acceleration dynamics get compromised as:

- the evaluated frequency range increases ($3.0-10$ Hz versus $10-30$ Hz)
- and the disturbance compensation control parameters increase.

This behavior is illustrated in Figure 16-7, where the 3D-plots of Figure 16-6 are rotated to the yz-plane (suspension setups against cabin criterion respectively). The measurements show that the active suspension units, with different disturbance compensation settings, are able to improve the comfort in the low frequency range, but at the same time compromise the vehicle's dynamics in the higher frequency ranges.

Considering the active damper unit concept and vehicle's controller structure, this behavior can be explained. To do so, a second look at the active damper unit's design is necessary.
As soon as an active damper force is demanded, the hydraulic pump generates a volume flow and the CDC valves "close" to allow a pressure to be build up in the system. Critical here is the resistance in the volume flow as a result of the activated CDC valves. Without this resistance, no active force would be generated, as the effect of the hydraulic pump would be minimal. The resulting volume flow would hardly be restricted and the damping fluid would just be pumped around in the system. The CDC valves are thus necessary to actively generate a force. As soon as the CDC valves restrict the system's volume flow however, the damping ratio is also effected. The more restricted the volume flow is, the firmer the damping gets. To generate an active force, the system's damping thus automatically becomes firm and high frequency excitation from the road is increasingly transmitted to the vehicle's body.
The attempt to subtract the additional volume flow, caused by movement of the wheels, with the K_v and K_a terms is, as it turns out, not sufficient to compensate for this firm damping. The theoretically fastest term K_a does not even has any noticeable effect on the system dynamics. It is therefore not shown here, instead, it is set to zero and no further considered. The velocity term K_v on the other hand does effect the system's damping. The Figures 16-6 and 16-7 show a slight reduction of the vehicle's body criterion in the middle frequency range as K_v increases (yellow versus purple graphs). The difference from the figures however is minimal and reducing the suspensions damping by increasing K_v is even questionable with respect to driving safety, as was previously shown by simulations.

The strongest effect between the different disturbance compensation suspension setups is in the low frequency range (cabin criterion $0.4-3.0$ Hz). The setting $\begin{bmatrix} K_s & K_v & K_a \end{bmatrix} = \begin{bmatrix} 0.7 & 0.3 & 0.0 \end{bmatrix}$ there definitely reduces the body acceleration the most. Furthermore, the velocity compensation term is relatively low in this setup, which is desired for a properly damped wheel (see Figure 13-8). This particular disturbance compensation setting is from now on revered to as "active" or "DC" for better readability. The effect of the velocity (or damping) compensation term K_v is more prominent when considering the driving behavior subjectively.

16-3-2 Subjective results

As soon as the velocity compensation term K_v increases, the system's damping is reduced. This can clearly be felt by the passengers in the vehicle. For $K_v \geq 0.7$, the damping is reduced in such an extend, that the wheel starts to flatter at high frequency road excitation. Although this undamped behavior did not compromise the drivability of the test vehicle during the controlled, non-critical test drives, it is unwanted as high fluctuations in the dynamic wheel load should be avoided to increase driving safety. Moreover, it does not improve the driving comfort.

The reduced body acceleration at low frequencies and compromised body acceleration at higher frequencies from the objective measurement evaluation are confirmed by the subjective assessment. A great reduction in the motion of the passenger cabin is noticed once the disturbance compensation algorithm is activated. Negative attention however is drawn to the driving comfort. As soon as the system is active, small sharp irregularities in the road profile e.g. manhole covers and curbstones, corresponding to high frequency road excitation, are transmitted to the passenger cabin stronger. Depending on the road section, this partly feels as if the vehicle would drive on low profile tires, or even on its rims.

From all the different test settings, the DC setup actually feels the most harmonic, which corresponds to the objective measurement results. Increasing the control parameters does slightly reduce the motion of the passenger cabin more, but this does not compensate for the corresponding compromised tire roll comfort. Lower control parameters increase this comfort, but only in such a small extend, that the differences are hardly noticed. The for lower control parameters corresponding increase in the passenger cabin's motion on the other hand is definitely noticed. Considering this and the objective test results, the DC parameter setting is the favored setup.

16-3-3 Road dependent setup

Appendix A shows the effect of the active suspension system, with the DC setup, with respect to the passive suspension in the time domain. Not only the DLK and Cobblestone tracks are plotted, but also the ORK and Concrete plates. Although the active and Soft Open measurements at each track are not exactly the same, some trends in the behavior are very clear.
As was concluded from the scatter plots, the active system compromises the comfort at higher frequencies. When and how distinct this happens however, turns out to be highly track dependent.

At the Cobblestone track, the active suspension setup only minimally tends to reduce the low frequency cabin criterion with respect to the inactive system, whereas it compromises the cabin criteria in the middle and high frequency ranges. The advantage gained in the low frequency range is so small, compared to the inactive suspension, that it does not compensate for the increased cabin criteria values in the higher frequency ranges. Together with the subjective assessment, it is therefore concluded, that is is better to drive with an inactive suspension setup, as soon as the road is as worse as the road surface of the Cobblestone test track.

The measurements at the ORK, with its smooth asphalted road surface and low frequency excitation profile, shows a completely different result. Here the low frequency cabin criterion is greatly reduced as soon as the suspension is active. Even in the middle frequency range, still an advantage is gained with the active system. Above that, the high frequency cabin criterion only shows marginally higher cabin criterion values, compared to the inactive suspension setup.
From within the passenger cabin, the effect of the active system at the ORK is impressive. The equal sine-wave excitation is hardly noticeable anymore and the vehicle seems to glide like a flying carpet. Also the roll (unequal sine wave) excitation is greatly reduced.

These two extremes show, that there is no single suspension setting that covers all possible road excitation. This motivates the development of an adaptation algorithm.

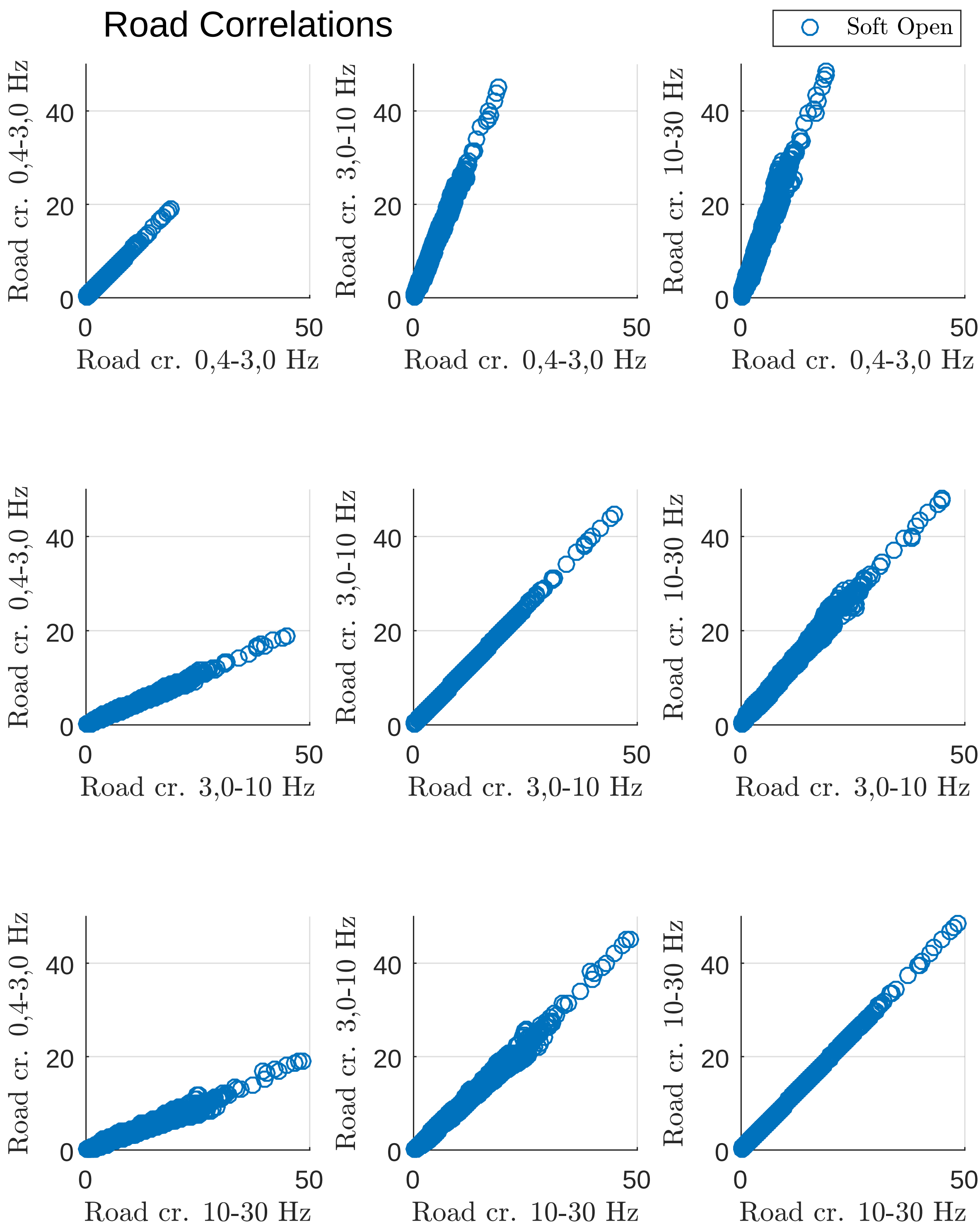

Figure 16-3: Scatter plots showing the correlation between the different frequency range road criteria. The almost perfect correlation independent of the frequency ranges indicates, that there is no use in defining multiple road criteria.

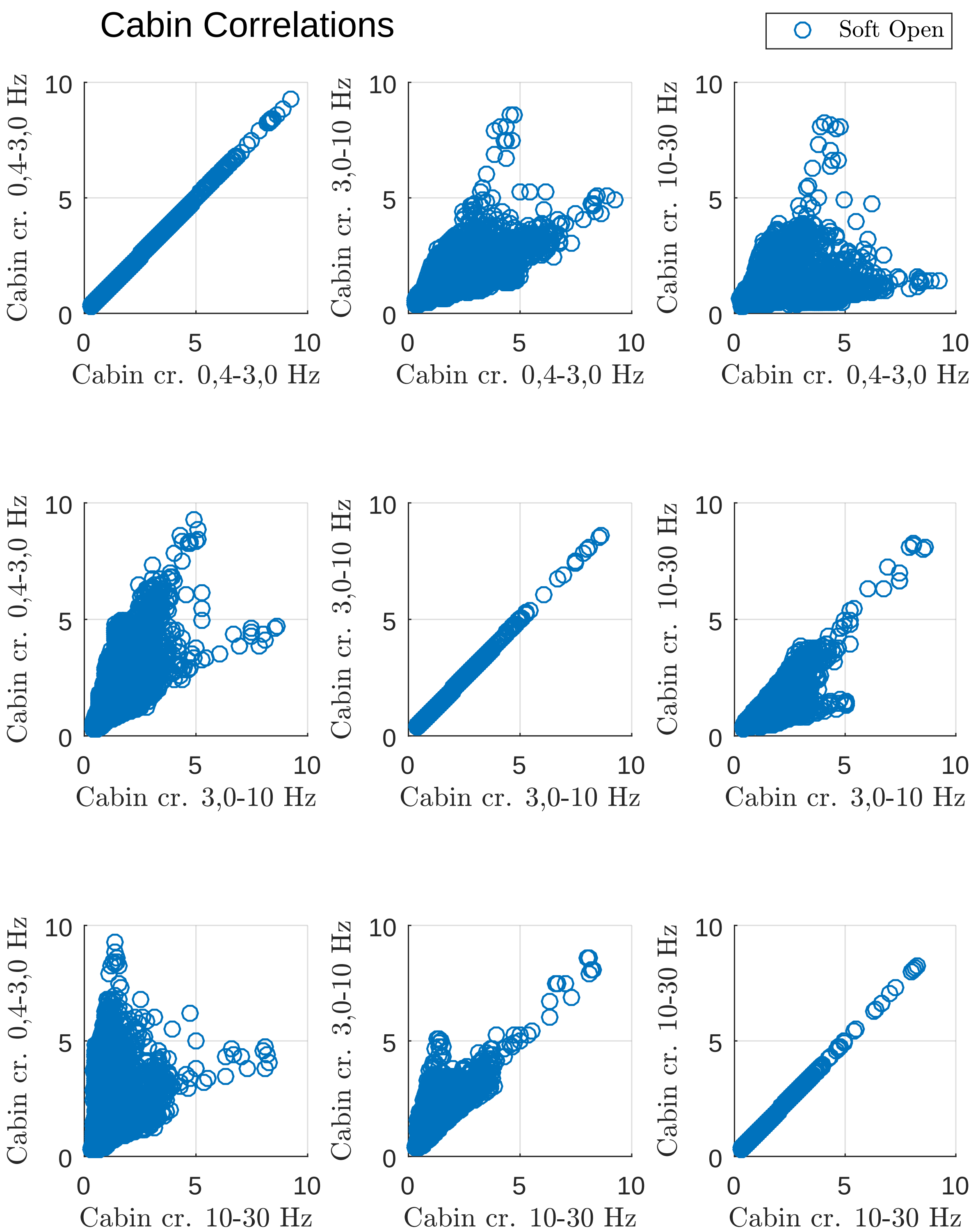

Figure 16-4: Scatter plots showing the correlation between the different frequency range cabin criteria. Spread in the correlations confirm, that the vehicle's body behaves different dependent on the frequency of the excitation.

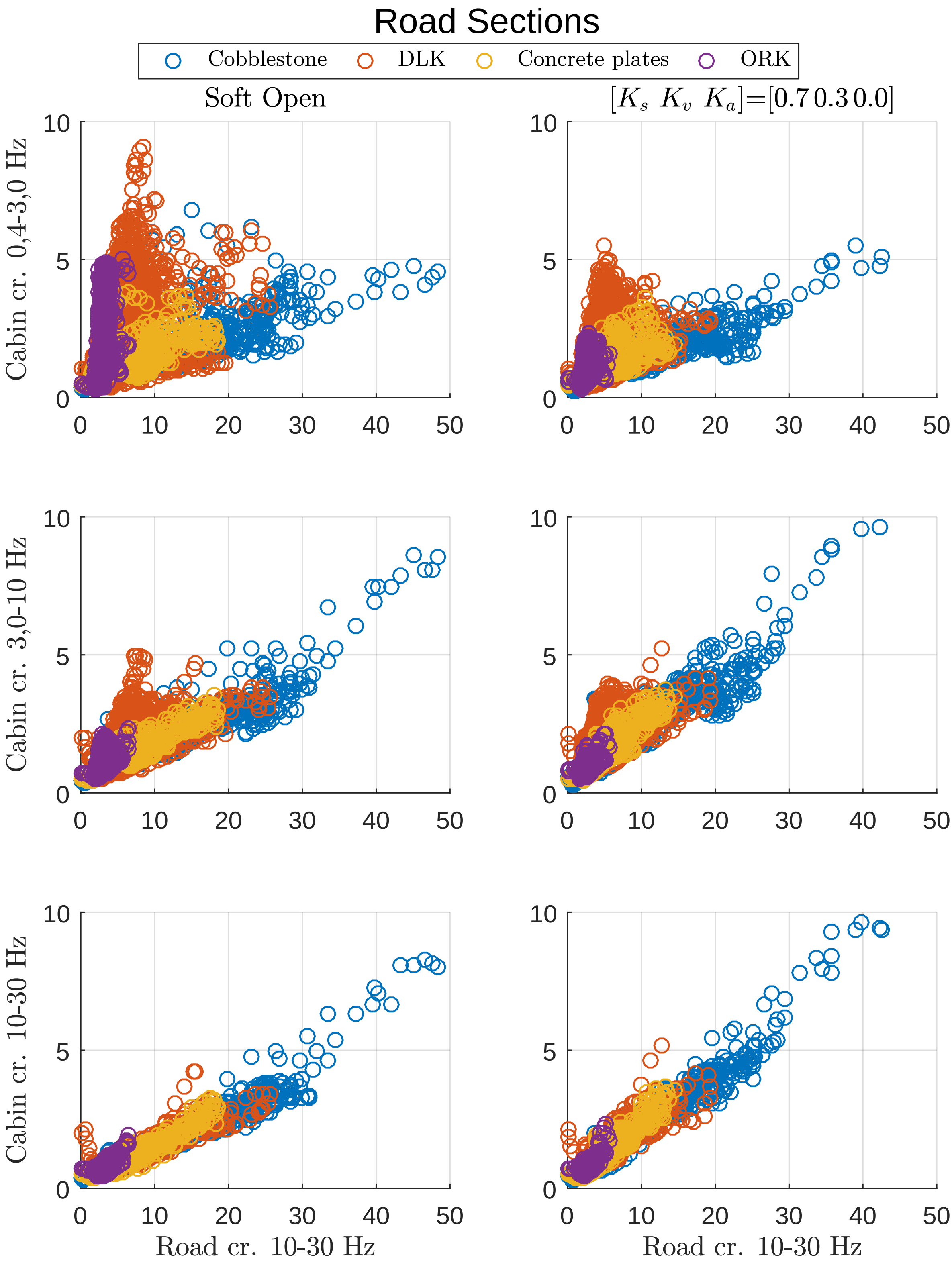

Figure 16-5: Scatter plots indicating the effect of the different test track road sections on the defined criteria. The Cobblestone and DLK road sections cover the complete range for both passive, as well as active suspension settings. This leads to the conclusion to confine the road test to these two road sections.

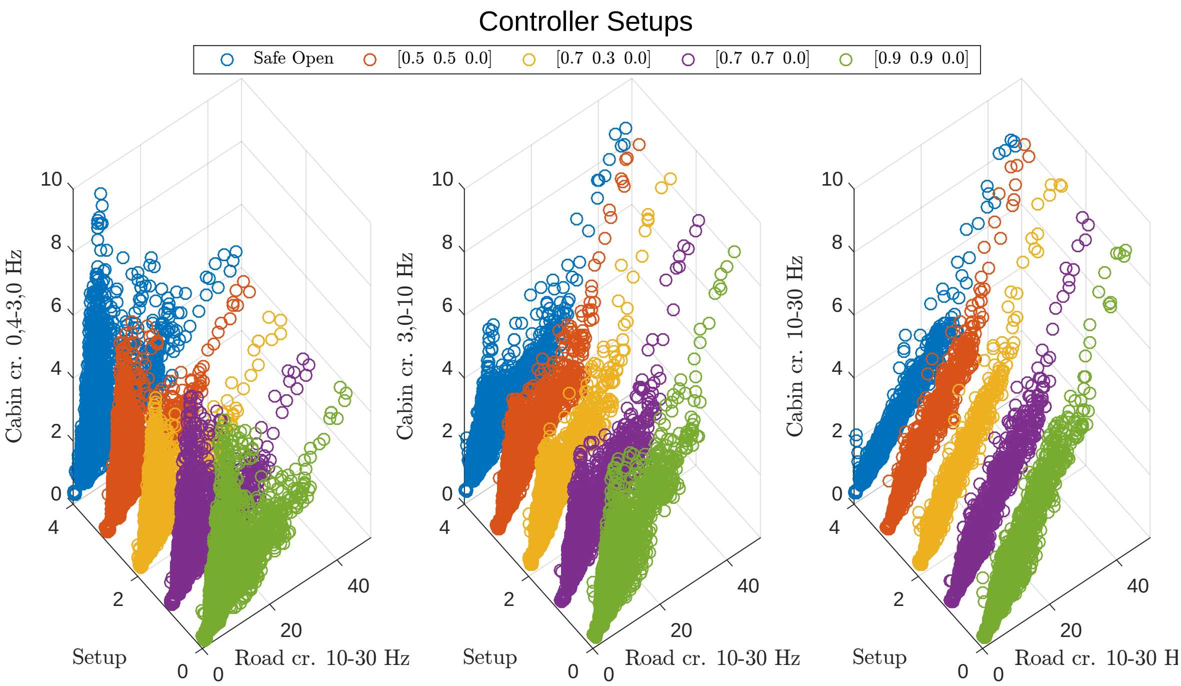

Figure 16-6: 3D-Scatter plots showing the result of the different suspension setups on the defined criteria. Effect of compromised comfort as the frequencies increase the disturbance control terms get higher follow from the middle and right plots.

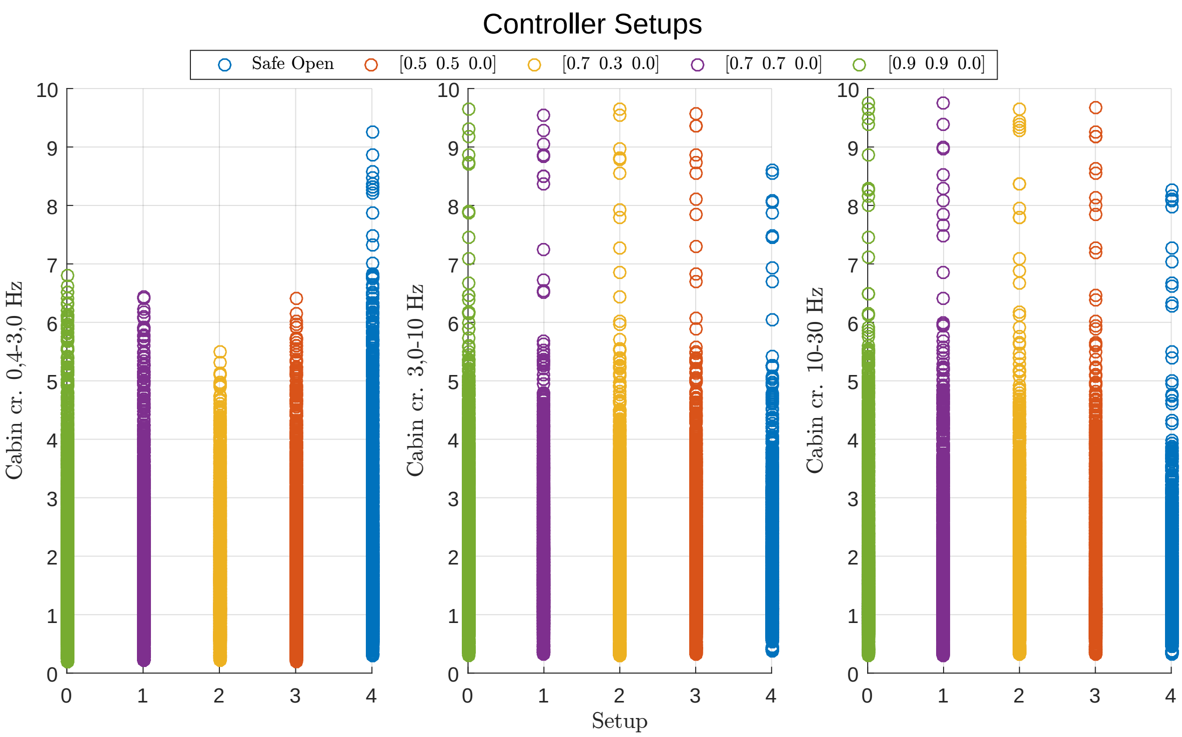

Figure 16-7: 2D-View of the 3D-Plots of Figure 16-6 to emphasize the effect of decreasing comfort at higher frequencies and disturbance compensation control parameters.

Chapter 17

Adaptation logic

The insights gained from the vehicle tests, show that there is no single disturbance compensation control setup, that offers the best driving dynamics on all possible road surfaces. Due to the physical working principle of the active damper unit, the system's damping increases as soon as an active actuator force is generated by the active damper unit, which compromises the tire roll comfort. This chapter introduces an adaptation logic specified for the disturbance compensation control algorithm to reduce this undesired effect. It also introduces a method that reduces this negative effect at rough road surfaces in combination with the Skyhook algorithm.

17-1 Road dependent disturbance control

The position compensation term K_s in the disturbance compensation control algorithm compensates for the suspension spring force and directly results in a desired active actuator force. From the linear actuator model in Figure 13-5, it follows, that this term is coupled to the CDC valve setting (linearly approximated by K_{CDC} in the figure). As a result of this, it primarily determines the damping ratio.

Figure 17-3 shows the inactive and active ($\begin{bmatrix} K_s & K_v & K_a \end{bmatrix} = \begin{bmatrix} 0.7 & 0.3 & 0.0 \end{bmatrix}$) setups overlapped in one figure for each cabin criterion frequency range against the road criterion. It clearly shows the previously explained disadvantage of the firm damping on the cabin criterion with respect to the inactive suspension as soon as the road surface gets worse and the evaluated frequency range increases. This behavior suggests to switch off the disturbance compensation controller and rely on the inactive suspension properties as soon as a certain threshold is violated.
This threshold is chosen to be dependent on the road criterion and it is exemplary represented in Figure 17-3 by a vertical boundary at a road criterion value of 17. The limit is indicated by the dotted vertical black line and accentuated by the separation of the active setup in green and red colors. If the suspension only is active up to this limit (green in the figure), then the inactive suspension characteristic (blue in the figure) is preserved as the road

surface gets worse. The areas in the figure above the continuous black lines in the two lower plots, corresponding to the area where the vehicle dynamics are compromised by disturbance compensation control, would then be avoided.

The threshold indicated in Figure 17-3 shows a complete and immediate on/off-switching of the disturbance compensation controller around the proposed limit. Moreover, this ”sharp” limit is not restricted to only the spring compensation force term K_s, as suggested above, but instead sets all active terms to zero. This means that the figure does not exactly represents the suggested resulting real system behavior. Nevertheless, it still does illustrate the idea behind the adaptation concept. The desired quantities and character of the threshold that affects K_s, have to follow from actual road test, which are looked into and evaluated in Chapter 18.

To facilitate tuning of the threshold during test drives, the value of K_s is multiplied with a factor implemented as a road criterion dependent characteristic map into the vehicle controller (see Figure 17-1). This allows a flexible configuration of the threshold and is also compatible with the `ControlDesk` software used during the test drives in the vehicle.

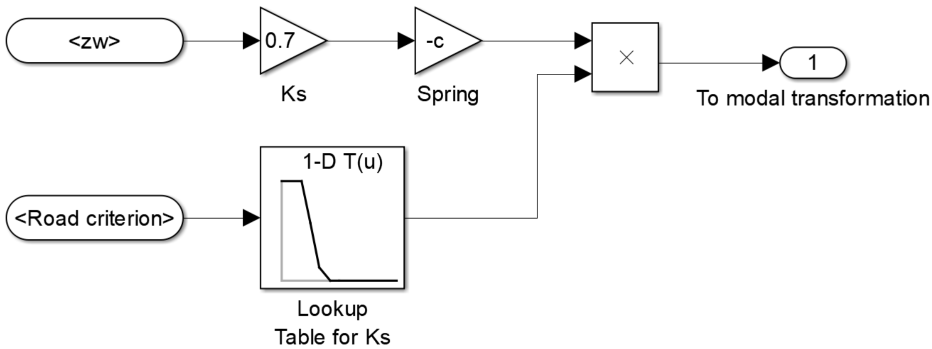

Figure 17-1: Road criterion dependent threshold on the spring compensation term K_s to reduce the negative effect on the system's damping coefficient at rough road surfaces.

17-2 Road dependent dead-zone

The introduced threshold unfortunately will also reduce the positive effect of the active suspension intervention on the low frequency cabin criterion. This is indicated by the encircled area in the upper plot of Figure 17-3. The aim of the adaptation logic therefore is to tune the threshold, such that this area is minimized, without compromising the higher frequency cabin criteria.

Since a disturbance compensation algorithm is essentially intended to enhance the vehicle dynamics by supporting other control algorithms, such as the Skyhook algorithm, a reduction of the encircled area in the figure could be achieved by a combination of control algorithms. Especially the Skyhook algorithm could reduce the encircled area, since it acts upon movement of the vehicle's body in the relatively low frequency range (around the body's eigenfrequency). The theoretical potential of both control algorithms already followed from the simulation results (see Figure 13-11), but up till now, the focus was on only the disturbance compensation algorithm.

A combination of different control algorithms is already foreseen by the vehicle controller's structure. The vehicle control structure (Figure 14-1) is arranged according to the Aktakon principle and adds all the forces resulting from the different body controller modules before transforming them, by means of an inverse modal transformation, into the desired forces for each active damper. This means, that as soon as multiple body control modules are active, they complement each other.
The sum of the desired actuator forces from single control modules however, could again result in desired active actuator forces upon high road criteria, leading to a reduction in the driving comfort. To overcome this problem, a road criterion dependent dead-zone is introduced and implemented immediately after the inverse modal transformation in the body controller. The width of this dead-zone, in which the required actuator forces are set to zero, is regulated by a road criterion dependent characteristic map. An increase in the road criterion increases the width of the dead-zone and vise verse. This is illustrated in Figure 17-2.
At rough road surfaces, this principle allows the Skyhook algorithm to reduce high relative

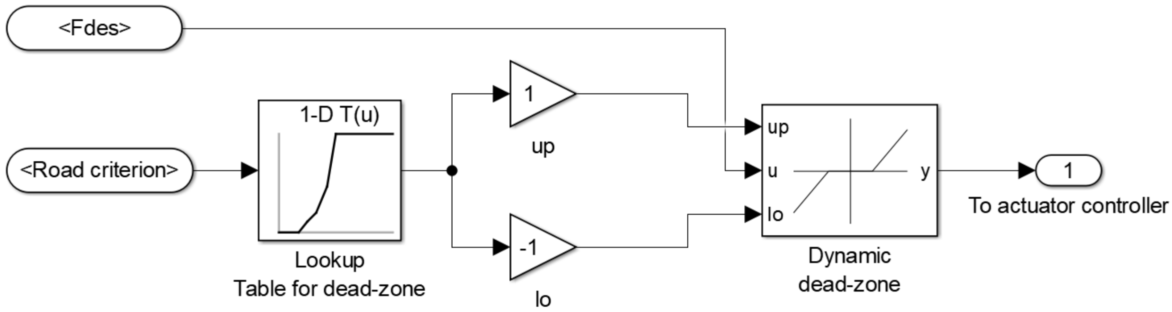

Figure 17-2: Road criterion dependent dead-zone to control the overall desired actuator forces and thereby enhance the driving comfort at rough road surfaces.

body velocities (body with respect to the "sky"), by letting through the corresponding high desired actuator forces F_{des}, but at the same time accepts a certain motion of the body, by canceling desired forces within the dead-zone.

The characteristic map that regulates the desired actuator force restriction is implemented into the vehicle controller and `ControlDesk` software, such that it can be tuned during test drives. Using the adaptation logic for the disturbance compensation algorithm and complementing it with dead-zone controlled Skyhook forces is subject of the next chapter and is expected to lead to the desired system behavior and a reduction of the encircled area in the upper plot of Figure 17-3.

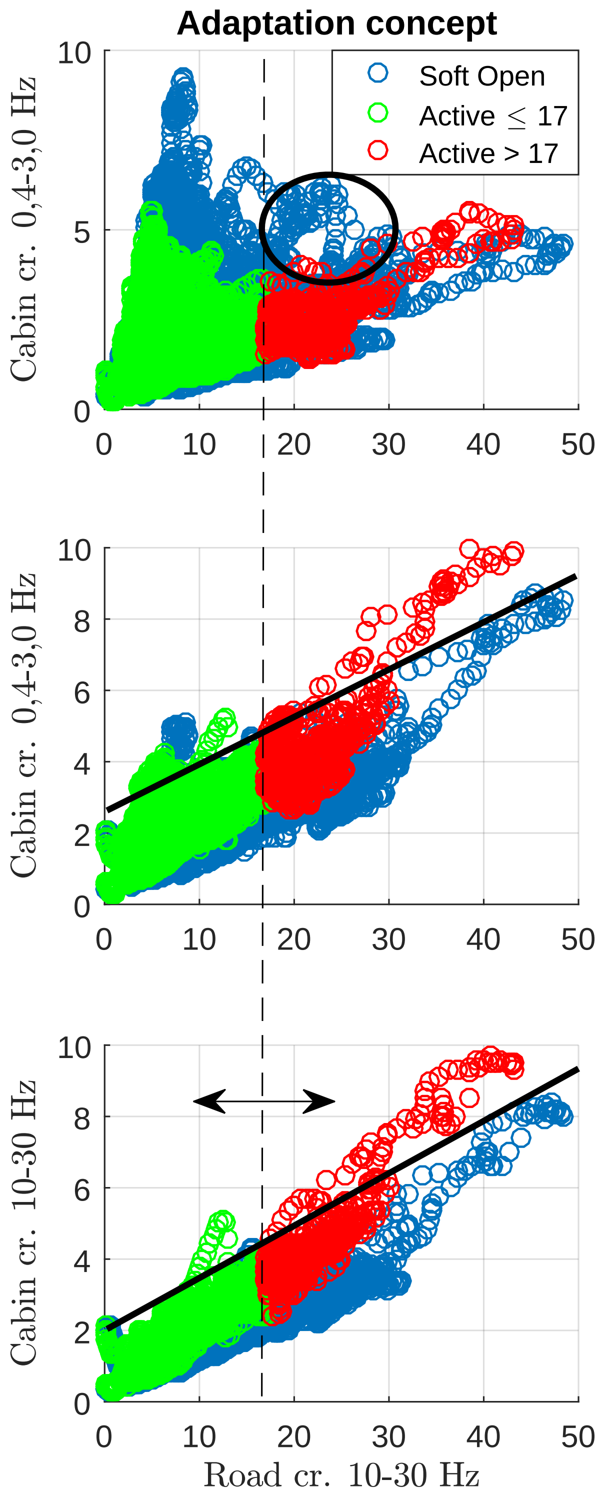

Figure 17-3: Passive (Soft Open) suspension setup vs. Active setup in one figure. The vertical dotted line illustrates the idea of the proposed adaptation logic. Limiting the desired active forces should enable to approach the passive suspension behavior at higher frequencies. The encircled area in the top plot is aimed for to be compensated by the Skyhook algorithm.

Chapter 18

Adaptation logic tests and evaluation

As with the initial disturbance compensation control implementation and testing, the adaptation algorithm is tested at the ATP test facility in Papenburg. Using the results of the first tests, the testing is confined to the Cobblestone and DLK road sections right from the beginning.

18-1 Test procedure

The tests are initiated with a repetition of measurements already executed in the first test drives. In the time between the first test and this test, work was done on the test vehicle and the sensor configuration has slightly changed. This explains why some of the values shown in figures in this chapter slightly deviate from previous results. The initialization measurements reassure comparability of the new measurements and cover the major changes in the system and test conditions.

For readability, the favored disturbance compensation control setup $\left[K_s\, K_v\, K_a\right] = \left[0.7\, 0.3\, 0.0\right]$ is as before abbreviated as DC and the Skyhook algorithm is abbreviated as SH. The performed road tests are listed in Table 18-1.

Table 18-1: Second road test procedure

Setup	**Aim**
Soft Open	Reference measurements for comparison to the passive system
SH	First assessment of the Skyhook algorithm's impact on the introduced criteria
DC	Measurement with the favored disturbance compensation control setup
SH + DC	First assessment of both algorithms working together

The tests are initially executed without the adaptation algorithm and dead-zone. Extra attention is paid to the occurring desired damper forces during these tests. Even in the Soft Open setting, the ”virtual” resulting controller forces, as a result of the road excitation (disturbance compensation) and cabin motion (Skyhook) are monitored. This helped to get an idea of the occurring active forces and provided a first orientation to initialize the threshold and dead-zone lookup tables.

The tests are repeated with activated threshold and dead-zone. An iterative process of measuring and evaluating finally results in a threshold characteristic that starts reducing K_s at a road criterion value of 7.5 all the way to zero at a road value of 12.5.
The boundary of the dead-zone is regulated from ± 10 N at a road criterion value of 0 (corresponding to standing still and accounts for unexpected disturbances in the sensor signals) up to ± 200 for a road criterion value of 15 and upwards.

18-2 Test results

The effect of the threshold and the dead-zone on the resulting desired damper forces, is shown in Figure 18-1. The desired Skyhook forces are only mildly restricted by the dead-zone. This was to be expected, since the operating range of the Skyhook algorithm acts at relatively low frequencies, where the negative effect of a change in the damping ratio is not that critical.
The threshold on the disturbance compensation on the other hand significantly restricts the desired damper forces and, by doing that, improves the driving experience. This is confirmed by the resulting cabin criteria, which are shown in Figure 18-2. As intended, the disturbance compensation does no longer compromise the high frequency system behavior as soon as the road criterion increases. Selective manipulations in the suspension forces even allow the active system (with disturbance compensation) to reduce the cabin criteria *below* the inactive suspension setup.

The unavoidable side effect on the cabin criterion values in the low frequency range (encircled area in the figure), by restricting the allowed disturbance compensation forces, is compensated for, as soon as the SH and DC work together. Their combination does however slightly increases the higher frequency cabin criteria values, when compared to the restricted disturbance compensation control only.

Since none of the test drives can exactly be replicated, they are all slightly different. This makes it difficult to qualitatively asses the controller's performance. The vehicle's speed, the position of the vehicle on the road, the drivers input and other factors all influence the measurement data. Above that, the system's performance still highly depends on the road surface. The measurements do however allow to assess the controller's performance quantitatively. The outlined plots in this research show, if there is more, or less movement of the body in a certain frequency range. Low frequency excitation is almost completely filtered out by the system (see the results on the ORK road section). High frequency excitation on the other hand is harder for the system to compensate for. With the adaptation logic that enhances the controller however, it is possible to reduce the body's movement without compromising the ride comfort to much (the inactive suspension behavior is approached by the active system in the higher frequency ranges).

Compared to the Skyhook algorithm, the disturbance compensation is able to enhance the vehicle dynamics in a higher frequency range. This is emphasized in Figure 18-3, where the plots of Figure 18-2 are repeated without showing the combined effect of both algorithms, such that the difference between the Skyhook and disturbance compensation control algorithms is accentuated.

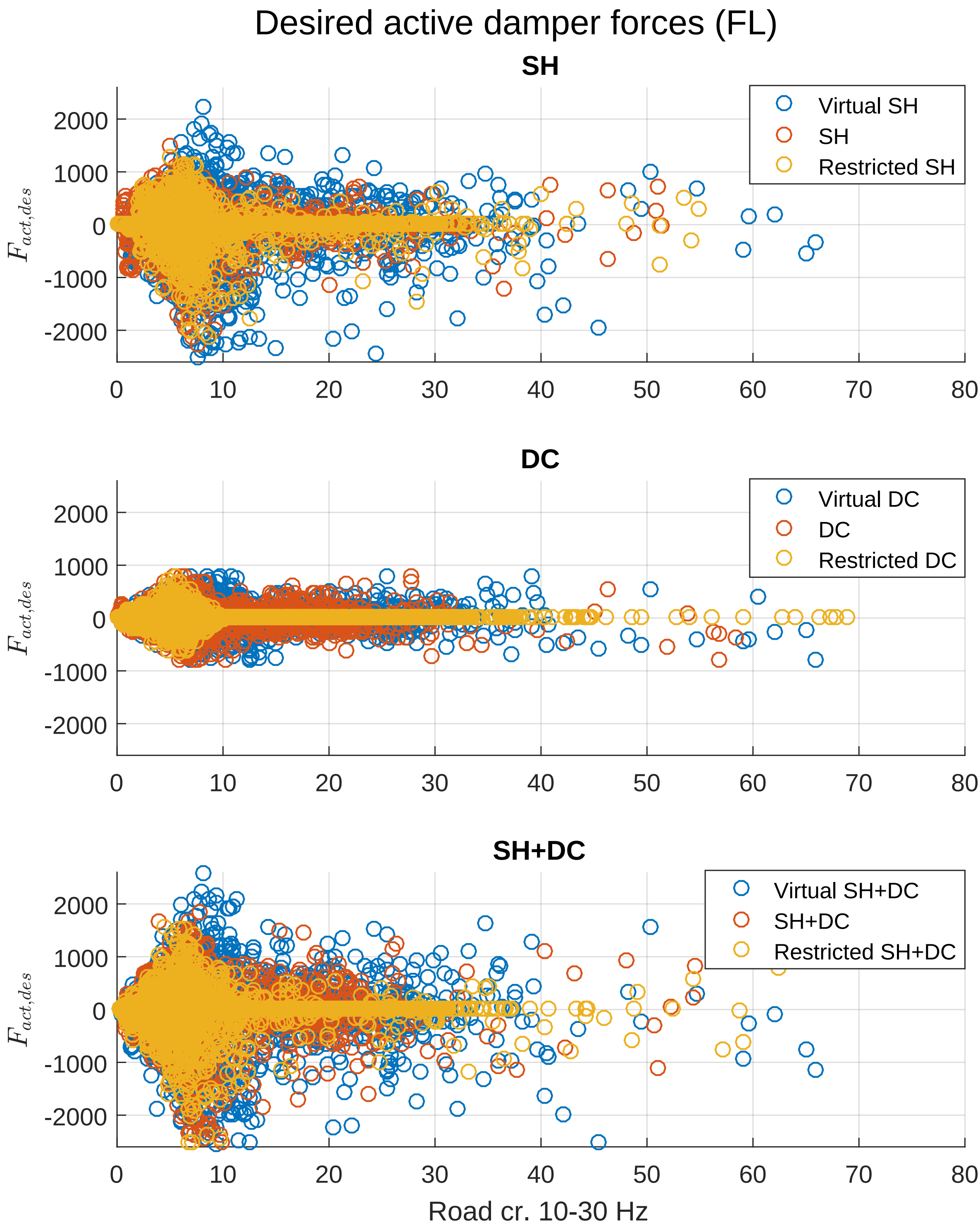

Figure 18-1: Effect of the adaptation logic and dead-zone on the desired active damper forces. The virtual forces (blue) are used to initialize the thresholds.

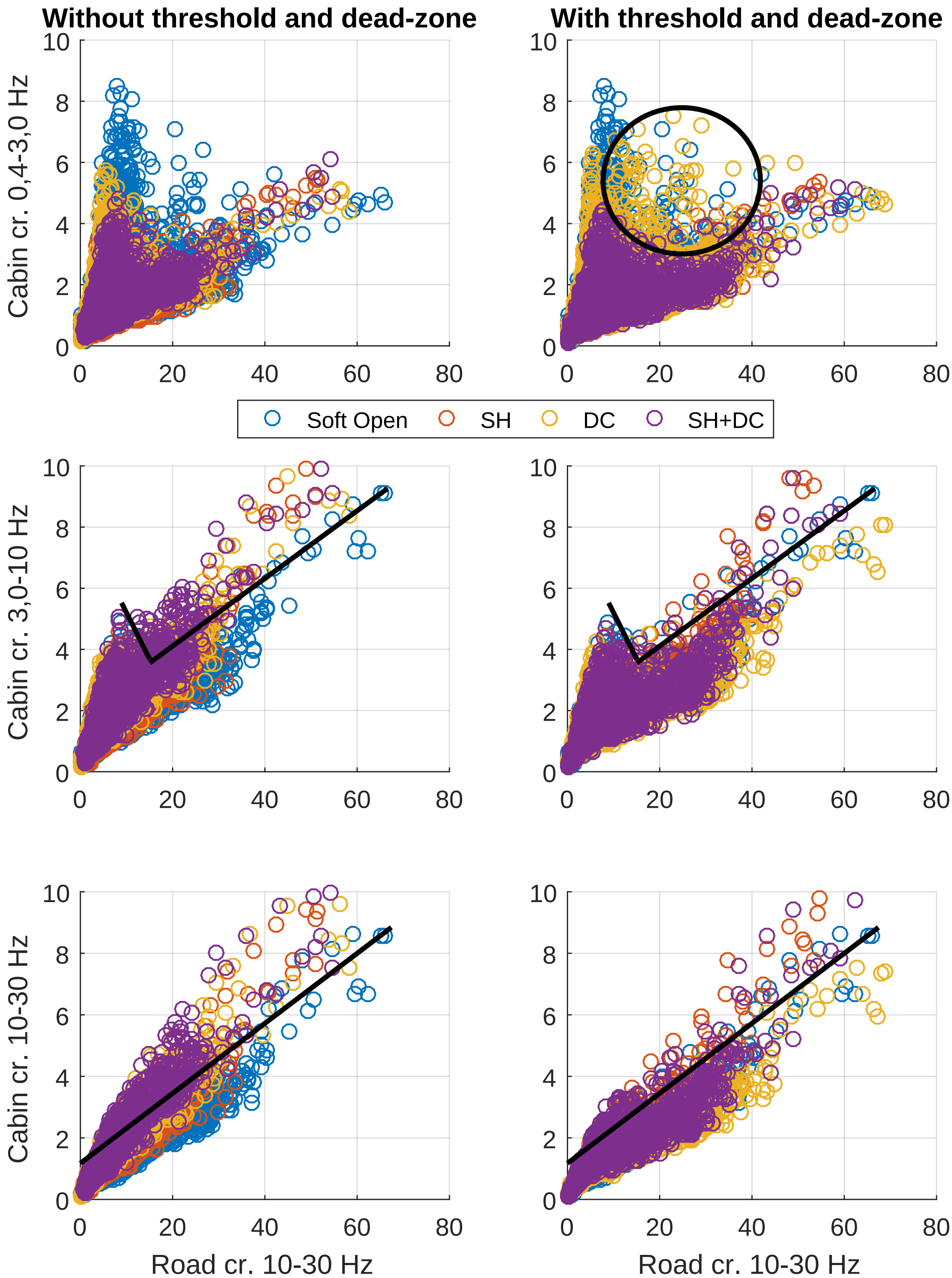

Figure 18-2: Scatter plots showing the result of the adaptation logic and dead-zone on the cabin criteria in the different frequency ranges. The combination of DC and SH achieves the desired result and reduces the high frequency cabin criteria down to the inactive suspension level.

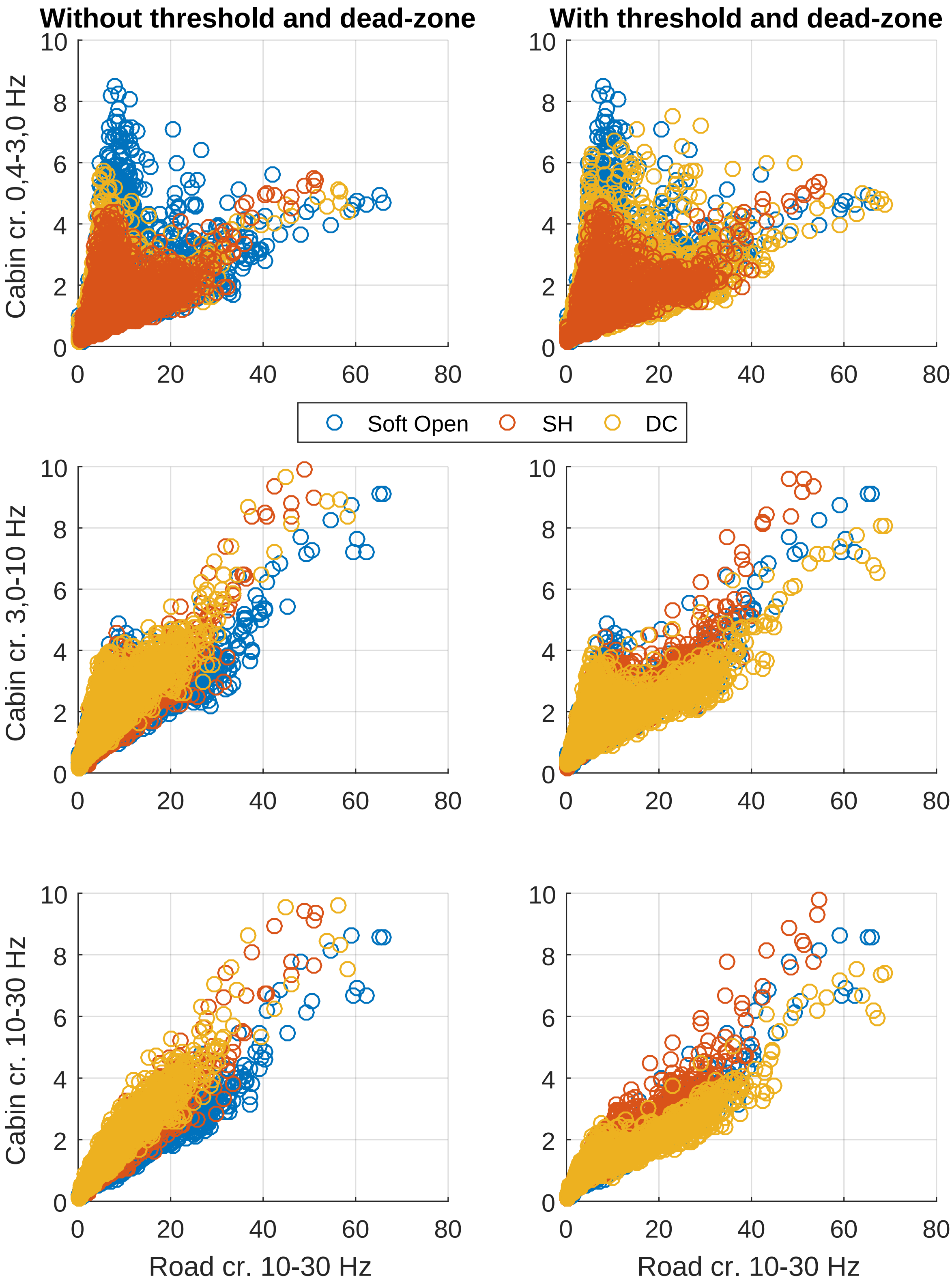

Figure 18-3: Scatter plots showing the result of the adaptation logic and dead-zone on the cabin criteria in the different frequency ranges. The difference between the disturbance compensation and Skyhook control is shown. The DC is able to reduce the cabin criteria more at higher frequencies than the SH does.

Chapter 19

Conclusion

In this work, a disturbance compensation control algorithm was proposed, implemented and extensively tested for the novel active damper units developed by ZF Friedrichshafen AG. These active damper units are designed, such that all the essential parts are integrated into the damper. This considerably simplifies implementation and facilitates packaging.

19-1 Discussion

In the search to find an applicable disturbance compensation controller for the active damping system, a signal based controller was proposed. This controller only uses the output of the wheel acceleration sensor and does not rely on a mathematical model of the vehicle. The advantage of this is, that it is highly implementable and the development could continue without the need for an advanced model of the suspension, which would require a test rig and corresponding system identification.

Despite the simplicity of the proposed algorithm, simulations showed, that the resulting algorithm is stable and has the desired effect on the vehicle's dynamics. The augmentation of the quarter car simulation model, by means of implementation of the linear approximated active damper unit model, allowed to reformulate the proposed algorithm. This modification led to extra control parameters. The resulting three disturbance compensation control parameters each affect different frequency ranges. This motivated the introduction of frequency range dependent performance criteria to assess the controller's performance.

Extensive real world tests confirmed the positive effect of the proposed algorithm on the vehicle's dynamics. The tests also revealed an undesired effect, related to the physical design of the active damper units, which was not considered before.
As soon as an active force is produced by the active damper units, the system's damping ratio changes and the roll comfort gets compromised. To reduce this undesired effect, an adaptation algorithm and dead-zone were introduced.

The adaptation algorithm dynamically restricts the desired active damper forces resulting from the position compensation term. The threshold that regulates this restriction is dependent on the state of the road surface. The velocity compensation term of the disturbance compensation algorithm is excluded from this restriction, since it has the desired effect, that it reduces the damping, by compensating for a disturbance induced volume flow in the system.

The introduced dead-zone further accounts for the active damper dynamics. It reduces the desired active damper forces resulting from active control modules in the body controller. It thereby makes sure, that the addition of multiple algorithms does not eventually lead to high desired forces on rough road surfaces, that compromise the high frequency behavior of the system.

19-2 Results and potential

With the adaptation logic and dead-zone implemented into the system, a combination of the disturbance compensation algorithm and Skyhook control was tested. The test show, that the negative effect is reduced down to the inactive suspension level. Furthermore, the test results show that the disturbance compensation algorithm can be used to complement other control algorithms.

The final disturbance compensation controller together with the adaptation logic and dead-zone limited Skyhook controller, considerably reduce the low frequency acceleration of the passenger cabin. At the same time, they reduce the higher frequency motion to an acceptable level (approximately the same as with an inactive suspension setup). The overall performance is however difficult to capture qualitatively. Dependent on the road section, the effect of the controller varies from impressive results, where the road excitation is almost completely compensated, to more moderate results, where only a small reduction of the cabin's motion compared to the inactive system is achieved. This will be improved as soon as the bandwidth of the active damper units is increased. After all, simulations have shown, that the introduced disturbance compensation algorithm has the potential to enhance the vehicle dynamics in the higher frequency range as well.

Chapter 20

Further research

The proposed disturbance compensation algorithm manages to reduce the motion of the passenger cabin and thereby increases the driving comfort. When applied to complement the Skyhook algorithm in combination with the adaptation logic, the results are even better and the behavior at high frequency excitation approaches the inactive suspension behavior. To approach the potential shown in the simulations even at high frequencies, further research is required.

20-1 Refinement and wheelbase-preview

More testing and fine-tuning are required to refine the disturbance compensation and adaptation algorithms. Also the performance criteria could be refined. Instead of using one road criterion (based on the measured acceleration of the two front wheels), individual terms could be looked into. As suggested by S. Spirk [32] a wheelbase-preview concept, could further enhance the system's performance. Using the measured signals at the front wheels of the car to calculate the upcoming excitation for the rear wheels, gives the rear suspension units more time to react.

20-2 Feed forward control

The system's performance at high frequencies is limited due to the physical damper layout of the damper. Bounded by the concept of the active damper unit, the damping ratio will always increase as soon as an active force is desired. Faster "on/off" switching of the CDC valves and faster pump dynamics could therefore increase the actuator bandwidth and enhance the total system performance.

A possible way to achieve faster CDC and pump dynamics is to use feed forward control. When the dynamic behavior of the CDC valves and pump are known, an individual inverse model of these dynamics could reduce their response time.

An inverse CDC model has actually been looked into at the time of this research and has been tested in the vehicle, with a predefined switching sequence. This model manages to reduce the response time of the valve switching. It has however not yet been implemented into the actual vehicle controller. This will probably follow in the near future, as the project continuous. The same could be done for the pump.

20-3 Model based controller

Another possibility to enhance the system performance would be to improve the signal quality and the quality of the estimated states. As long as no preview system is considered, this can eater be achieved with better sensors, or by a better estimation method.
Instead of just integrating the wheel's vertical acceleration signal, multiple signals could be combined (e.g. acceleration and displacement signals). M. Fröhlich [7] shows in his research, that a combination of Kalman techniques and conventional filtering should lead to the best state estimates. He assesses the methods by considering both practicality as well as signal quality. This however does require an accurate (at least quarter car) model of the vehicle and will involve system identification on a test rig. When such a method would be considered, it is recommended to start with a test rig, equipped with high-end sensors. During this research, high fluctuations in the sensor read outs were not uncommon. This caused a lot of problems and delays in the development of the controller. Starting with more expensive, but more reliable sensors will make the development of a model based algorithm a lot less problematic. It is easier to downgrade the model and sensor quality in the end, than the other way around, as soon as a functional controller is developed.

20-4 Considering hysteresis

E. Pellegrini et al. [24] improve their controller as they take into account dynamic effects in the damper force generation by employing a hysteresis model. They show, that the hysteresis model describes their damper behavior considerably better than static characteristics do.
It is known, that the active damper unit of this research is affected by hysteresis. This however is not considered in the current model. Further research could focus on improvement of the current active damper model, to get a better description of its dynamic behavior. This could be realized with the existing test rig of the active damper unit (without suspension spring) available (at another facility) within the project at ZF Friedrichshafen AG.

Appendix A

Evaluated measurements

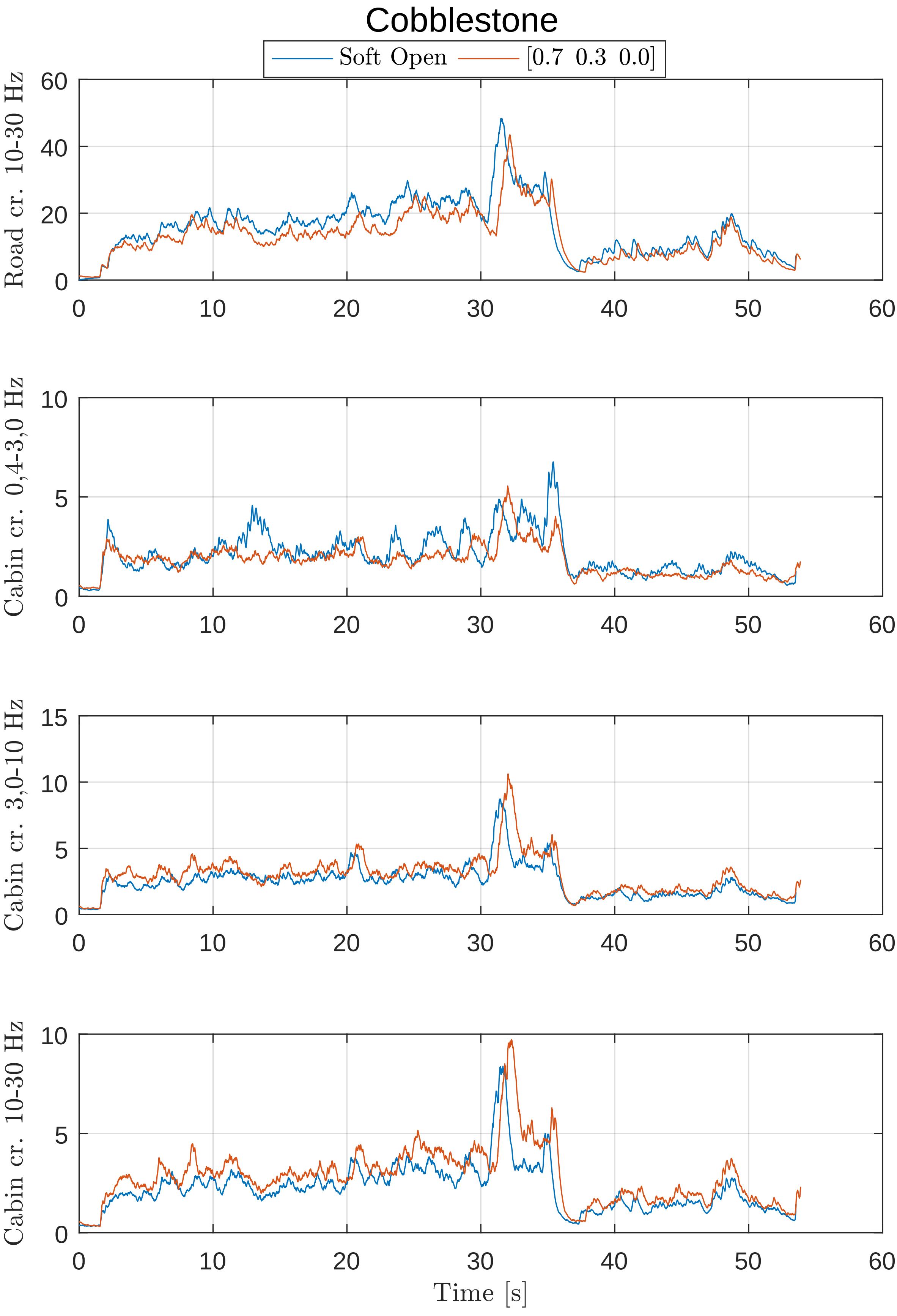

Figure A-1: Passive (Soft Open) vs. Active suspension setup in the time domain. Disturbance compensation control does only minimally reduce the low frequent cabin criterion. The higher frequency ranges are compromised.

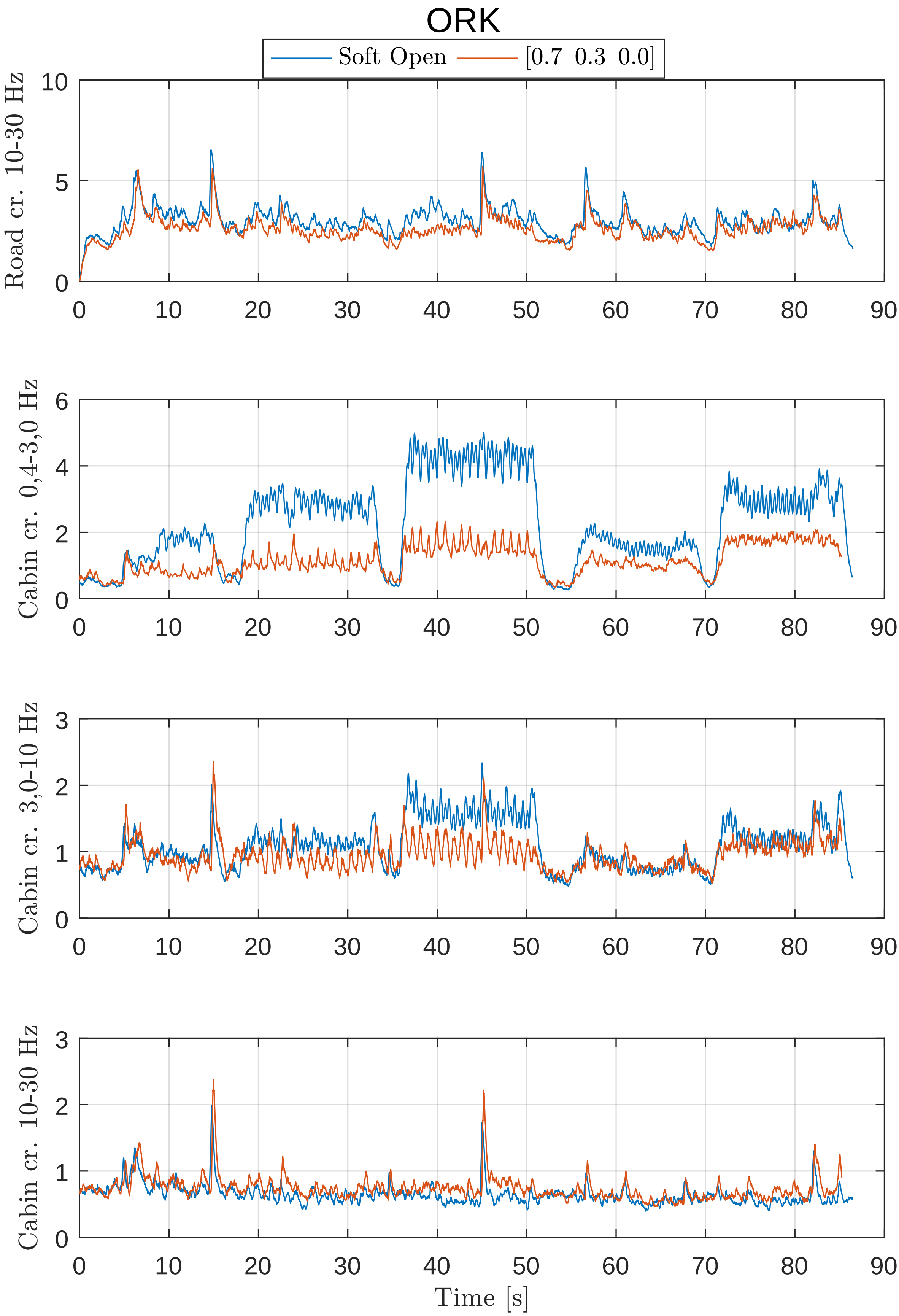

Figure A-2: Passive (Soft Open) vs. Active suspension setup in the time domain. Impressive results are achieved with the active setup on the smooth road surface of the ORK test track.

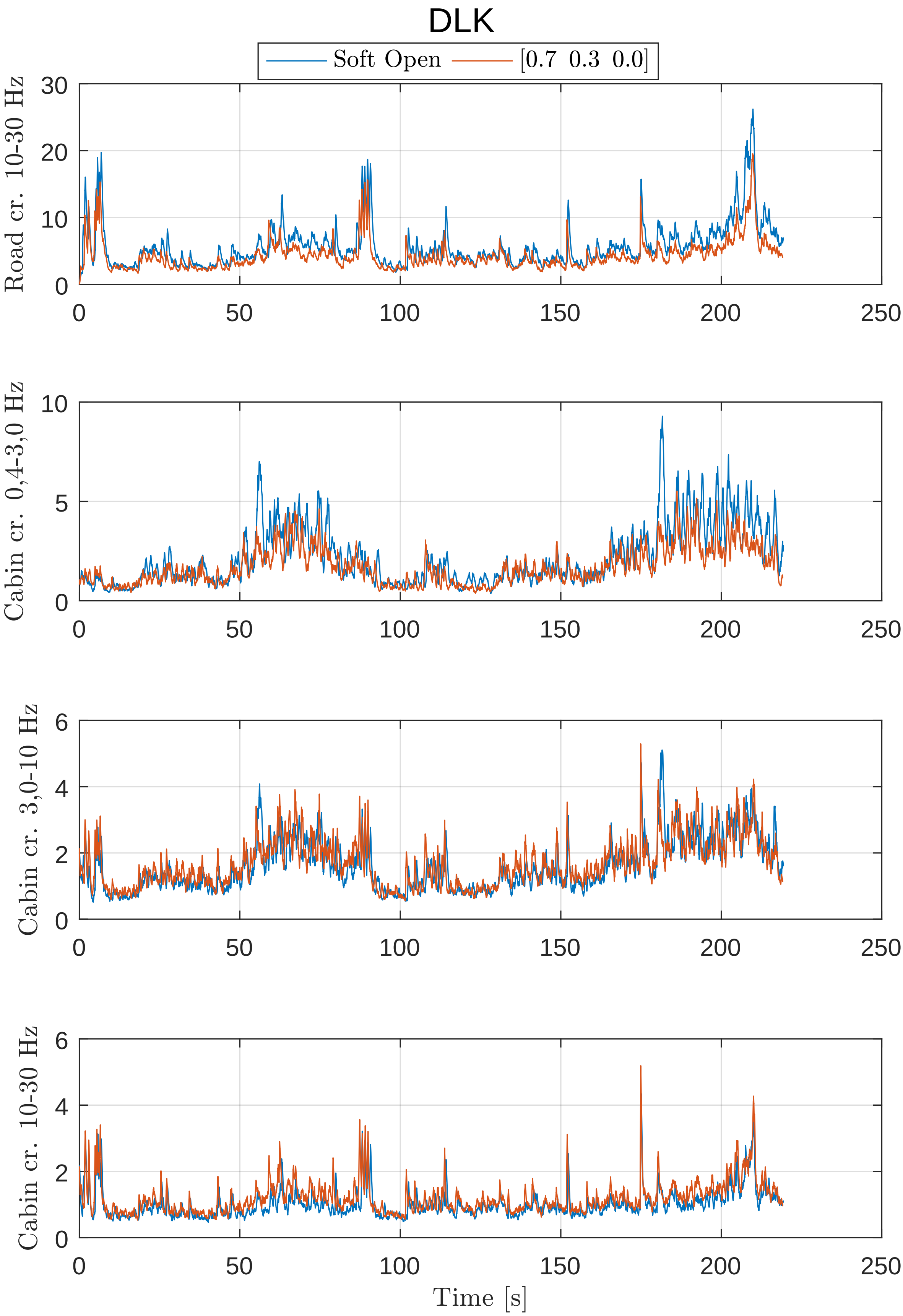

Figure A-3: Passive (Soft Open) vs. Active suspension setup in the time domain. The active disturbance compensation controller reduces the low frequent body motion, but tents to compromise the higher frequent cabin criteria.

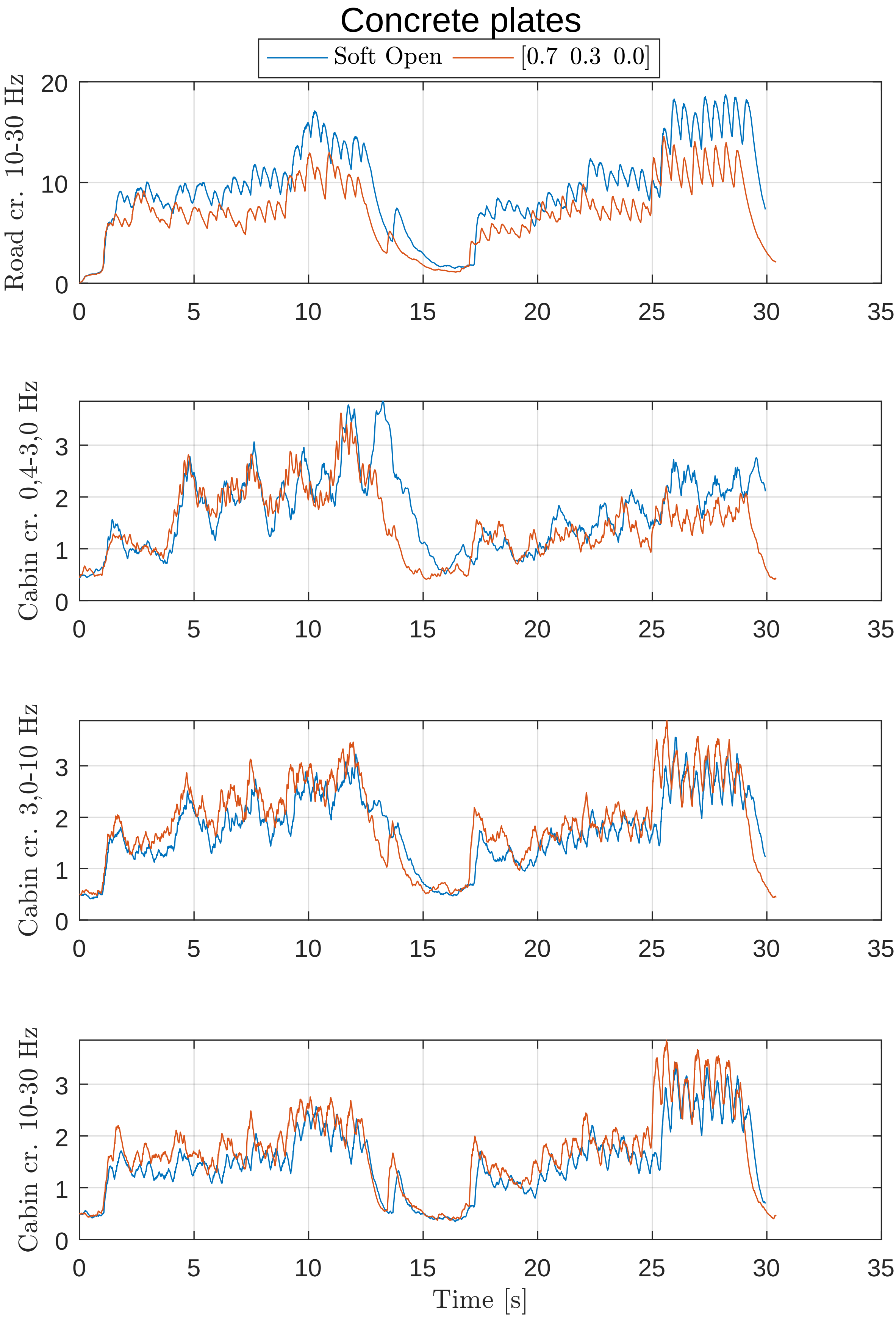

Figure A-4: Passive (Soft Open) vs. Active suspension setup in the time domain. The disturbance compensation controller cannot make a crucial difference on the concrete plates section.

Appendix B

Augmented state-space model

Model's state vector is augmented, such that it includes

- the appropriate filtered signals (also for the Skyhook algorithm),
- the Skyhook (K_{SH}) and disturbance compensation (K_s, K_v and K_a) terms,
- the actuator dynamics.

The augmented system state vector is

$$\underline{x} = \begin{bmatrix} z_c & \dot{z}_c & z_w & \dot{z}_w & \dot{z}_{c_1} & \dot{z}_{c_2} & \dot{z}_{w_1} & \dot{z}_{w_2} & z_{w_3} & \dot{z}_{w_3} & x_a & x_i & \omega_P & \Delta_p \end{bmatrix}^T \tag{B-1}$$

The filtered signals required for the Skyhook algorithm are acquired using the same strategy as described in Chapter 12.

- $\ddot{z}_{c_1}$ one time high-pass filtered body acceleration signal
- $\ddot{z}_{c_2}$ two times high-pass filtered body acceleration signal (required for the offset free vertical velocity of the body $\dot{z}_{c_2}$)

The resulting system is written in state-space form

$$\dot{\underline{x}} = A\,\underline{x} + B\,u, \tag{B-2}$$

$$y = C\,\underline{x} + D\,u. \tag{B-3}$$

The matrices A and B are given on the next page. The systems output y is determined by the choice of the matrices C and D .

$$A = \begin{bmatrix}
0 & 1 & 0 & 0 & 0 & 0 & 0 & 0 & 0 & 0 & 0 & 0 & 0 & 0 \\
-\frac{c_c}{m_c} & 0 & \frac{c_c}{m_c} & 0 & 0 & 0 & 0 & 0 & 0 & 0 & 0 & 0 & 0 & \frac{A}{m_c} \\
0 & 0 & 0 & 1 & 0 & 0 & 0 & 0 & 0 & 0 & 0 & 0 & 0 & 0 \\
\frac{c_c}{m_w} & 0 & -\frac{c_c+c_w}{m_w} & 0 & 0 & 0 & 0 & 0 & 0 & 0 & 0 & 0 & 0 & -\frac{A}{m_w} \\
-\frac{c_c}{m_c} & 0 & \frac{c_c}{m_c} & 0 & -\frac{1}{T} & 0 & 0 & 0 & 0 & 0 & 0 & 0 & 0 & \frac{A}{m_c} \\
-\frac{c_c}{m_c} & 0 & \frac{c_c}{m_c} & 0 & -\frac{1}{T} & -\frac{1}{T} & 0 & 0 & 0 & 0 & 0 & 0 & 0 & \frac{A}{m_c} \\
\frac{c_c}{m_w} & 0 & -\frac{c_c+c_w}{m_w} & 0 & 0 & 0 & -\frac{1}{T} & 0 & 0 & 0 & 0 & 0 & 0 & -\frac{A}{m_w} \\
\frac{c_c}{m_w} & 0 & -\frac{c_c+c_w}{m_w} & 0 & 0 & 0 & -\frac{1}{T} & -\frac{1}{T} & 0 & 0 & 0 & 0 & 0 & -\frac{A}{m_w} \\
0 & 0 & 0 & 0 & 0 & 0 & 0 & 0 & 0 & 1 & 0 & 0 & 0 & 0 \\
\frac{c_c}{m_w} & 0 & -\frac{c_c+c_w}{m_w} & 0 & 0 & 0 & -\frac{1}{T} & 0 & -\frac{1}{T^2} & -\frac{2}{T} & 0 & 0 & 0 & -\frac{A}{m_w} \\
0 & 0 & 0 & 0 & 0 & -\frac{K_{CDC}\,K_{SH}\,d_{SH}}{A\,T_a\,V_P} & 0 & -\frac{A\,K_v}{T_a\,V_P} & -\frac{K_{CDC}\,K_s\,c_c}{A\,T_a\,V_P} & 0 & -\frac{1}{T} & 0 & 0 & 0 \\
0 & 0 & 0 & 0 & 0 & -\frac{K_2\,K_{CDC}\,K_{SH}\,d_{SH}}{A\,V_P} & 0 & -\frac{A\,K_2\,K_v}{V_P} & -\frac{K_2\,K_{CDC}\,K_s\,c_c}{A\,V_P} & 0 & 0 & 0 & -K_2 & 0 \\
-\frac{A\,K_a\,c_c}{V_P\,m_w} & 0 & \frac{A\,K_a\,(c_c+c_w)}{V_P\,m_w} & 0 & 0 & -\frac{K_{SH}\,d_{SH}\,H}{A\,J} & \frac{A\,K_a}{T_a\,V_P} & -\frac{A\,K_v\left(K_1+\frac{J}{T_a}\right)}{J\,V_P} & -\frac{K_s\,c_c\,H}{A\,J} & 0 & -\frac{1}{T} & \frac{1}{J} & -\frac{K_1}{J} & \frac{A^2\,K_a}{V_P\,m_w}-\frac{K_P}{J} \\
0 & -\frac{A}{C} & 0 & \frac{A}{C} & 0 & 0 & 0 & 0 & 0 & 0 & 0 & 0 & \frac{V_P}{C} & -\frac{K_{CDC}}{C}
\end{bmatrix}, \tag{B-4}$$

with

$$H = K_P + \frac{K_1\,K_{CDC}}{V_P} + \frac{J\,K_{CDC}}{T_a\,V_P}$$

$$B = \begin{bmatrix} 0 & 0 & 0 & \frac{c_w}{m_w} & 0 & 0 & \frac{c_w}{m_w} & \frac{c_w}{m_w} & 0 & \frac{c_w}{m_w} & 0 & 0 & -\frac{A\,K_a\,c_w}{V_P\,m_w} & 0 \end{bmatrix}^T \tag{B-5}$$

Bibliography

[1] ATP Automotive Testing Papenburg GmbH. https://www.atp-papenburg.de. Accessed: 2019-01-12.

[2] Auto motor und sport. https://www.auto-motor-und-sport.de/marken-modelle/vw/touran/iv-typ-5t/technische-daten/. Accessed: 2019-02-06.

[3] dspace. https://www.dspace.com. Accessed: 2019-03-08.

[4] Anton van Beek. *Advanced Engineering Design*. TU Delft, 2012.

[5] Michael Fleps-Dezasse. *Linear Parameter-Varying Control of Full-Vehicle Vertical Dynamics using Semi-Active Dampers*. PhD thesis, Universität der Bundeswehr München, 2018.

[6] Gene F. Franklin, J. David Powell, and Abbas Emami-Naeini. *Feedback Control of Dynamic Systems*. Pearson, 2010.

[7] Martin Fröhlich. *Ein robuster Zustandsbeobachter für ein semiaktives Fahrwerkregelsystem*. PhD thesis, Technische Universität München, 2007.

[8] Wolfgang Gomoll. Der fliegende Teppich von ZF. *Auto Bild*, 2018.

[9] Bernd Heißing and Metin Ersoy. *Chassis Handbook*. Vieweg + Teubner, 2011.

[10] Thorsten Hestermeyer. *Entwurf, Implementierung und Realisierung einer modellgestützten Regelung für ein Fahrzeug mit volltragendem aktivem Fahrwerk und Motorpumpeneinheiten*. PhD thesis, Universität Paderborn, 2003.

[11] Norbert Hohenbichler and Klaus Six. Potentials of active and semi-active skyhook control laws applied to the secondary suspensions of railway vehicles. *at - Automatisierungstechnik, vol. 54, no. 3*, 2006.

[12] ISO. 2631-1 mechanical vibration and schock-evaluation of human exposure to whole body vibration. Technical report, International Standard Organisation, 1997.

[13] Jaguar and Land Rover. Future jaguar and land rover vehicles will help reduce motion sickness. https://www.jaguarlandrover.com/news/2018/11/future-jaguar-and-land-rover-vehicles-will-help-reduce-motion-sickness. Accessed: 2018-11-06.

[14] Tamás Keviczky. *Lectures Control Theory*. Delft Center for Systems and Control, 2015.

[15] Guido Koch. *Adaptive Control of Mechatronic Vehicle Suspension Systems*. PhD thesis, Technische Universität München, 2011.

[16] Guido Koch, Sebastian Spirk, and Boris Lohman. Reference model based adaptive control of a hybrid suspension system. In *6th IFAC Symposium Advances in Automotive Control*. IFAC, 2010.

[17] Guido Koch, Sebastian Spirk, Nils Pletschen, and Boris Lohmann. Hybrides Fahrwerkskonzept mit fahrzustandsadaptiver Regelung. Technical report, ATZ, 2012.

[18] Hong Li and Roger M. Goodall. Linear and non-linear skyhook damping control laws for active railway suspensions. *Control Engineering Practice 7*, 1999.

[19] Markus Lienkamp. *Vorlesung Grundlagen des Kraftfahrzeugbaus*. Fachschaft Maschinenbau, Technische Universität München, 2015.

[20] Christoph Lungwitz. Ausblick auf den neuen A8: vollaktives Fahrwerk bietet Flexibilität nach Maß. *Audi MediaInfo*, 2017.

[21] Mercedes-Benz. Magic Body Control. *Mercedes-Benz Newsletter*, 2018.

[22] Manfred Mitschke and Henning Wallentowitz. *Dynamik der Kraftfahrzeuge*. Springer Vieweg, 2014.

[23] Enrico Pellegrini. *Model-Based Damper Control for Semi-Active Suspension Systems*. PhD thesis, Technische Universität München, 2012.

[24] Enrico Pellegrini, Guido Koch, Sebastian Spirk, and Boris Lohman. A dynamic feedforward control approach for a semi-active damper based on a new hysteresis model. In *Preprints of the 18th IFAC World Congress*. IFAC World Congress, 2011.

[25] Nils Pletschen, Sebastian Spirk, and Boris Lohmann. Frequency-selective adaptive control of a hybrid suspension system. Technical report, Institute of Automatic Control, Technische Universität München, 2013.

[26] Schaeffler. *Technisches Taschenbuch*. Schaeffler, 2012.

[27] Erika Schäfer. *Modular-hierarchische modellbasierte Entwicklung und Optimierung einer Regelung für ein aktives Federungssystem*. PhD thesis, Universität Paderborn, 2009.

[28] Erika Schäfer, Torsten Bruns, and Andreas Wielenberg. Potential einer Störgrößenaufschaltung bei der Regelung aktiver Fahrwerke am Beispiel eines geländegängigen Nutzfahrzeugs. In *Entwurf mechatronischer Systeme*. Paderborner Workshop Universität Paderborn, 2006.

[29] Erika Schäfer, Karl-Peter Jäker, and Andreas Wielenberg. Aktive Federeung für ein geländegängiges Nutzfahrzeug. In *VDI/VDE-Fachtagung zur Steuerung und Regelung von Fahrzeugen und Motoren*. AUTOREG, 2006.

[30] Andreas Schindler. *Neue Konzeption und erstmalige Realisierung eines aktiven Fahrwerks mit Preview-Strategie*. PhD thesis, Universität Karlsruhe (TH), 2009.

[31] Sebastian Spirk and Kay-Uwe Henning. Wheel load oriented control of semi-active and active suspension systems using pre-located road sampling. In *Lecture Notes in Electrical Engineering 201*. SAE-China and Fisita (eds.), 2013.

[32] Sebastian Spirk and Chenhui Hu. Traktionsorentierte Regelung aktiver Fahrwerke mittels Straßenprofilabtastung oder radstadbasierter Schätzung. Technical report, Lehrstuhl für Regelungstechnik, Technische Universität München, 2013.

[33] Ralph H. Streiter. *Entwicklung und Realisierung eines analytischen Regelkonzeptes für eine aktive Federung*. PhD thesis, Teschnische Universität Berlin, 1996.

[34] Andreas Unger. *Serientaugliche quadratisch optimale Regelung für semiaktive PKW-Fahrwerke*. PhD thesis, Technische Universität München, 2012.

[35] Verein Deutscher Ingenieure. *VDI Norm 2057 - Human exposure to mechanical vibrations*. Beuth, 2002.

[36] Michel Verhaegen and Vincent Verdult. *Filtering and system identification*. Cambridge University Press, 2007.

Glossary

List of Acronyms

RMS-value root mean square value

MBC Magic Body Control

ABC Active Body Control

VDI Verein Deutscher Ingenieure

ISO International Standard Organisation

CDC Continuous Damping Control

Aktakon Aktive Aufbau Kontrolle

Ammakon Additive Modular Modale Aufbau Kontrolle

EDC Electronic Damper Control

ATP Automotive Testing Papenburg

ORK High Speed Oval

DLK Durability Road

SWS Rough Road

ECU Electronic Control Unit

MAB Micro-Autobox II

MPU Motor Pump Unit

Index